Universidade de Aveiro Departamento de Química
Ano 2020

AFONSO CERQUEIRA MARTINS

LÍQUIDOS IÓNICOS COMO HIDRÓTROPOS – A CHAVE PARA O AUMENTO DA SOLUBILIDADE

IONIC LIQUIDS AS HYDROTROPES – THE KEY TOWARDS SOLUBILITY INCREASE

Universidade de Aveiro Departamento de Química
Ano 2020

AFONSO CERQUEIRA MARTINS

LÍQUIDOS IÓNICOS COMO HIDRÓTROPOS – A CHAVE PARA O AUMENTO DA SOLUBILIDADE

IONIC LIQUIDS AS HYDROTROPES – THE KEY TOWARDS SOLUBILITY INCREASE

Dissertação apresentada à Universidade de Aveiro para cumprimento dos requisitos necessários à obtenção do grau de Mestre em Bioquímica, realizada sob a orientação científica da Doutora Tânia Ereira Sintra, Estagiária de Pós-doutoramento do CICECO, Universidade de Aveiro, e coorientação do Doutor Nicolas Gislain Schaeffer, Investigador Júnior do CICECO, Universidade de Aveiro.

o júri

presidente

Professor Doutor Brian James Goodfellow
Professor Auxiliar do Departamento de Química da Universidade de Aveiro

arguente

Professor Doutor Simão Pedro de Almeida Pinho
Professor Coordenador do Departamento de Tecnologia Química e Biológica do Instituto Politécnico de Bragança

orientador

Doutor Nicolas Gislain Schaeffer
Investigador do Departamento de Química da Universidade de Aveiro

agradecimentos

Aos meus orientadores, por me terem sábia e pacientemente acompanhado num caminho para mim completamente novo, do qual tirei o maior proveito e que me permitiu descobrir novas e interessantíssimas facetas desta área científica;

Ao PATh, que me deu a oportunidade de experimentar um núcleo onde a ciência se faz com grande qualidade;

Ao DQ, que por várias razões se tornou “a minha casa”, esperando sempre ter-lhe dado tanto quanto pude nos anos em que o foi;

E finalmente à UA, que com os seus mais e os seus menos traça o seu caminho como uma Universidade única, à qual devo muito, e que nunca deixarei de recordar.

aos meus avós, Alzira e Adelino

palavras-chave

Hidrotropia, líquidos iónicos, compostos hidrofóbicos, solubilidade, sais

resumo

A solubilidade em água de compostos hidrofóbicos é um fator crucial na formulação de fármacos, produtos de limpeza e de higiene pessoal. Assim, a tecnologia que permite aumentar a solubilidade e a taxa de dissolução dos mesmos tem atraído um considerável interesse não só a nível académico como industrial. Neste sentido, os hidrótropos têm sido alvo de muita atenção. Estes compostos são caracterizados como moléculas com capacidade de promover um drástico aumento da solubilidade aquosa de compostos fortemente hidrofóbicos, aumento este em várias ordens de magnitude. Recentemente, os líquidos iónicos foram apontados como uma classe promissora de hidrótropos cataniónicos, uma vez que quer o catião como o anião pode contribuir para o aumento da solubilidade. Embora haja um vasto número de trabalho de revisão com foco na hidrotropia, o mecanismo de ação por detrás deste fenómeno ainda não está claramente entendido. Este trabalho pretende averiguar o impacto da adição de um sal no fenómeno de hidrotropia com o intuito de melhor compreender o seu mecanismo, experimentalmente e através de simulação. A adição de cloretos a soluções aquosas de um líquido iónico demonstrou prejudicar a solubilidade ao promover a agregação do hidrótropo, com um comportamento com várias nuances, mas limitadamente sob uma ordenação de acordo com a valência do catião do sal adicionado. Interações hidrofóbicas mostraram-se centrais no efeito de agregação do hidrótropo em volta do soluto, que parece conduzir a hidrotropia. As interações entre o hidrótropo e o soluto apresentam um grau de especificidade de local, perdido com a adição de sal. A agregação do hidrótropo mostrou-se prejudicial para o efeito hidrotrópico, refutando uma das principais teorias justificativas do mecanismo da hidrotropia.

keywords Hydrotropy, ionic liquids, hydrophobic compounds, solubility, salts

abstract

Water solubility of hydrophobic compounds is a crucial factor in the formulation of drugs, cleaning products and personal hygiene. Therefore, technology that allows us to increase their solubility and dissolution rate has attracted considerable interest not only at an academic level but also at an industrial one. In this sense, hydrotropes have been under the spotlight. These compounds are characterized as molecules possessing the capacity of promoting a drastic, several-fold increase in aqueous solubility of highly hydrophobic compounds. Recently, ionic liquids have been appointed as a promising class of catanionic hydrotropes, since both the cation and anion can contribute to the solubility increase. Although there is a vast amount of reviewing work centred on hydrotropy, its underlying mechanism is not yet fully understood. This work proposes to study the impact of salt addition on the hydrotropy phenomenon as to better understand its mechanism, both experimentally and through simulation. Herein the addition of chloride salts to aqueous solutions of an ionic liquid was found to hinder solubility by promoting aggregation of the latter, with a notably nuanced behaviour according to the salt cation valence. Hydrophobic interactions were found to be central to the aggregative effect of the hydrotrope around the solute, which seem to drive hydrotropy. The interactions between the hydrotrope and the solute presented a degree of site-specificity, lost with salt addition. Hydrotrope aggregation showed to be detrimental to the hydrotropic effect, disproving one of the dominant theories justifying the mechanism of hydrotropy.

abbreviations

$[C_4mim]Cl$	1-butyl-3-methylimidazolium chloride
AA	All-atom
API	Active pharmaceutical ingredient
CG	Coarse-grained
CMC	Critical Micellar Concentration
CN	Coordination/cumulative number
EM	Energy minimization
FF	Force field
FST	Fluctuation Solution Theory
GROMACS	GROningen MAchine for Chemical Simulations
HS	Hofmeister series
IL	Ionic liquid
IS	Inorganic salt
KB	Kirkwood-Buff
LJ	Lennard-Jones
MD	Molecular dynamics
MHC	Minimum Hydrotrope Concentration
NMR	Nuclear Magnetic Resonance
OPLS	Optimized Potential for Liquid Simulations
PBC	Periodic boundary conditions
PME	Particle-mesh Ewalds
RDF	Radial Distribution Function
SANS	Small-Angle Neutron Scattering
SASA	Solvent-Accessible Surface Area

SDF	Spatial Distribution Function
TRAVIS	TRajectory Analyzer and VISualizer
TSP	Trimethylsilylpropanoic acid
VdW	Van der Waals
VMD	Visual Molecular Dynamics

index

Chapter I – Introduction

1. Opening remarks…….....3
2. Hydrotropy as a solubility phenomenon……3
    a. Mechanism of hydrotropy and existing controversy……5
3. Current applications of hydrotropes……9
4. Different types of hydrotropes……11
    a. Ionic liquids as catanionic hydrotropes……12
5. Effect of different salts on aqueous solutions of ionic liquids……13
6. Molecular Dynamics……...15
7. Objectives……18

Chapter II – Methodology

1. Experimental hydrotropic solubility tests…….....21
    a. Materials……..21
    b. Hydrotropic solubility curves……22
    c. Nuclear Magnetic Resonance……..23
    d. Dynamic Light Scattering……..23
2. Molecular Dynamics……...24
    a. Simulation details……..25
    b. Analysis……...27

Chapter III – Results and discussion

1. Hydrotropic solubility tests……33
2. Determination of hydrotrope-solute interactions……39
    a. Ionic liquid aqueous solutions…….....39
    b. In the absence of salt……40
    c. Salted ionic liquid aqueous solutions……..45
    d. Salted ionic liquid aqueous solutions with vanillin……..48

3. Molecular Dynamics……...53
    a. Probing aggregate formation……53
    b. Probing site-specific solute-hydrotrope interactions……57
        i. Ionic liquid-vanillin interactions……58
        ii. Solute-water interactions……67
4. Summary of findings……...71

Chapter IV – Conclusions and future work……75

Chapter V – Bibliography……81

Supporting Information……..91

List of Figures

Figure 1. Solubility curve of vanillin in an aqueous solution of 1-butyl-3-methylimidazolium chloride ([C_4mim]Cl), as measured by the optical density at 280 nm, showcasing the sigmoidal nature of the hydrotropic solubilization curve. ……..……..……...6

Figure 2. Schematic representations of the three proposed mechanisms for hydrotropy. (a) exemplifies the pre-clustering model, where hydrotropes are aggregated before solute addition; (b) exemplifies the water-disrupting model, where hydrotropes disrupt the water structure creating cavities that the solute can then occupy; and (c) exemplifies the co-aggregation model, where solute addition drives the aggregation of the hydrotrope around the solute. ……..…7

Figure 3. Examples of the several types of hydrotropes. As an anionic hydrotrope, ammonium xylenesulfonate (1); as a cationic hydrotrope, tetrabutylammonium bromide (2); as a neutral hydrotrope, urea (3); as a catanionic hydrotrope, the ionic liquid 1-butyl-3-methylimidazolium thiocyanate ([Bmim][SCN]) (4). ….……12

Figure 4. Schematic representation of the time and special scales reachable by molecular dynamics simulation methods, as well as some structure and occurrences related to membrane biophysics [Nielsen *et al.*]. ……..….16

Figure 5. Chemical structures of 1-butyl-3-methylimidazolium ([C_4mim]Cl, left) and vanillin (protonated, right). ……21

Figure 6. Schematic of the experimental workflow of the vanillin solubility tests. Addition of vanillin to an ionic liquid (hydrotropic) solution (1); agitation to promote vanillin dissolution, through several days (2). When no vanillin can be observed, step (1) is performed again, followed by (2), as many times as needed. When the solid vanillin precipitate amount is constant for 48h (3), supernatant absorbance is read at 280 nm (4). ……23

Figure 7. Example of a determination of an RDF using vanillin and water. In this case, the reference atom is the oxygen atom of the aldehyde functional group of vanillin and the selection is water. *r* denotes the chosen radius at which the probability of finding water will be calculated and expressed as *g(r)*. ……28

Figure 8. Solubility curves for vanillin in a 0,5 M [C_4mim]Cl aqueous solution and in the presence of different salts. Error bars represent the standard deviation from three independent measures. Vanillin solubility in water as determined by Cláudio *et al.* ….……33

Figure 9. Solubility curves for vanillin in a 1,5 M [C_4mim]Cl aqueous solution and in the presence of different salts. Error bars represent the standard deviation from three independent measures. Vanillin solubility in water as determined by Cláudio *et al*. ……...…34

Figure 10. Evaluation of a correlation between the Gibbs free energy of hydration of the studied salt cations and their respective disruption of the hydrotropic effect, expressed through the ratio between vanillin solubility in the presence of salt, *S*, and in its absence, S_{nosalt}. Referent to the series in 0,5 M IL. ……..……..37

Figure 11. Evaluation of a correlation between the Gibbs free energy of hydration of the studied salt cations and their respective disruption of the hydrotropic effect, expressed through the ratio between vanillin solubility in the presence of salt, *S*, and in its absence, S_{nosalt}. Referent to the series in 1,5 M IL.
(*)YCl^3 concentration in this point is 0,5 M, the maximum successfully tested.…….38

Figure 12. Chemical shifts of the hydrogens of the C_4mim cation in 1,5 and 2,25 M solutions of [C_4mim]Cl in water when compared to a 0,5 M solution. ……..……40

Figure 13. Chemical shifts of the hydrogens of the IL cation in a 1,5 M solution of [C_4mim]Cl in water, saturated with vanillin, when compared to an aqueous 1,5 M IL solution with no solute……..42

Figure 14. Chemical shifts of the hydrogens of vanillin in a 1,5 M solution of [C_4mim]Cl in water, saturated, when compared to vanillin dissolved in water, saturated. ……..…43

Figure 15. Chemical shifts of the hydrogens of the C_4mim cation in a 1,5 M solution of [C_4mim]Cl in water, saturated with vanillin, when compared to the same solution without vanillin. ……...…44

Figure 16. Chemical shifts of the hydrogens of vanillin in a 1,5 M solution of [C_4mim]Cl in water, saturated, when compared to vanillin dissolved in water, saturated. ……..……45

Figure 17. Chemical shifts of the hydrogens of the C_4mim cation in 1,5 M solutions of [C_4mim]Cl in water with 1,0 M of added salts, when compared to a similar solution without added salt. ……..…47

Figure 18. DLS measurement of aggregate presence in 1,5 M [C_4mim]Cl salted solutions without vanillin, logarithmic scale. ……..……...48

Figure 19. Chemical shifts of the hydrogens of the C_4mim cation in 1,5 M solutions of [C_4mim]Cl in water, with added vanillin to saturation and with 1,0 M of added salts, when compared to a similar solution without added salt. ……..……49

Figure 20. Chemical shifts of the hydrogens of vanillin in 1,5 M solutions of [C_4mim]Cl in water, with added vanillin to saturation and with 1,0 M of added salts, when compared to a similar solution without added salt. …….50

Figure 21. Chemical shifts, normalized to the valence of the salt cation added, of the hydrogens of the ionic liquid cation (a) and vanillin (b) in 1,5 M solutions of [C_4mim]Cl in water, with added vanillin to saturation and with 1,0 M of added salts, when compared to a similar solution without added salt. …….51

Figure 22. Aggregate presence in 1,5 M [C_4mim]Cl salted solutions saturated with vanillin in a (a) normal and (b) logarithmic scale. ……..…….52

Figure 23. Solvent-accessible surface area for the [C_4mim]$^+$ cation in all conditions. …….54

Figure 24. Density curves for the IL cation, vanillin, and water across the simulation boxes. The five conditions are (a) IL in water, (b) 10 vanillin in water, (c) 10 vanillin in IL and water, (d) 20 vanillin in IL and water, (e) 20 vanillin in IL and water with 100 NaCl molecules. Note that in (b) and (c) vanillin is present below its solubility limit, and in (d) and (e) above it. The depicted curves are smoothed running averages of the actual raw curves. ..……56

Figure 25. [C_4mim]$^+$ cation (left) and vanillin (right) all-atom models with labelling of the atoms for which RDF analyses were performed. ……..……..57

Figure 26. Radial distribution functions for the H0S hydrogen of the vanillin ring as reference, and the four hydrogens of the IL cation as selection, for the following conditions: 10 vanillin molecules in aqueous IL (top), 20 vanillin molecules in aqueous IL (middle), and 20 vanillin molecules in aqueous IL with 100 NaCl molecules added (bottom). ……59

Figure 27. Radial distribution functions for the O0A oxygen of the vanillin aldehyde group as reference, and the four hydrogens of the IL cation as selection, for the following conditions: 10 vanillin molecules in aqueous IL (top, with respective ampliation on the right), 20 vanillin molecules in aqueous IL (middle), and 20 vanillin molecules in aqueous IL with 100 NaCl molecules added (bottom). ……..…….61

Figure 28. Different examples of IL-vanillin aggregates and possible hydrogen bonding. Depicted are vanillin (with red oxygen atoms), the IL cation (with blue nitrogen atoms) and chloride (green). ……..62

Figure 29. Spatial Distribution Functions of water (blue), chloride (yellow), vanillin (red), the IL cation head (green), and the IL cation tail (purple) with vanillin as the reference molecule, for condition (c) 10 vanillin in aqueous 100 IL (left) and (d) 20 vanillin in aqueous 100 IL (right)……..…63

Figure 30. Spatial Distribution Functions of water (blue), chloride (yellow), vanillin (red), and the IL cation head (green) with the IL cation as the reference molecule, for condition (c) 10 vanillin in aqueous 100 IL (left) and condition (d) 20 vanillin in aqueous IL (right). ……..…...65

Figure 31. Vanillin (with red oxygen atoms) and IL cation (with blue nitrogen atoms) aggregates evidencing ring stacking. Van der Waals (left) and licorice (right) representations……..…65

Figure 32. Radial distribution functions for the three selected functional group oxygens and hydrocarbon ring hydrogen of vanillin as reference, and water as selection. ……..……68

Figure 13. Radial distribution functions for the four selected hydrogens of the IL cations as reference, and water as selection. ……..…69

Figure 34. General interactions studied throughout this work. From the hydrotrope in solution (1), the addition of salt will promote hydrotrope aggregation, with preference for interactions involving the hydrophobic tail. This aggregation is due to dehydration induced by strong ion-water interactions (2). The addition of solute will promote aggregation of the hydrotrope but around the solute, central in hydrotropy. The main interactions are hydrophobic (3). The addition of both salt and solute will promote larger and less organized aggregates, but the salting will hinder solubility (4). ……..……..……...73

Figure 35. All-atom (left) to coarse-grain (right) modelling by the MARTINI model attempted in this work for the $[C_4mim]^+$ cation. The ring was represented by beads NP1, of bead type SP5, polar ring bead with very high polar affinity, NQ2, of bead type SQd, charged ring bead acting as hydrogen bond donor, and CC3, of bead type SP1, polar ring bead with low polar affinity, and the tail by bead C4, of bead type SC1, apolar bead with low polar affinity…..…79

Figure 36. All-atom (left) to coarse-grain (right) modelling by the MARTINI model attempted in this work for the vanillin molecule, with beads C1, of bead type SNda, nonpolar bead acting as both donor and acceptor of hydrogen bonds, C2, of bead type SC4, apolar bead with high polar affinity, C3, of bead type SQa, charged bead acceptor of hydrogen bonds, O4, of bead type SC5, apolar bead with high polar affinity, and C5, of bead type SC4. ……..…….79

List of Figures for the Supporting Information

Figure SI:1. NMR spectra of $[C_4mim]Cl$ in water, at different concentrations: 0,5 M (red), 1,5 M (green), and 2,25 M (blue). ……..95

Figure SI:2. NMR spectra of $[C_4mim]Cl$ and vanillin in water. 1,5 M IL in water (red), 1,5 M IL with vanillin to saturation (green), and vanillin in water to saturation (blue). …….95

Figure SI:3. NMR spectra of 1,5 M $[C_4mim]Cl$ in water with added salts: 1,5 M IL in water without added salt (red), 1 M NaCl (olive), 1 M LiCl (green), 1 M $MgCl_2$ (blue), 1 M YCl_3 (purple). ……..……96

Figure SI:4. NMR spectra of 1,5 M $[C_4mim]Cl$ in water with added LiCl: 1,5 M IL in water without added salt (red), 1 M LiCl (olive), 2 M LiCl (turquoise), 6 M LiCl (purple). …..…….96

Figure SI:5. Chemical shifts of the hydrogens of the C_4mim cation in 1,5 M solutions of $[C_4mim]Cl$ in water, with added LiCl, when compared to a similar solution without salt. ……97

Figure SI:6. Chemical shifts of the hydrogens of the C_4mim cation in 1,5 M solutions of $[C_4mim]Cl$ in water, with added vanillin to saturation and with 1,0 M of added salts, when compared to a similar solution without vanillin. …….97

Figure SI:7. Radial distribution functions for the O0H oxygen of the vanillin methoxy group as reference, and the four hydrogens of the IL cation as selection, for the following conditions: 10 vanillin molecules in aqueous IL (top), 20 vanillin molecules in aqueous IL (middle), and 20 vanillin molecules in aqueous IL with 100 NaCl molecules added (bottom). ……..98

Figure SI:8. Radial distribution functions for the O0N oxygen of the vanillin hydroxyl group as reference, and the four hydrogens of the IL cation as selection, for the following conditions: 10 vanillin molecules in aqueous IL (top), 20 vanillin molecules in aqueous IL (middle), and 20 vanillin molecules in aqueous IL with 100 NaCl molecules added (bottom). ……....99

Figure SI:9. Spatial Distribution Functions of water (blue), chloride (yellow), vanillin (red), the IL cation head (green), and the IL cation tail (purple) with vanillin as the reference molecule, for condition (e) 20 vanillin in aqueous 100 IL with 100 NaCl. ……100

Figure SI:10. Spatial Distribution Functions of water (blue), chloride (yellow), vanillin (red), the IL cation head (green), and the IL tail (purple) with the IL cation as the reference molecule, for condition (e) 20 vanillin in aqueous 100 IL. ……..……..…100

Figure SI:11. Spatial Distribution Functions of water (blue) and vanillin (red) with vanillin as the reference molecule, for condition (b) 10 vanillin in water. ……..…101

Figure SI:12. Spatial Distribution Functions of water (blue), chloride (yellow) and the IL cation imidazolium ring (green) with the $[C_4mim]^+$ cation as the reference molecule, for condition (a) 100 IL in water. ……...101

Figure SI:13. Sequence of eight frames depicting typical observed interactions between vanillin (with red oxygen atoms), the IL cation (with blue nitrogen atoms), and chloride (green). Deserving special emphasis, the planar interactions, the methyl chloride interactions, IL tail-vanillin interactions, and the possible structuring effect of chloride in frames 7 and 8. Water hidden for clarity. Snapshots taken from condition (d) 20 vanillin in aqueous IL. ..…..102

List of Tables

Table 1. Common file formats for GROMACS and their function. ……..24

Table 2. Detailed composition and properties of the five all-atomistic MD systems. These will oftentimes be referred by their designated letter (a) through (e). ……..……30

Table 3. Thermodynamic parameters of the tested salt cations at 298,15 K. *r* denotes the ions' radius, *Δr* the radius of its hydration shell, *n* the number of water molecules within the hydration shell, $\Delta_{hyd} S^{o}$ the absolute value of the conventional standard molar entropy of hydration, and $\Delta_{hyd} G^{*}$ the experimental value of the molar Gibbs free energy of hydration, according to Marcus. ……..……..36

Table 4. Summary of radial distribution function values for the first peak obtained for the systems including both IL and vanillin. ……...66

Table 5. Summary of radial distribution function values for the first peak obtained for the systems including IL or vanillin in water. ……..70

List of Tables for the Supporting Information

Table SI:1. Experimental results for the hydrotropy tests referent to the 0,5 M IL condition. The vanillin concentration expressed is the mean value deriving from three independent tests. Note that the value in the absence of salt was obtained from a previous study, and as such is not subject to any deviation. ……..…….93

Table SI:2. Experimental results for the hydrotropy tests referent to the 1,5 M IL condition. The vanillin concentration expressed is the mean value deriving from three independent tests. Note that the value in the absence of salt was obtained from a previous study, and as such is not subject to any deviation. ……..…….94

Chapter I

Introduction

1. Opening remarks

Scientific progress has been increasingly tied with the development of a more sustainable industry and economy at a global level, especially in the current millennium. Green chemistry is now a staple of the scientific production in the fields of chemistry and chemical engineering, aiming at the elimination or substitution of methods and compounds with associated environmental risk through the development of more friendly alternatives.[1] Solvents are of utmost importance to this finality, attracting research relevant to industry, pharmaceuticals, and academia. Ionic liquids (ILs) have, at the turn of the century, caught much interest as novel designer solvents. Effectively, their tuneability, high product yields and recycling potential made them promising contenders in the world of green solvents.[2] Current knowledge states that ILs are not always green – but there is still an enormous role for them to play when they are. Some of these compounds have recently been recognized as hydrotropes, agents very soluble in water that drastically improve the solubility of other sparingly soluble hydrophobic compounds.[3,4] Hydrotropy has been successfully applied to industry and pharmacy alike, and the combined advantages from this phenomenon and ILs appears to be a promising branch of research. The hydrotropic mechanism of solubilisation has been the target of much work, and despite having become clearer in recent advances is not yet fully understood. The present work intends to probe the interactions at play in this mechanism by analysing the effect inorganic salts (ISs) have on the hydrotropic solubilisation effect of an imidazolium-based ionic liquid on vanillin, a much-studied molecule in the field of extractions by ILs, and a natural antioxidant and anti-inflammatory. Herein it is also intended to analyse the aggregation behaviour and interactions by both hydrotrope and solute, through experimental methodology and the application of molecular dynamics (MD) simulations.

2. Hydrotropy as a solubility phenomenon

There are currently several known techniques of solubility enhancement for poorly water-soluble substances, of which many are used with pharmacological interest for active pharmaceutical ingredient (API) solubility improvement: cosolvency,[5] addition of salting-in electrolytes,[6] use of surfactants, including use of surfactants alongside an oil to create a microemulsion,[7,8] micronization,[9] nanosuspension,[10] use of precipitation inhibitors,[11] complexation (i.e. with cyclodextrins),[12] solid dispersion technique,[13] and hydrotropy,

among others. The hydrotropic solubilization emerges amidst this panoply of techniques with the advantages of its simplicity, as it only requires the mixing of the hydrotrope with the solvent in aqueous media and does not demand any chemical modification of the solute nor use of organic solvents or emulsion preparation, its independency of pH and the fact that hydrotropic solutions can easily precipitate the solute upon dilution.[14,15]

Hydrotropy is, by definition, a solubilization phenomenon in which a compound significantly increases the solubility of hydrophobic or otherwise poorly soluble substances in water or in aqueous media. This phenomenon was first reported by Neuberg in 1916, who then coined the term “hydrotropy”.[16] Neuberg’s hydrotropes were organic salts with short alkyl chains. Since then, a large amount of research has been done on the subject, and currently hydrotropic compounds find a broad range of uses, especially in chemical industrial processes and pharmaceutical development.[4,17–21] Typical hydrotropes used in industry possess an amphiphilic molecular structure and are very water soluble, most consisting of a phenyl group linked to an anionic group – hydrophobic and hydrophilic moieties, respectively. Counter ions for these molecules are diverse, such as sodium, potassium, calcium and ammonium.[22] It is of important to emphasise that hydrotropes are not considered surfactants: they do not spontaneously self-assemble into distinct structures and phases in aqueous media as their hydrophobic moiety is too short for these phenomena to occur.[23,24] There is evidence of their self-aggregation, but they are less surface active than classical surfactants. The microenvironments of hydrotrope aggregates are comparable to those of micelles in terms of polarity and microviscosity - the differences lie in the higher and step-wise ordered solubilization by micelles and the low cooperativity shown by hydrotropes in the aggregation process.[25]

The process of solubilization requires the breakage of bonds, whether covalent or ionic, between the molecules of solute, allowing them to interact with the solvent molecules and occupy the spaces existing in the solvent matrix. This process happens under a dynamic equilibrium, as during solubilization the two processes of solute dissolution and phase joining - such as precipitation in the case of solid solutes - occur simultaneously at different rates, until solubility equilibrium is reached and these rates become equal. The extension to which a given non-gaseous solute solubilizes in a given solvent is dependent of a) the physicochemical properties of the solute, such as the particle size, shape (i.e. in polysaccharides and isomeric alcohols, more branching generally means increased solubility) and molecular size, affecting the surface area available to the solvent, and its polarity since it greatly affects solute-solvent interaction forces; b) the physicochemical

properties of the solvent; c) temperature, as increased temperature generally translates into increased solubility.[26]

a. Mechanism of hydrotropy and existing controversy

Hydrotropes present a characteristic sigmoidal solubility curve which appears to show the existence of a threshold where solubility drastically increases, usually known as the minimum hydrotrope concentration (MHC).[27] An exemplifier curve is presented in Figure 1, referring to the actual solubility in vanillin in [C_4mim]Cl previously determined.[3] In low hydrotrope concentrations, below the MHC, there is little to no increase in solubility. Upon reaching it there is a sudden spike in solubility, which eventually comes to a plateau after a few molars of hydrotrope concentration. Every hydrotrope promotes its effect to a different extent. The hydrotropic capacity of different compounds relative to a given solute can be known through the determination of their hydrotropy constant, K_{Hyd}. In turn, this constant is determined through the application of the Setschenow equation,[28] modified:

$$\log\ (S/S_0) = K_{Hyd} \times\ C_{Hyd} \quad (1)$$

where S and S_0 represent the solubility of the solute in the hydrotrope aqueous solution and in pure water, respectively, and C_{Hyd} represents the concentration of the hydrotrope in aqueous solution. Therefore, the higher the value of K_{Hyd}, the more solute can be solubilized by the hydrotropic solution, and the higher is the capacity of the compound in question to act as a hydrotrope.

Although a considerable amount of research has been made on this topic, the exact mechanism underlying hydrotropy is not yet understood to its full extent. There are currently three central theories that try to describe the mechanism behind the enhanced solubilisation phenomenon, schematized in Figure 2:

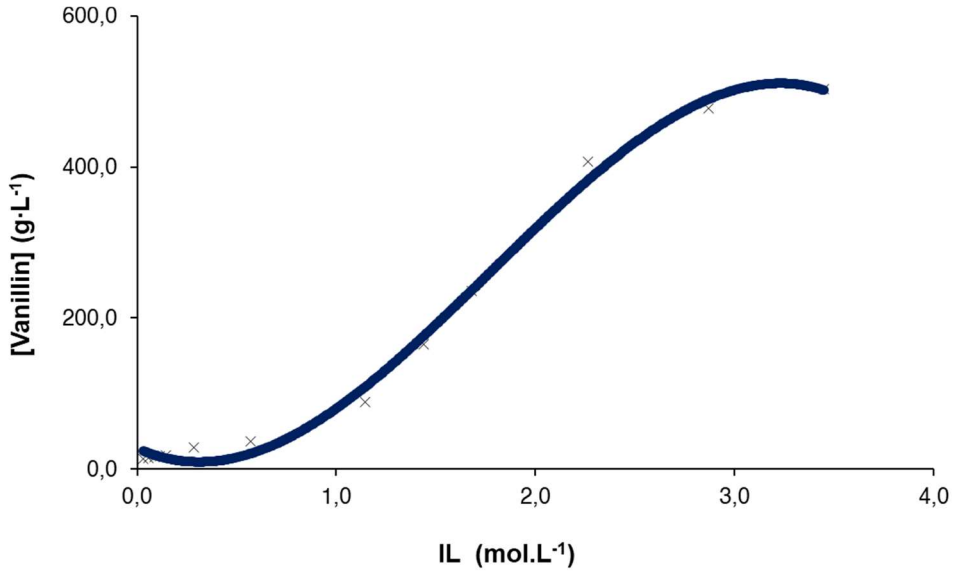

Figure 1. Solubility curve of vanillin in an aqueous solution of 1-butyl-3-methylimidazolium chloride ([C_4mim]Cl), as measured by the optical density at 280 nm, showcasing the sigmoidal nature of the hydrotropic solubilization curve.[6]

(a) The self-aggregation of hydrotropes theory that several authors propose affirms that the formation of a cluster of hydrotrope molecules in the bulk phase occurs (pre-clustering). That structure can accommodate solute molecules, thus forming a solute-hydrotrope complex and increasing solubility. This theory can be seen with some parallelism with micellar solubilization. Yet, considering the hydrotropes' weak tendency to form such complex structures due to their short hydrophobic moiety, there is plenty of space for debate on whether this is truly the driving force for the enhanced solubilization mechanism.[29]

(b) Other authors suggest that hydrotropes interfere with the solvent structure, modifying the water distribution around the solute molecule. This means that hydrotropes do not directly bind to solute molecules; instead, the hydrotrope breaks the water structure around the hydrophobic solutes, causing facilitated solubilization, which would explain the hydrotropy mechanism. This rationale is based on the so called "iceberg" model that suggests that hydrophobic moieties enhance local structuring of water.[30] However, other works have determined that such effect is non-existent, if not contrary, as hydrophobic entities seem to be accommodated in the disordered bulk-like water structure without any increased "ice-like" structuring.[31,32]

(c) Recently, the co-aggregation of the solute with the hydrotrope, further detailed below, has been a strong proposal to explain the mechanism. It generally states hydrotrope-solute are the preferential interactions, and that solute presence induces hydrotrope aggregation around it, while pre-clustering of hydrotropes hinders the hydrotropic effect.[33,34]

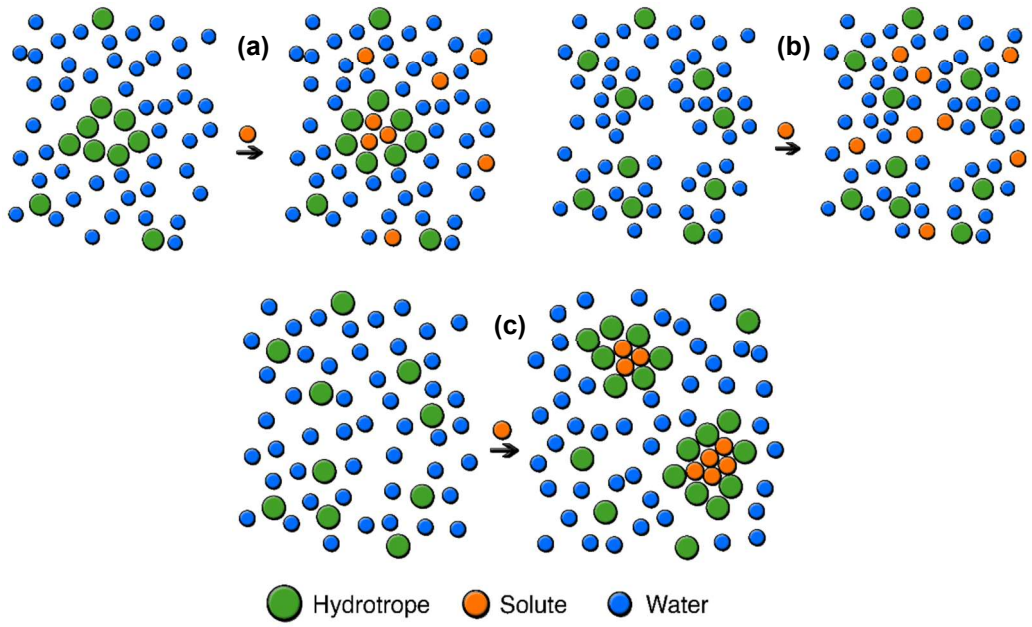

Figure 2. Schematic representations of the three proposed mechanisms for hydrotropy. (a) exemplifies the pre-clustering model, where hydrotropes are aggregated before solute addition; (b) exemplifies the water-disrupting model, where hydrotropes disrupt the water structure creating cavities that the solute can then occupy; and (c) exemplifies the co-aggregation model, where solute addition drives the aggregation of the hydrotrope around the solute.

The sigmoidal solubility curve such as seen in Figure 1 is indicative that hydrotropic-mediated solubilisation is a cooperative phenomenon,[25] meaning intermolecular interactions are involved in its mechanism of action. Bearing in mind the similarity between MHC for hydrotropes and the critical micellar concentration (CMC) for surfactants, the belief that it is the self-aggregation of hydrotropes that drives the increased solubility arose. Nonetheless, more recent studies have verified that the MHC still occurs when the self-aggregation and micellization of hydrotropes does not, disproving this theory.[33] As such, further study was needed to understand the nature of MHC and thus to shed light on the mechanism of hydrotropy. Recently, through the application of the Kirkwood-Buff (KB) theory, an exact, no-approximation statistical thermodynamics theory, it has been shown

that the great increase in solubility is caused by the solute-induced increase in hydrotrope-solute interactions from the bulk solution, and the MHC is caused by hydrotrope aggregation in presence of the solute. Also, micelle formation reduces the efficiency of solubilization per hydrotrope molecule and prevents the achievement of the MHC.[34] Hence, hydrotropes are molecules whose structuring in water is enforced by the presence of a third, poorly water-soluble compound, and that enforced structuring is what drives the hydrotropic effect that leads to the increased solubility of the hydrophobic molecules. As such, further understanding of the mechanism underlying hydrotropy should be centred on how the hydrotrope molecules behave around the solutes, not on the bulk phase self-interaction of hydrotropes, as previously thought. Moreover, the existence of the MHC has recently been subject of doubt by several authors, since a considerable amount of experimental data indicates a more gradual increase of solubility as the hydrotrope concentration rises, instead of the MHC-typical spike followed by a plateau.[35] Some relate it with inaccuracy in experimental measurements and others with faulty interpretation of experimental data.[35,36]

Hatzopoulos *et al.*[37] compared physicochemical properties of sodium salts of benzoate of varying alkyl chain lengths in the *p* position. Shorter alkyl chains are mostly associated with common hydrotropes, whereas longer ones give compounds associated to regular surfactants. Conductivity measurements of CMC lead to the finding that longer chain homologues give a curve with sharp bends, but the shorter ones provide a smoother, rounded curve, indicating micelle formation at the CMC for the former and step-wise aggregation with less free-energy for the latter. As such, while compounds with longer alkyl chains tend to form micelles of well-defined size at a specific concentration, typical hydrotrope-like compounds with shorter chains aggregate over a broader concentration range, with less defined sizes, in a stepwise manner. This further casts doubt on the existence of the MHC, and its claim of a sudden spike in solubility. Nevertheless, the same authors performed Small-angle Neutron Scattering (SANS) experiments on homologous sodium *p*-alkylbenzoates which showed nearly the same aggregation behaviour for both long and short chain homologues. That aggregation occurred at a defined concentration, more resembling of surfactants than hydrotropes. Overall, it may be considered that for amphiphilic molecules consisting of a large organic anion and a small inorganic cation, description that can encompass a very significant portion of the most well-studied hydrotropes, there can be a cross-over from hydrotropes to surfactants.[15]

So far, the specificities of the molecular mechanism that drives the hydrotropic effect are yet to be detailed. Studies with nicotinamide have claimed that the formation of solute-hydrotrope complexes based on π-π interactions play a major role in the effect. This kind

of interactions promote the stacking complexation between solute and hydrotrope molecules, in which the exposure to water of the hydrophobic regions of both are reduced. Such complexes would be the result of interactions between an aromatic solute and aromatic moiety of a hydrotrope, especially when involving planar molecules. The stacking could form 1:1 solute to hydrotrope complexes or 1:2 “sandwich” complex consisting of 1 molecule of solute in-between two of complexing hydrotrope.[29] Nevertheless, it has been shown that despite most common hydrotropes possessing aromatic anions in their structure, non-aromatic cations also induce the hydrotropic effect.[3]

In sum, data points to the fact that hydrotropes have the capacity to self-aggregate, but to a much lesser extent than common surfactants. This aggregation is also not sudden nor subject to a specific concentration, as it happens throughout a broad concentration range. Crucially, hydrotropes do tend to cluster around a hydrophobic solute in its presence, above a certain hydrotrope concentration range. As described by Booth, Abbott and Shimizu,[38] using statistical thermodynamics through the application of the fluctuation solution theory (FST), a rigorous, model-free approach, there are two conflicting driving forces to this clustering: the attraction force between the hydrotrope and the solute, and the interaction between the hydrotrope and water, where there increased entropy when water is relieved of contact with the hydrotrope molecules. This second force is also related to the self-association of the hydrotrope in the bulk phase, showing that the greater it is, the lesser the per-molecule of hydrotrope solubilization efficiency. The same work also undoubtedly dispels the idea that hydrotropic self-association enhances solubility, as micellar self-association does. Only above a sufficient concentration of hydrotropes in the presence of the solute does the clustering of hydrotrope molecules become considerable, driving the so-called hydrotropic effect that, summarizing, originates from solute-induced interaction between hydrotrope molecules above a certain hydrotrope concentration range. Hence, the enthalpic effect of hydrotrope-water interaction is insufficient to explain the mechanism in question, and one should also look at the entropic effect at play in the hydrotrope-solute interaction relative to the hydrotrope-water.[15]

3. Current applications of hydrotropes

The current practical applications of hydrotropes are showcased mostly in the pharmaceutical and industrial fields.[4,17–21] In pharmacy, many of the compounds in early stages of drug development are highly hydrophobic and poorly water-soluble. Good solubility in water is a key physicochemical property to account for in the development of

novel pharmaceuticals. This property allows the achievement of a desired concentration of a drug in systemic circulation, thus providing high bioavailability, which in turn greatly impacts the overall effectiveness of a drug.[39] Even regardless of administration route and bioavailability, preclinical and toxicological studies require that the drug be tested at relatively high concentrations, demanding good enough water solubility.[18] As such, solubility enhancement of potential pharmaceutical compounds is an active research topic. Hydrotropic solutions have shown the ability to greatly improve the solubility of poorly water-soluble drugs.[4,18,33] It is important to acknowledge that the development of hydrotropic systems for drug solubilization should consider how to maximize the beneficial hydrotropic effect, while maintaining the hydrotrope dosage in the formulation minimal, to avoid possible issues.[18]

More recently, the mixed hydrotropy technique has emerged. It uses a combination of several hydrotropic agents in a solution, instead of one in conventional hydrotropy. Maheshwari and Jagwani[40] reported an increase in furosemide solubility of 660 times in a 40% w/v urea + sodium benzoate + sodium citrate solution in a 15:20:5 ratio when compared to solubility in water. Furosemide solubility in 40% w/v of exclusively sodium benzoate was only enhanced by 296 times in the same study. These authors then combined mixed hydrotropy with the solid dispersion technique by dissolving furosemide in the mixed solution and evaporating water. During dissolution rate studies, these solid dispersions almost completely dissolved in 1 minute, while conventional furosemide tablets only dissolved about 82% after 30 minutes. No solute-hydrotrope interactions or complex formation were reported. Other authors have performed analogous studies with different drugs with consistent results,[41,42] supporting the idea that mixed hydrotropy can be an additional technique to further improve the solubility of poorly water-soluble substances, and that it can be combined with the solid dispersion technique as an extremely useful procedure to enhance drug solubility and bioavailability, presenting a promising route for further research.

In industry, hydrotrope applications were initially pointed at by McKee,[43] who most remarkably noted the ability of hydrotropic solutions to precipitate the solute on dilution with water, since as described above the characteristic increased solubilization is only seen above a certain hydrotrope concentration, that is, above the MHC. To industry, this is an important phenomenon as it allows the ready recovery of the solvent for re-use, making hydrotropic solvents green and economic solvents. McKee also pointed several advantages in favour of hydrotropic versus conventional solvents in electrochemical, organic and inorganic reactions, and most notably the potential role of hydrotropic solutions in the field

of separations.[43] Using these solutions, separation factors in extractive separations, extractive distillations and crystallizations have been shown to be higher than compared to conventional methods, while they also provide highly selective separation for industrial mixtures. Difficult-to-separate solid mixtures are separated using hydrotropes by either a solubilization and precipitation technique, in which a mixture is solubilized in a hydrotropic solution followed by the selective precipitation of a desired component by simple dilution with water, or by leaching, in which the solubilization is partial and controlled, so that one of the components of the mixture is left in solid phase with improved purity. Combining the hydrotropic solutions high selectivity and separation potential with the easy recovery of products makes these solutions very good candidates for a wide array of industrial uses.[19,21]

4. Different types of hydrotropes

Most common substances associated to the concept of hydrotrope are salts with an amphiphilic bulky anion, mainly a short alkylbenzene sulfonate. Examples of such are xylenesulfonate and cumenesulfonate. Another well-known hydrotrope is urea, a neutral molecule that is both a good donor and acceptor of hydrogen bonds. Because it forms a near-ideal mixture with water, and so should not self-associate to a great extent, but still exhibits hydrotropic properties, it defied the theory that it is the self-association of hydrotropes that promotes hydrotropic solubility. Also due to this fact, urea has a very high per-molecule solubilization efficiency.[38] Cationic hydrotropes such as tetraethylammonium chloride and polypropylene oxide ammonium chloride have also had work reported on them,[44,45] but not many more are known to a considerable extent at the current stage. Some work is reported on quaternary ammonium compounds such as tetrabutylammonium bromide, aniline hydrochloride and toluidine hydrochloride, mostly tested together with anionic surfactants and reporting synergistic effects between the two and mixed micelle formation.[46] Recently, ionic liquids (ILs) have been reported as a promising class of catanionic hydrotropes, since both the cation and anion may contribute towards the augmented solubility effect on hydrophobic substances.[3] Therefore, one can consider the existence of several hydrotrope types: anionic, cationic, neutral and catanionic. Some are exemplified in Figure 3.

Catanionic hydrotropes consist exclusively of ionic liquids and will be further detailed in the text below.

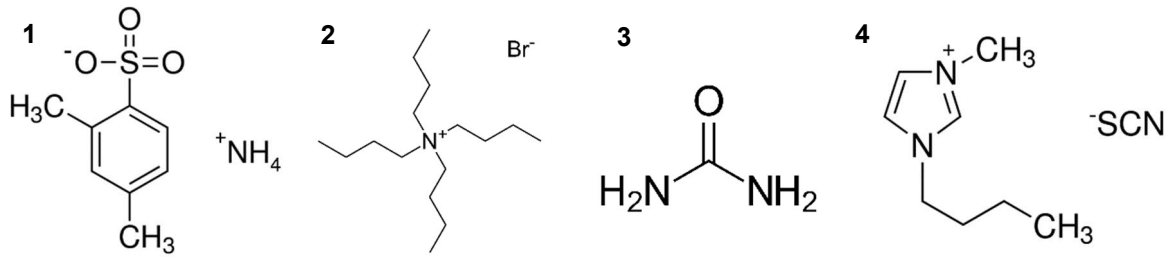

Figure 3. Examples of the several types of hydrotropes. As an anionic hydrotrope, ammonium xylenesulfonate (1); as a cationic hydrotrope, tetrabutylammonium bromide (2); as a neutral hydrotrope, urea (3); as a catanionic hydrotrope, the ionic liquid 1-butyl-3-methylimidazolium thiocyanate ([Bmim][SCN]) (4).

a. Ionic liquids as catanionic hydrotropes

Ionic liquids are salts entirely composed of ions, usually large organic cations and organic or inorganic anions, with low melting points (typically lower than 100°C), since one or both ions have a dispersed charge, and their asymmetry hinders the formation of an ordered crystalline structure. The increasing attention paid to ILs is largely justified by their unique properties, such as their negligible vapour pressure, high chemical and thermal stability, and high solvation ability.[47] Furthermore, these ionic compounds can be considered as “designer solvents’’ due to their tuneable properties, which means that they can be arranged and tuned for a wide array of specific applications by the selection of the adequate cation/anion combination. Adding to this, there is the advantage of one being able to independently modify the properties of both cation and anion while maintaining the ILs main properties, allowing for extensive design of new compounds and materials.[48]

Due to their good solvation ability for a wide range of solutes, they have been proposed as potential alternatives for conventional organic solvents used in extraction and separation processes. The use of aqueous solutions of ILs for the extraction of value-added compounds from biomass have been reported, namely for the extraction and purification of phenolic compounds, such as gallic acid and vanillin.[49,50] The research on these kind of organic compounds bears its relevance since they possess beneficial properties for human health. Vanillin is a known antioxidant, anti-inflammatory, radical scavenger and antimicrobial compound found in natural vanilla, having as well great importance in food flavouring and preservation.[51]

Considering the current knowledge on both the good solvation ability of ILs and the hydrotropic solubilization phenomenon, it is with some ease that an interesting question arises: can ILs act as hydrotropes? Relevantly, the solubility of vanillin in aqueous solutions has been shown to increase in the presence of conventional hydrotropes such as nicotinamide, resorcinol, citric acid and sodium salicylate.[52] We know that typical hydrotropes are amphiphilic molecules and that characteristic is essential to the occurrence of the hydrotropic effect. Similarly, ionic liquids also present amphiphilic behaviour, since evidence shows that they interact with solutes differently depending on the environment, as they arrange themselves in the form of a nanostructured fluid with polar and nonpolar domains – it is this structure and amphiphilic behaviour that grants ILs their differentiated solvation ability and allows them to solvate such a wide array of compounds when compared to common solvents.[53] Answering the previous question, it has in fact been proved that ionic liquids may act as hydrotropes. Cláudio *et al.*[3] reported 40-fold increases in gallic acid and vanillin solubility in ILs solutions when compared to pure water. The same study provided support for the more recent dismissal of the MHC, since a sudden spike in solubility was not identified; instead, solubility increased in a more continuous, linear fashion. Rengstl *et al.*[54] showed that choline carboxylates, bio-derived ionic liquids, behave like hydrotropes and dissolve Disperse Red 13, a hydrophobic dye, exponentially with increasing hydrotrope concentration. Sintra *et al.*[4] clearly showed the ability of ILs to act as hydrotropes for ibuprofen, reporting 60- to 120-fold increases in its solubility with concentrations of 1M for $[C_4C_1im][SCN]$ and $[C_4C_1im][N(CN)_2]$, respectively. These authors also compared the hydrotropic activity of $[C_4C_1im]$- and sodium-based cations and noticed activity higher than $[C_4C_1im][TOS]$ for $[C_4C_1im][SCN]$ and $[C_4C_1im][N(CN)_2]$, while the combination of dicyanamide and thiocyanate with the sodium cation presented much inferior activities. These results support the idea that ILs contribute to the hydrotropic effect synergistically with both cation and anion, an important and distinguishing factor from conventional hydrotropes. This effect was confirmed both experimentally and through simulation.

5. Effect of different salts on aqueous solutions of ionic liquids

It is now a known fact that ionic liquids can act as catanionic hydrotropes, providing increased solubility of hydrophobic compounds. They are comprised of an anion and a cation and are good solvents. As such, one can easily understand that there are several chemical interactions at play in the solubilisation of any compound in solutions of ionic liquids. Therefore, an interesting approach that can potentially have influence over the

solubilisation phenomenon is the addition of different salts to the ionic liquid/water/solute system. This salt introduction increases the amount of overall possible interactions between the system components and could therefore lead to beneficial or otherwise elucidative changes in solubility.

The addition of electrolytes to aqueous solutions and subsequent determination of solubility rates for hydrophobic compounds has been subject of some work. Changes in solubility can be observed due to two phenomena: salting-in and salting-out. Generally, the macroscopic influence of electrolytes in a system, as is the case of the solubility of proteins and other molecules, can be arranged according to the Hofmeister series (HS).[55] This series explained, at its establishment, that ions can increase or decrease the water structuring in a solution, and can be ordered according to the relative strength of that effect. Several works have reported the use of ISs in IL solutions, and found consistency with the HS and also with the Gibbs free energy of hydration of the ions.[56–59] However, more recently the HS has been portrayed as not so universal, effectively showing a spectrum between direct, reverse, and altered versions of it.[60]

The presence of inorganic salts in a solution of ILs has been shown to provide a salting-out effect in relation to a certain solute if the solute-salt ion interaction is less favourable than both solute-water and salt ion-water interactions. The addition of sodium sulphate to aqueous media has shown to have a salting-out effect on the solubility of phenolic compounds such as vanillin, the rate of which increased with the increase of salt concentration. This effect is owed to the strong tendency of ionic solutes to tightly bind water in their hydration shells, reducing the amount available to solvate the phenolic compounds and thus reducing their solubility. Temperature also seems to play a role in the solubility rate, as increases in temperature translate in slight increases in solubility.[61] An extreme manifestation of the salting-out effect is the formation of aqueous biphasic systems above a certain salt concentration. In the existence of a stronger solute-salt ion interaction the salting-in of the solute is verified, providing an increase in solubility.[62] Solvent systems consisting of ionic liquids with added lithium salts have been tested for cellulose solubility by Xu *et al.*[63] and have shown to enhance it when compared to solutions of only the ionic liquid. The authors suggest, using ^{13}C Nuclear Magnetic Resonance (NMR) spectrometry, that this augmented solubility arises because of the disruption of an intermolecular hydrogen bond, as the Li^+ ion interacts with the oxygen atom in cellulose involved in this bond. Ionic liquid aggregation in aqueous media is dependent of IL interaction with water.[64] Therefore, addition of electrolytes in the form of inorganic salts can influence this interaction and affect self-aggregation rate. IL self-aggregation seems to be correlated to phase

separation in IL mixtures.[56] It also may be behind the solubilization power of ILs, to a certain extent.[65] Therefore, salting IL solutions may have a direct impact on their ability to solubilize hydrophobic compounds.

There is yet insufficient knowledge in both the hydrotropic properties of ionic liquids, as well as how the salting of hydrotropic solutions of ILs influences the solubility degree of hydrophobic compounds. It is then a researching prompt that could translate in a better comprehension of the hydrotropic mechanism, of IL behaviour in heavily electrostatic charged environments and in the perspectivation of novel applications for ionic liquids as solvent media and hydrotropes.

6. Molecular Dynamics

Molecular dynamics refers to the computer simulation method of analysing atomic and molecular physical movements with the purpose of understanding the properties of the structure of molecular assemblies and the interactions among them. In general, MD simulations act as a complement to conventional experiments, providing insight about specificities that are difficult to experimentally determine.[66] As such, MD simulations are an important complimentary tool to understand the hydrotropic solubilization processes as well as to appreciate the influence of IL aggregation and salt effect on the latter, with many work on both hydrotropy and ILs so far reported.[67–70] The following paragraphs detail the relevant simulation tools for the analysis of the obtained data and how to use them to visualize and gain insight over the phenomenon.

Molecular dynamics simulations take an inputted finite-sized molecular configuration and evolve it through time, in a step-by-step fashion. The limitations on the time and length scales of the runs are majorly defined by the computational power available. Time and space scales within the scope of MD can be seen in Figure 4. Typically, MD runs simulate a system for no more than a few nanoseconds of real time. From this bottleneck, two very important considerations have to be made: a) it is absolutely necessary to convey a statistical analysis to the simulation averages obtained, as to realistically estimate error, and b) prior to the MD run, it is essential to guarantee that the system is in equilibrium, as it is essential to ensure that the own run has made the system reach an equilibrium before the resulting calculations can be considered. Besides the molecular models of the molecules to use in a system one wants to simulate, there is also the need for an appropriate force field, as well as an appropriate software suite. All-atom (AA) or atomistic models are the ones traditionally used in molecular dynamics, as they represent each molecule in a system,

solvents included, with each of their atoms considered explicitly. Evidently, the full description of all atomic coordinates in a system is the most adequate to obtain results of the highest detail and precision possible. However, the more chemical detail one inputs in a model, the higher the computational requirements to run said model, and the higher the restrictions to what time and size scales are viable to simulate (Figure 3). Such limitations led to the development of coarse-grained (CG) models such as the MARTINI[71] model, a simplified version of AA in which several of the atoms in a molecule are grouped together and represented in a simplified, bead-like structure, acting as a single interaction site.

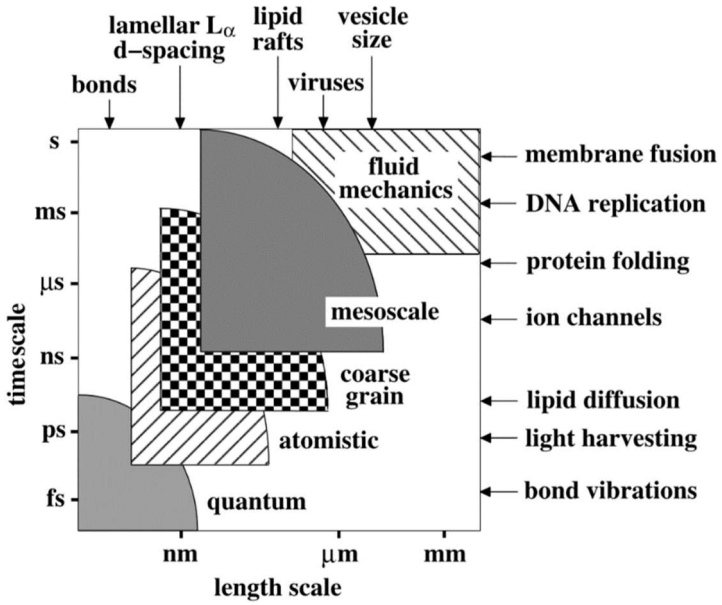

Figure 4. Schematic representation of the time and special scales reachable by molecular dynamics simulation methods, as well as some structure and occurrences related to membrane biophysics (Nielsen *et al.*)[72].

Classical MD simulations ultimately come down to the numerical integration of Newton's equations of motion for the involved interaction centres, or particles. These forces can be expressed as deriving from potential functions, representing the potential energy of the system for a specific spatial arrangement of the particles within. These particles are subject to two major distinct forces: an attractive force at long ranges, mostly the van der Waals force, and a repulsive force at short ranges, originating primarily from overlapping electron orbitals, that is, Pauli repulsion. Widely used to represent these forces in the MD field is the Lennard-Jones (LJ) potential, a mathematical model proposed in 1924:

$$V^{LJ}(r_{ij}) = 4\varepsilon\left[\left(\frac{\sigma_{ij}}{r_{ij}}\right)^{12} - \left(\frac{\sigma_{ij}}{r_{ij}}\right)^{6}\right] \quad (2)$$

where ε represents the strength of the interaction or the depth of the potential well (the minimum of potential energy), σ represents the finite distance at which the inter-particle potential is zero and r represents the distance between particles. There are two parameters present in the LJ potential, also known as the 6-12 potential, r^6 and r^{12}. The first is related with attraction between dipoles, while the second one is the repulsion-related term, acting between electron clouds. Mostly, in a force field the forces fall under two categories: non-bonded and bonded interactions. Non-bonded interactions are described by the LJ potential, which in practice defines the interaction strength through the well depth ε_{ij}, dependent of the interacting particles commonly referred as *i* and *j* and defines the effective size of particles through the σ parameter. Beyond the LJ interaction, the interaction between charged groups is described by a Coulombic energy function:

$$V_C(r_{ij}) = f\frac{q_i q_j}{\varepsilon_r r_{ij}} \quad (3)$$

that considers the electrostatic interactions between charged particles (i and j) separated by a distance r.

Bonded interactions are instead described by bond-stretching, angle-bending, improper and proper dihedrals are considered for bonded interactions, and LJ interactions between nearest particles are inhibited. Both bond-stretching and angle-bending are described through harmonic functions, the former being the harmonic bond length fluctuation between two covalently linked atoms, and the latter the angle variation of three covalently linked atoms. Dihedrals are defined as the angles between the two planes that encompass three atoms each, with two atoms in common.

In terms of the simulation parameters, their variety is quite large, but key ones include the timestep, neighbour list update frequency and cut-off radii for the nonbonded potentials, the distance between particles at which the LJ potential is excluded. Neighbour lists strongly influence the energy conservation of the system, an important factor to avoid accentuated fluctuations in energy. Evidently, the more frequent the list update, the higher the computational requirements.[71]

GROMACS (GROningen MAchine for Chemical Simulations)[73] is a molecular dynamics software package currently available to simulate a wide range of systems,

biological or not. In MD, a software such as GROMACS computes a range of system parameters, most importantly particle trajectory, velocity and coordinates, during a simulation on which a chosen FF is applied to every molecule/atom according to the previous equations of motion described. In a complete simulation, several steps are prerequired to the actual final run. The first of them is the energy minimization (EM), when the system reallocates the molecules within as to avoid clashes and promote an energy-minimized system. Following, an NVT or canonical and an NPT or isothermal-isobarical equilibration ensembles are performed, respectively, as the former sets the desired temperature and the latter the desired pressure for a system. NVT stands for conservation of amount of substance (N), volume (V), and temperature (T), while NPT stands for conservation of amount of substance, pressure (P) and temperature. Equilibrium must be verified at the end of each step by analysing the thermodynamic properties of the system and ensuring they reached a plateau along the running time. Only then the final stage, the production run, is performed.

7. Objectives

This work is then aimed at verifying and rationalizing the effects of chloride inorganic salts on the hydrotropic solubilization effect of $[C_4mim]Cl$, an imidazolium-based IL, towards vanillin. This is to better the understanding of how ILs as hydrotropes behave in an environment with many electrolytes, probing their structuring and the synergistic effect between the IL anion and cation. The elucidation of the mechanism of hydrotropy is as well intended through the study of hydrotrope-water, hydrotrope-solute, and hydrotrope-hydrotrope interactions, as well as through the characterization of IL-vanillin aggregates, both experimentally and through MD simulations.

Chapter II
Methodology

1. Experimental hydrotropic solubility tests

Several different approaches were used to assess the influence of the presence of different salts on the hydrotropic solubility of vanillin and the structuring of the IL and solute in [C_4mim]Cl aqueous solutions. The selected salts possess cations varying in charge, ranging from mono- to trivalent, as to provide further insight over the effect cation charge may present. The analytical methods chosen consist of the determination of the solubility curves of vanillin in aqueous IL solutions with varying concentrations of salt by ultraviolet (UV) spectrophotometry, and the analysis of IL and vanillin in solution by nuclear magnetic resonance (NMR) and dynamic light scattering (DLS).

a. Materials

1-butyl-3-methylimidazolium ([C_4mim]Cl) IL was from IoLiTec Ionic Liquids Technologies GmbH, with a stated purity of at least 99,0 wt. %. Regarding the salts, sodium chloride, NaCl, was supplied by José Manuel Gomes dos Santos, with a stated purity of at least 99,8 wt. %; potassium chloride, KCl, was purchased from Chem-Lab NV, with a stated purity of at least 99,5 wt. %; lithium chloride, LiCl, was from Merck KGaA; magnesium chloride, $MgCl_2$, anhydrous, was provided by Sigma-Aldrich; calcium chloride, $CaCl_2$, anhydrous, was from Panreac, with a stated purity of at least 95,0 wt. %; yttrium chloride was purchased from Aldrich Chemical Company, with a stated purity of at least 99,9 wt. %. Vanillin was from Sigma-Aldrich, with a stated purity of at least 99,0 wt. %. Deuterium oxide used in NMR analyses was acquired from Aldrich with at least 99,96 wt. % D atoms. The 3-(trimethylsilyl)propionic-2,2,3,3-d4 acid sodium salt (TSP) was purchased from Aldrich Chemical Company with at least 98 mol % D atoms. The chemical structures of the utilized IL and vanillin are represented in Figure 5.

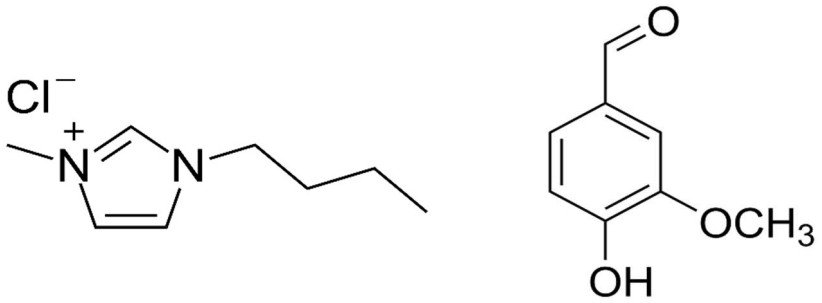

Figure 5. Chemical structures of 1-butyl-3-methylimidazolium ([C_4mim]Cl, left) and vanillin (protonated, right).

b. Hydrotropic solubility curves

Vanillin solubility tests were performed on 0,5 M and 1,5M [C_4mim]Cl solutions. For each of these concentrations, salted IL solutions were made in which the salt concentration ranged from no salt up to near the solubility limit in water for each specific salt, as described in Table SI:1. Each of these solutions was prepared in a glass vial for a volume of 2,5 mL, from which three 0,7 mL aliquots were transferred to 1,5 mL *Eppendorf's*, as to perform this test in triplicate. Small amounts of vanillin were initially added to each *Eppendorf*, followed by agitation, until no further dissolution was observed. *Eppendorf's* were then kept at 303,15 K and constant 1050 rpm agitation in an Eppendorf Thermomixer. Vanillin was added whenever necessary as to keep all solutions saturated over time. Accumulation of a clear gel-like substance was often observed on the upper wall section of the *Eppendorf*'s, out of the bulk solution. This accumulated solid was removed prior to subsequent addition of more vanillin, as it was verified to be of difficult solubilization. Reaction was stopped after 48h of no evident further vanillin dissolution, in the presence of visible precipitate. Samples were then diluted, prior to analysis, as to obtain UV readings in the range of 0,2 to 1,0 absorbance. All 1,5 M IL solutions were at most diluted with distilled water in two dilutions, of 0,1:200 and 1:10 ratios; 0,5M IL solutions were diluted at most in a 0,1:200 ratio only. After dilution, vanillin concentration was determined by UV spectrophotometry with a SHIMADZU UV-1700 Pharma-Spec spectrometer at 280 nm, through the application of the Beer-Lambert law:

$$A = \varepsilon c l \tag{4}$$

where A stands for the absorbance of light through a substance, ε the molar absorption coefficient, c the molar concentration and l the optical path length. The absorbance of a sample is given by the inverse logarithm of the transmittance:

$$A = -\log T \tag{5}$$

where T represents the transmittance of a substance, the ratio of transmitted light intensity over total incident light intensity. The globality of the sample preparation method is schematized in Figure 6. 10mm path length quartz cuvettes were used. The calibration curve used for this spectrophotometric approach originated from the previous determination

of absorbance of aqueous solutions of known concentrations of [C_4mim]Cl.[3] The control samples utilized were of equal composition, but without vanillin.

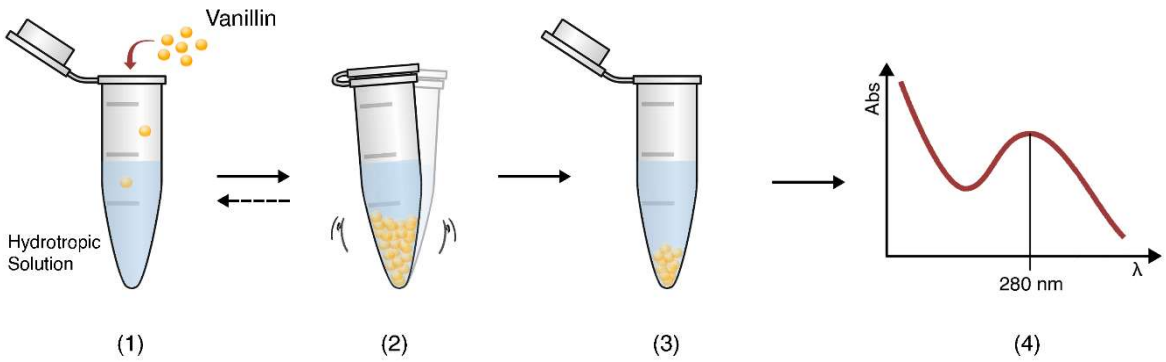

Figure 6. Schematic of the experimental workflow of the vanillin solubility tests. Addition of vanillin to an ionic liquid (hydrotropic) solution (1); agitation to promote vanillin dissolution, through several days (2). When no vanillin can be observed, step (1) is performed again, followed by (2), as many times as needed. When the solid vanillin precipitate amount is constant for 48h (3), supernatant absorbance is read at 280 nm (4).

c. Nuclear Magnetic Resonance

^{1}H and ^{13}C NMR analyses were performed to provide insight on the alterations of the chemical environment of the IL and vanillin promoted by the addition of salt, and on the interactions between the IL and vanillin, that is, between the hydrotrope and the solute. Samples were prepared in a similar fashion as the ones previously described for the hydrotropy tests. Samples were analysed in a glass NMR tube with an added sealed capillary with D_2O, with TSP as an internal reference, in a coaxial insert. Measurements were performed on a Bruker Avance 300 NMR spectrometer operating at 300 MHz, at 298 K.

d. Dynamic Light Scattering

Assessment of IL-vanillin aggregates was made by DLS, using the Zetasizer Nano-ZS photometer from Malvern Instruments. Prior to the analyses, all samples destined to DLS were treated as to avoid air bubbles and to promote sedimentation of eventual impurities that would create artifacts in the readings. After formulation, sample solutions

went through sonication in an ultrasonic bath for 5 minutes, to promote particle dispersion and degassing, and were then left to rest overnight. Immediately before analysis samples were aspirated to a syringe, excluding the bottommost portion in the container, and were finally filtered through a nylon 0,45 µm syringe filter into a 10 mm path length quartz cuvette. Samples were analysed at 193,15 K, with an equilibration time of 120 seconds. Irradiation was performed at a wavelength of 565 nm by a Helium-Neon laser and scattered light detected at a backscattering angle of 173º. Viscosity for both 0,5 M and 1,5 M aqueous IL solutions was determined beforehand to be 1,315 and 1,730 mPa.s. Automatic mode was used for both measurements and data processing. Analyses were performed in triplicate and extracted results are averages.

2. Molecular dynamics

All MD simulations were performed with the GROMACS package, version 2019.4.[74] The main simulations consisted of five all-atomistic systems describing different binary, ternary and quaternary conditions containing the IL, vanillin, water and/or NaCl. Table 1 summarizes common file formats widely used throughout the MD workflow.

Table 1. Common file formats for GROMACS and their function.

File format	Function
.mdp	Contains run parameters (thermostat, barostat, simulation time, timestep, etc.).
.gro	GROMACS format, contains molecular structure and coordinates information.
.top	Topology file, contains system composition information and individual .itp files.
.itp	Includes topology for a specific system component.
.ndx	Index file, contains specific groupings of atoms or residues available for selection.

.tpr	Contains system topology, parameters, coordinates and velocities.
.trr	Contains trajectories obtained from simulation runs.
.edr	Includes energies, temperature, pressure, box size, density, and virials.

The GROMACS software package provides a versatile molecular dynamics program that can be run on single processors. GROMACS allows to define a systems' size, shape, number, and type of molecules within and both initial coordinates and velocities of said molecules. The typical workflow in a simulation run consists of the building the simulation box, the insertion of molecules, minimization of energy, several equilibration steps and finally the production MD. The energy minimization (EM) step ensures the absence of steric clashes and provides the initial system geometry. After EM come the several steps of the system equilibration. This procedure is divided into a constant Number of particles, Volume, and Temperature (NVT) ensemble, followed by a constant Number of particles, Pressure, and Temperature (NPT) one. These steps ensure proper optimization of the solvent against the solute, as well as the pretended system temperature, and finally, through applied pressure, the proper density. Analysing the progression, once we find them stable over time, we have an equilibrated system. As such, we are now ready to run the actual simulation in experimental conditions. The next run will release the position restraints and will simulate the system properly for data collection. Simulation outputs are analysed using GROMACS' built-in tools as well as other programs such as VMD (Visual Molecular Dynamics).[75] This way, through MD simulation we can build an initial idea of what are the molecular dynamics of an organic solvent in an ionic liquid and salt aqueous system. Such data must be, indispensably and as stated, statistically valid and compared to actual experimental data.

a. Simulation details

All simulation boxes were created with the *gmx insert-molecules* tool, allowing the placement of all the desired molecules within them with random initial positions. Following this step, and prior to the MD production runs, all systems went through an equilibration process consisting of three steps: a) energy minimization, conducted using the steepest descent algorithm with a tolerance of 10 kJ/mol/nm, meaning convergence is achieved when the maximum force falls below this value; b) NVT equilibration, as to achieve a plateau

in system temperature. Temperature was fixed at 298K through coupling with a modified Berendsen thermostat.[76] Velocities were randomly generated according to a Maxwell distribution at 298K. Long range dispersion corrections for energy were applied. c) NPT equilibration, an ensemble with the purpose of stabilizing pressure, and as such, the density of a system. Pressure was fixed at 1 bar through isotropic coupling with a Parrinello-Rahman barostat,[77] and temperature as described for NVT equilibration. for For the ionic liquid cation the force field parameters used were developed by Canongia Lopes *et. al*[78], based on the OPLS-AA/AMBER framework.[78,79] The OPLS-AA FF was used for sodium and vanillin, and for water the SPC/E model.[80]

For both equilibration steps and the production run, the used algorithm was the leap-frog integrator.[81] Neighbouring search type was grid search and the neighbour list set to update every 20 steps. The Verlet cut-off scheme was used, with a cut-off radius of 1.2 nm. LJ and Coulombic interactions had equally a short-range cut-off radius of 1.2 nm, with Particle-Mesh Ewald (PME)[81] electrostatics function applied to long-range electrostatic interactions in NPT equilibration and MD production. For LJ interactions, potential-shift with the Verlet cutoff-scheme was selected for NPT equilibration and MD production. For Coulombic interactions in the NVT equilibration step the potential-shift with the Verlet cutoff-scheme was also used. Periodic boundary conditions (PBC) were accounted for in all directions. The LINear Constraint Solver (LINCS) algorithm[81] was used to constrain all bonds, resetting them to their correct lengths after an unconstrained update and providing a warning for any bond rotations greater than the set amount of 90º. In the MD production runs, temperature and pressure coupling were performed as described above for the equilibration steps. These runs were performed over 1.0 ms of simulation time. A cubic box shape was used for all simulations.

All MD simulations and, when pertinent, prior equilibration steps where evaluated as to guarantee a state of equilibrium through visual analysis of molecule positions and trajectories, to ensure the absence of any unwanted aggregations, phase transitions or otherwise unevennesses, and through the use of the *gmx energy* tool of GROMACS to analyse bulk system properties, namely temperature, pressure and potential, that one would expect to have reached a plateau or to be stable throughout the run if equilibrium is in fact reached.

Table 2 details the composition and properties of the five systems simulated under the scope of this work and further discussed below.

b. Analysis

Equilibration was verified by the analysis of total system temperature, pressure, and potential, ensuring all of these reached a plateau during run time. Post-processing and analysis were mainly performed over two dimensions: visual and statistical. Visual analysis was performed resorting to the molecular visualization software package Visual Molecular Dynamics (VMD)[75] which allowed the direct observation of all the molecules' coordinates and distribution throughout the duration of the simulations. The presented simulation snapshots throughout this work were taken use the VDW (Van der Waals) visualization mode, representing approximately the total volume of each atoms, and the "licorice" mode, presenting bonds as cylinders and atoms as spheres of equal radius, providing a clearer and more eye-pleasing picture. Statistical analysis consisted of using the GROMACS tools *gmx sasa* to obtain the solvent-accessible surface area (SASA) profiles, *gmx density* to obtain partial density profiles, and *gmx rdf* to obtain radial distribution functions (RDFs), as well as the TRAVIS – Trajectory Analyzer and Visualizer[82] software package to obtain spatial distribution functions (SDFs). The GROMACS tool *gmx make_ndx* was previously used to index specific atoms or groups of atoms to be selected or used as a reference for the described analyses.

The *gmx sasa*[83] tool was used to obtain the SASA profiles for the IL cation. This analysis uses the double cubic lattice method algorithm, applying two cubic lattices in space, one for grouping neighbouring atomic centres, and the other for grouping neighbouring surface dots of an atom. *gmx sasa* utilizes the van der Waals (vdW) radii of the molecules/atoms within a system to calculate the totality of contact points between the reference molecule or atom(s) and the solvent. Hence, it returns the totality of the area of the reference available to contact with the solvent, thus solvent-accessible surface area.

The *gmx density* tool is used to calculate partial densities across the simulation box. This tool divides the box into slices and obtains the density of a given chosen atom or set of atoms, starting from one end of a cartesian coordinate and ending on the other or starting from the centre of the box and out. The plotting of these profiles returns peaks and depressions directly showcasing aggregation or absence of the given reference on a given box coordinate.

The *gmx rdf* tool was used to obtain the RDF profiles. The radial distribution functions are a description of the probability of finding a given particle at a distance r from another given reference particle. The RDF between two particle types A and B is given by:

$$g_{AB}(r) = \frac{[\rho_B(r)]}{[\rho_B]_{local}} \quad (6)$$

Where $[\rho_B(r)]$ is the B particle type density at a distance r around particles of A type, and $[\rho_B]_{local}$ the B particle type density averaged over all spheres around particles of type A with a maximum defined radius, in this case half the box length.[74] The vertical axis of an RDF plot therefore provides a measure of the density of A in comparison to the bulk density of the solution ($g(r) = 1$), against a scale of distance from the reference, r, in the horizontal axis. Together with the RDF plots, the coordination number (CN) or cumulative number is also usually plotted, showing the average number of particles within a distance r of the reference. Figure 7 provides a quick visual reference to these concepts using vanillin and water.

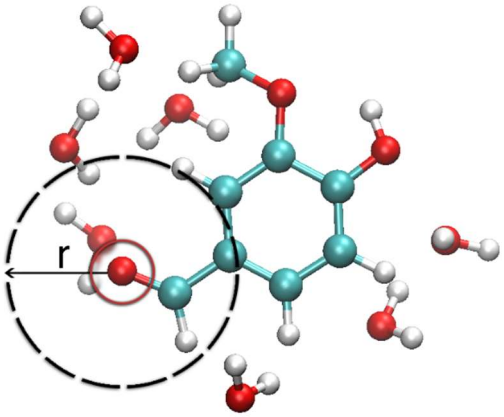

Figure 7. Example of a determination of an RDF using vanillin and water. In this case, the reference atom is the oxygen atom of the aldehyde functional group of vanillin and the selection is water. *r* denotes the chosen radius at which the probability of finding water will be calculated and expressed as *g(r)*.

The SDFs herein presented and discussed, obtained with the TRAVIS software, are a representation of the three-dimensional density distribution of a given selected molecule or atom(s) around a given reference molecule or atom(s). In simple terms, while the RDF provides a detailed plotting of the molecular environment around the reference, the SDF provides a more visual 3D plotting of it, allowing a more free and comfortable exploration and representation. For each SDF representation, an isovalue must be defined. The isovalue defines the extent of the represented surfaces and has a range dependent on the quantity of molecules or atoms contributing towards the density distribution. An isovalue of 0 will consider densities across the whole box, and as this number is increased this

consideration will be progressively restricted to the densities nearing the reference molecule. The results presented in this work will sometimes, for the same condition, present several different isovalues, as very restricted ones often proved insightful. Chosen represented isovalues are among 2/3, 4/5 and 9/10 of the maximum isovalues.

Table 2. Detailed composition and properties of the five all-atomistic MD systems. These will oftentimes be referred by their designated letter (a) through (e).

System	n_{IL}	[IL]		$n_{vanillin}$	[Vanillin]		n_{NaCl}	[NaCl]		n_{H_2O}	T (K)	Sim. t (µs)	Box size (nm^3)
		mol.kg^{-1}	wt. %		mol.kg^{-1}	wt. %		mol.kg^{-1}	wt. %				
[C_4mim]Cl in water (a)	100	0,51	8,85	-	-	-	-	-	-	10000	298,15	0,06	6,89[3]
Vanillin in water below solubility limit (b)	-	-	-	10	0,055	0,84	-	-	-	10000	298,15	0,06	6,71[3]
Vanillin in aqueous [C_4mim]Cl below solubility limit (c)	100	0,50	8,78	10	0,050	0,77	-	-	-	10000	298,15	0,1	6,90[3]
Vanillin in aqueous [C_4mim]Cl above solubility limit (d)	100	0,50	8,71	20	0,099	1,52	-	-	-	10000	298,15	0,06	6,90[3]
Vanillin in aqueous [C_4mim]Cl above saturation with NaCl (e)	100	0,48	8,46	20	0,097	1,47	100	0,48	2,83	10000	298,15	0,06	6,90[3]

Chapter III
Results and discussion

1. Hydrotropic solubility tests

Aiming to assess the influence of the presence of salts on the hydrotropic solubilization capacity of [C_4mim]Cl, an array of solubility tests that allowed the extrapolation of solubility curves was performed. All the tested salts belong to the chloride family of salts and therefore salting-out was to be expected, reducing the solubilization capacity of the IL solution to a certain extent. By using all salts with a common anion, the cation effect could be observed with increased exclusivity. Beforehand knowledge of the hydrotropic behaviour of [C_4mim]Cl in the tested conditions guaranteed that the limiting factor in the maximum experimented concentration of each salt was its own solubility in aqueous media, and that no phase separation should be observed, allowing saturation of all tested solutions with vanillin to occur without impediment. [C_4mim]Cl was chosen also because it is a much-studied IL and one of the most reported for a wide variety of applications, besides being a known hydrotrope for vanillin.[49] Cl^- as the IL counter-anion was chosen as to match the anion of the studied salts. Two different concentrations of IL were tested: a lower one at 0,5 M (9 wt. %) in Figure 8 and a higher one at 1,5 M (26 wt. %) in Figure 9. Table SI:1 and Table SI: 2 compilate all obtained data points. The experimented salt concentrations were selected based upon the maximum concentration possible to achieve for each salt.

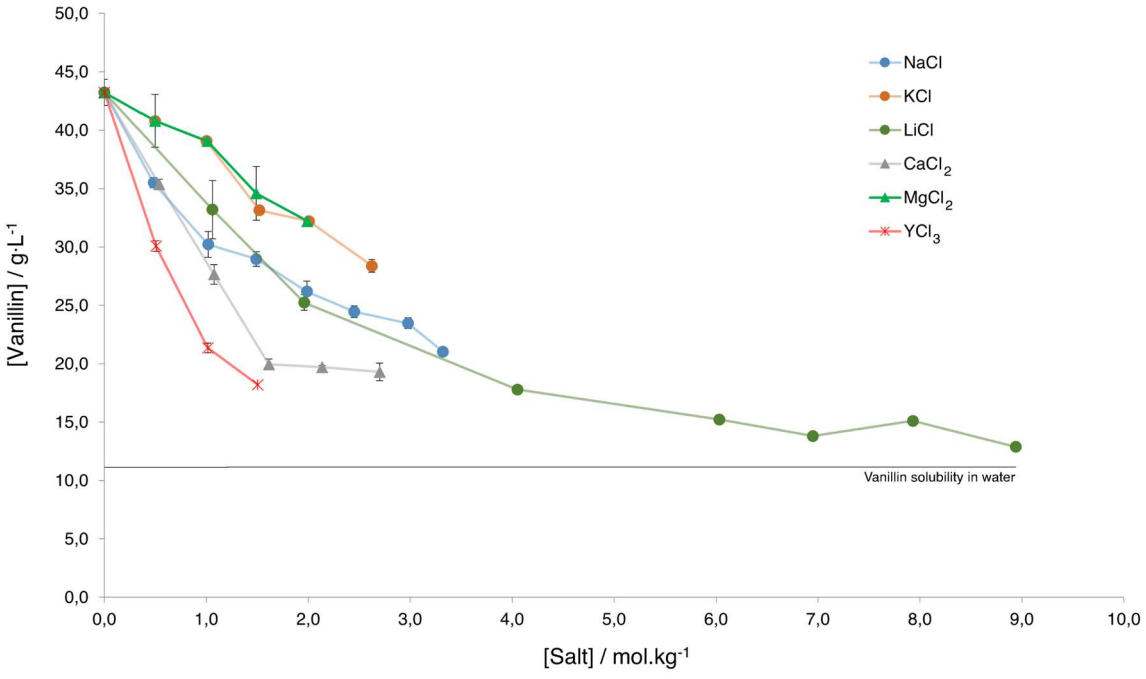

Figure 8. Solubility curves for vanillin in a 0,5 M [C_4mim]Cl aqueous solution and in the presence of different salts. Error bars represent the standard deviation from three independent measures. Vanillin solubility in water as determined by Cláudio *et al*.[3]

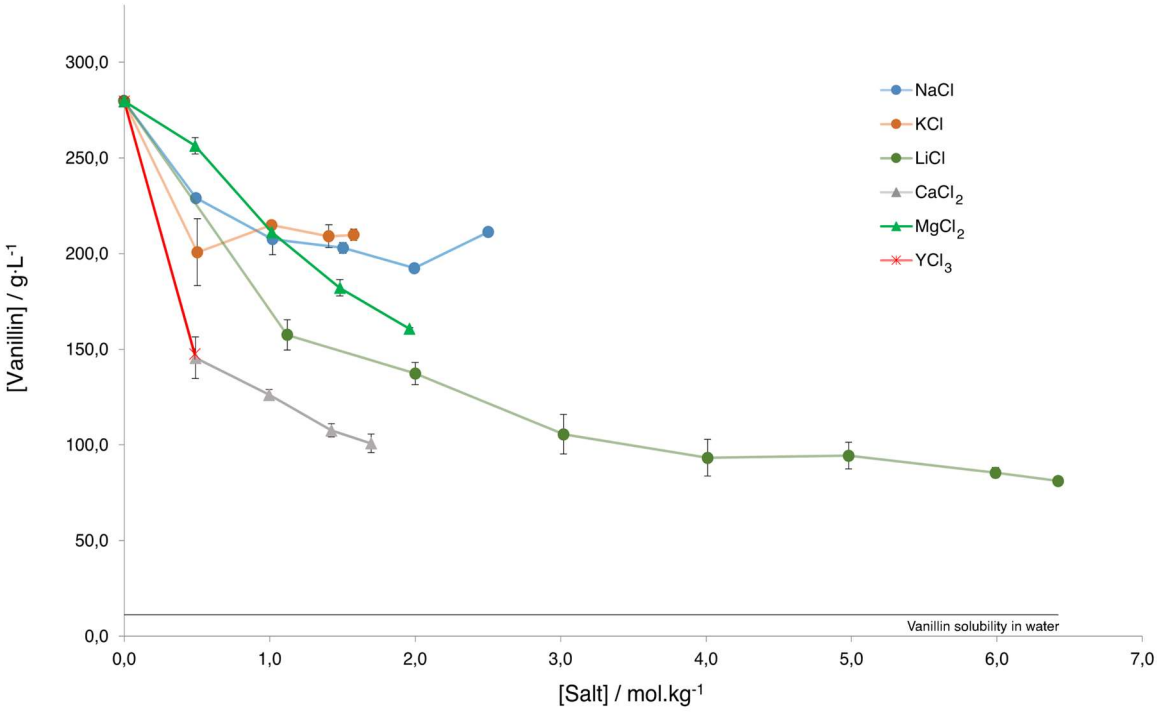

Figure 9. Solubility curves for vanillin in a 1,5 M [C_4mim]Cl aqueous solution and in the presence of different salts. Error bars represent the standard deviation from three independent measures. Vanillin solubility in water as determined by Cláudio *et al*.[3]

The lower 0,5 M IL concentration proved to be an advantage in itself, as it allowed for a more expansive range in terms of maximum salt concentrations and data points fitted into the solubility curves when compared to 1,5 M. NaCl and LiCl showed a significantly more detrimental effect on vanillin solubility than their monovalent counterpart, KCl. In turn, $MgCl_2$ showed a much lower effect than $CaCl_2$. YCl_3, despite only providing a relatively low maximum concentration, showed the most detrimental effect on vanillin solubility, with $CaCl_2$ with the second strongest effect. LiCl, due to its high solubility in aqueous media and low molar mass, allowed the probing of much higher salt concentrations, showing the reaching of a plateau on solubility decrease, without ever falling below the solubility of vanillin in water. Overall, all salting of IL solutions diminished their solubilization capacity to different extents. An eventual cation valence correlation with the strength of the detrimental effect on solubility is not directly evident. Nevertheless, the fact that YCl_3 shows a stronger effect than $CaCl_2$ which in turn shows a stronger effect than NaCl, LiCl and KCl poses such a suggestion. Regarding the higher 1,5 M concentration of IL, the general trend can still be verified, especially at lower salt concentrations. Above 1,0 M KCl is still the least detrimental

for vanillin solubility and LiCl the most, for monovalent salts. $MgCl_2$ once again shows a much less detrimental effect than $CaCl_2$, while YCl_3 is still very detrimental despite the low maximum salt concentration possible to reach, at 0,5 M. These results present a clear overview of the salting-out effect chloride salts have on a hydrophobic solute in an aqueous $[C_4mim]Cl$ solution. In general, this effect increases, regardless of salt, with its concentration, except for sodium and potassium chloride added to 1,5 M IL, seemingly stabilising, and even increasing solubility above 1,0 M of salt concentration.

To rationalize these results, the thermodynamic hydrotropy model proposed by Shimizu[33,84] will be considered, where hydrotropic solubilization is mainly driven by solute-hydrotrope interactions and water activity depression, the latter having as major contributions hydrotrope-hydrotrope interactions but also other pair-wise interactions such as solute-solute, water-solute and water-hydrotrope interactions. As so, a hydrotrope is a compound for which its interaction with a given solute is strong and greatly overcomes the hydrotrope-hydrotrope one, and thus its self-aggregation.[34,84] In the present work a third component is introduced in a hydrotrope/solute system. The addition of inorganic salts will have two main effects: (a) due to their strong binding of water molecules, these salts will reduce solute-water and hydrotrope-water interactions, effectively dehydrating them, and (b) due to their salting-out nature, originating from their greater charge density in comparison to the IL cation, these salts will promote hydrotrope-hydrotrope interactions. Simultaneously, these two effects translate into increased hydrotrope aggregation and decreased hydrotrope-solute interactions, therefore diminishing the strength of the hydrotropic effect, and with it, vanillin solubility. As so, for any of the considered salts, vanillin solubility should be expected to be inferior in the salted solutions when compared to the non-salted ones, that is:

$$\frac{[S]}{[S_{nosalt}]} < 1 \tag{7}$$

where S is the solubility of vanillin in each system with added salt, and S_{nosalt} the solubility of vanillin in the system without added salt. The magnitude of this ratio should be dictated by the salting-out potential of each of the added salts, which in turn is based on their Gibbs free energy of hydration, a measure of how strong an ion binds water molecules, and dependent on its radius and shell of hydration. Table 3. provides hydration-related thermodynamical parameters of the relevant ions. When following the energy of hydration parameter, a sequence such as $Y^{3+} > Mg^{2+} > Ca^{2+} > Li^{+} > Na^{+} > K^{+}$ would be expected in

terms of vanillin solubility, ranging from the salt cation most detrimental to it to the one the least detrimental. However, at a salt concentration of 1,0 M, the apparent trend is Y^{3+} > Ca^{2+} > Li^{+} and Na^{+} > K^{+} and Mg^{2+} for 0,5 M IL, and (Y^{3+}) > Ca^{2+} > Li^{+} > Na^{+}, K^{+}, and Mg^{2+} for 1,5 M IL, with magnesium chloride apparently the most uncorrelated salt. Worthy of mentioning is also how the Hofmeister series, starting from the most salting-out cation, runs in the following fashion: Ca^{2+} > Mg^{2+} > Li^{+} > Na^{+} > K^{+}.

Table 3. Thermodynamic parameters of the tested salt cations at 298,15 K. *r* denotes the ions' radius, *Δr* the radius of its hydration shell, *n* the number of water molecules within the hydration shell, $\Delta_{hyd} S^{o}$ the absolute value of the conventional standard molar entropy of hydration, and $\Delta_{hyd} G^{*}$ the experimental value of the molar Gibbs free energy of hydration, according to Marcus.[85,86]

Ion	r (nm)	Δr (nm)	n	$\Delta_{hyd} S^{o}$ (J.K^{-1}.mol^{-1})	$\Delta_{hyd} G^{*}$ (kJ.mol^{-1})
Li^{+}	0,069	0,172	5,2	-142	-475
Na^{+}	0,102	0,116	3,5	-111	-365
K^{+}	0,138	0,074	2,6	-74	-295
Mg^{2+}	0,072	0,227	10,0	-331	-1830
Ca^{2+}	0,100	0,171	7,2	-252	-1505
Y^{3+}	0,090	0,228	12,0	-483	-3450

Attempts to establish a correlation between the ratio of solubilities and the free Gibbs energy of hydration of salt cations, as seen in Figures 10 and 11, did not produce a strong trend. Note that for the first figure salt concentration is higher than IL concentration, while the opposite is true for the second figure. As so, despite experimental verification of the expected salting-out effect of the added salts towards vanillin, this effect can only be generally attributed but not completely explained by the referred energy differences, showcasing a more nuanced behaviour. Lommelen *et al.*[87] recently produced a similar conclusion when testing the effect of chloride salts on solvent extraction of metal ions, verifying that ion hydration and ion-solvent interactions are the underlying factors explaining

the different effect different salt cations have, while also taking into account the possible deviation-causing cation-anion association of some salts.

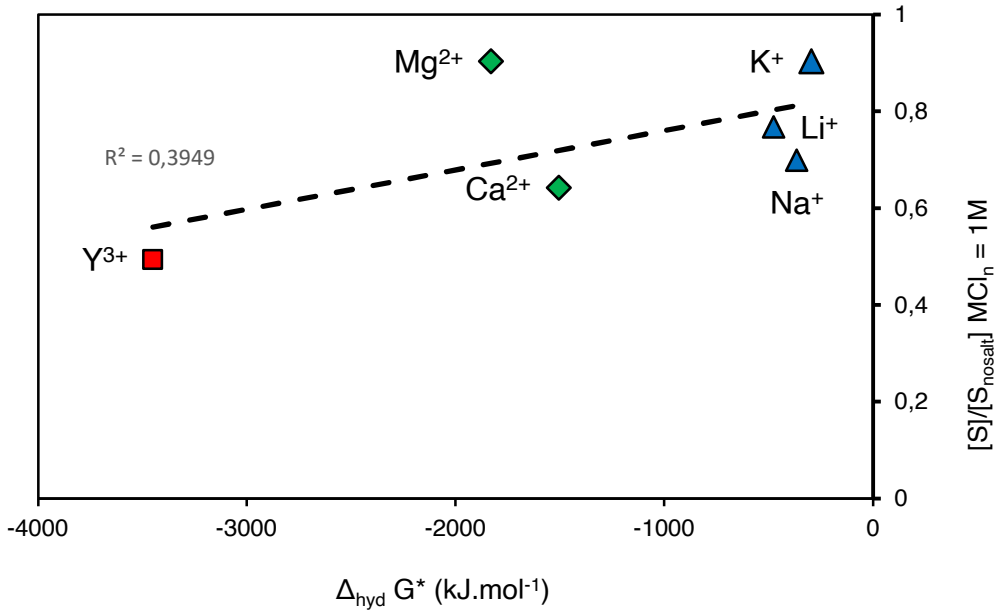

Figure 10. Evaluation of a correlation between the Gibbs free energy of hydration of the studied salt cations and their respective disruption of the hydrotropic effect, expressed through the ratio between vanillin solubility in the presence of salt, *S*, and in its absence, S_{nosalt}. Referent to the series in 0,5 M IL.

Considering the studied salts, magnesium chloride presents itself as the major outlier, and invokes further consideration over its action towards vanillin solubility. A possible explanation for its seemingly odd behaviour may lie in the fact that the tendency of divalent metal cations to form ion pairs is considerably superior to the one of monovalent ones, with the stability of $[Mg(Cl)]^+$ and $[Ca(Cl)]^+$ complexes being reported six times higher than that of [Na(Cl)] and [K(Cl)].[88] Noting how in the absence of salt the ionic strength of the aqueous phase is *I*=0,5 and *I*=1,5 for the 0,5 M and 1,5 M conditions respectively, with the addition of salt only further increasing it, the formation of these complexes is greatly promoted. Considering that the probability of occurrence and stability of $[Mg(Cl)]^+$ are high and that these ion pairs have a lower charge density when compared to the freely solvated ions and as so effectively reduce the hydration ability of the salt solution, one could hint at how this translates into a less detrimental effect over vanillin solubility for magnesium and potassium. Note that the molecular structuring of $[Mg(Cl)]^+$ is very unlikely a contact ion pair but rather a solvent-separated one, namely double-solvent-separated or solvent-shared ion pairs.[89]

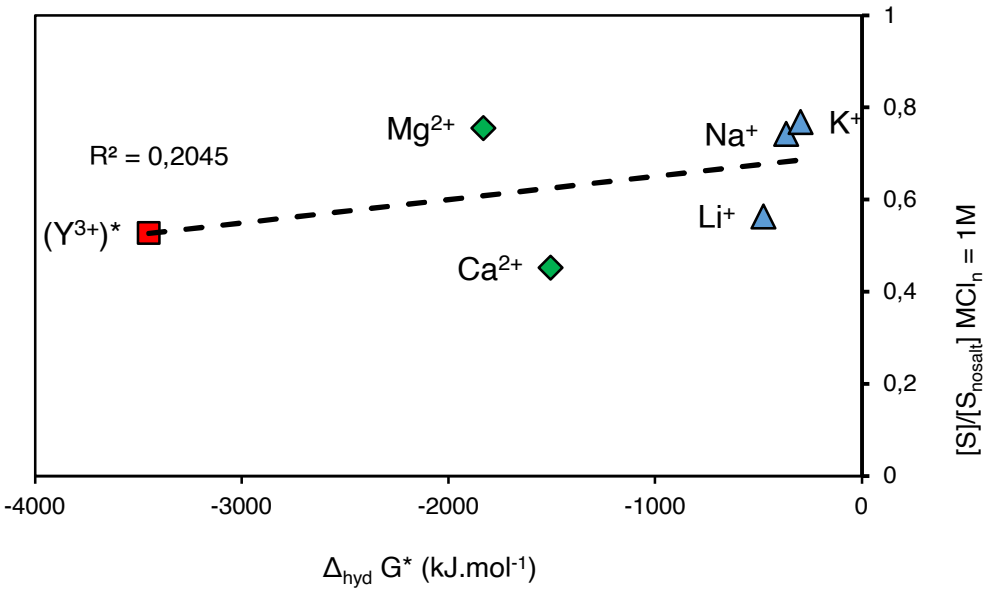

Figure 11. Evaluation of a correlation between the Gibbs free energy of hydration of the studied salt cations and their respective disruption of the hydrotropic effect, expressed through the ratio between vanillin solubility in the presence of salt, *S*, and in its absence, S_{nosalt}. Referent to the series in 1,5 M IL.
(*)YCl^3 concentration in this point is 0,5 M, the maximum successfully tested.

Moreover, magnesium and calcium dications likely have two different mechanisms for anion and water exchange: a dissociative mechanism for Mg^{2+} and an associative mechanism for Ca^{2+}, while the former shows a much greater rate of dissociation with water than the latter, boasting additional relevance for biological systems, constituting another clue for interpreting the present experimental results[90,91] - as the magnesium cation has a more fixed hydration number, meaning that water molecules remain for longer when compared to calcium, the effective radius of the Mg^{2+} cation becomes the ionic plus the hydration radii, resulting in an bigger overall effective volume, which in turn results in a smaller charge density, reason for its weaker salting-out effect. Beyond this possible reasoning for the elevated vanillin concentration achieved with the addition of $MgCl^2$, an interesting additional justification for the discrepancy verified among alkali metal cations may lie in the radius of influence of the ion over water molecules, as both Na^+ and K^+ have very weak influence over water molecules beyond their first hydration sphere,[92] while Li^+ has been reported to possess a second hydration sphere,[93] furthering its influence over water, and hinting at the verified higher detrimental effect over vanillin solubility. However, Mg^{2+} also possesses a second hydration sphere, while being less detrimental towards vanillin solubility than Ca^{2+}, making such rationalization rather difficult. In addition, the strong effect bolstered by YCl^{3+}

may also be potentiated by the fact that yttrium, as all rare-earth elements, presents limited complexation with chloride, such that $[Y(Cl_2)]^+$ or $[Y(Cl_3)]$ complexes are unlikely to be created.[94]

2. Determination of hydrotrope-solute interactions

Towards a further understanding of the intermolecular interactions at play in the hydrotropic solubilization of vanillin, NMR and DLS analyses were performed on several combinations of IL/salt/vanillin solutions. NMR analyses were performed with deuterium oxide and with TSP as an internal reference. The hydrotropic solubility tests presented prior showed the extent to which each salt promotes the salting-out of vanillin, the tested hydrophobic solute. The aim of the present NMR analyses will be to take a closer look at which interactions effectively are at play, namely which moieties of the hydrotrope and solute interact and how they interact, towards a rationalization of the strength of the detrimental effect the added salts have on vanillin solubility. The following four **a)** to **d)** sections are organized in a sequence that runs from the simplest systems to the most complex ones: it shows firstly how the hydrotrope in question interacts with itself, that is, the extent of hydrotrope-hydrotrope interactions; following next, the interactions of the hydrotrope with the solute in question, vanillin, that is, hydrotrope-solute interactions; afterwards, the influence of salting is assessed on hydrotropic solutions, allowing hydrotrope-hydrotrope interactions to be probed in the presence of salt; and finally, the last sequence gives insight on how hydrotrope-solute interactions are affected by salt doping.

a) Ionic liquid aqueous solutions

The initial analysis was performed on several concentrations of IL in water, without solute nor salt, as to evaluate potential interactions between the IL cations: in other words, hydrotrope-hydrotrope interactions. Figure 12 depicts the chemical shift observed in 1,5 M and 2,25 M IL solutions when compared to the lowest tested concentration of 0,5 M. An immediate correlation between the concentration of the IL solution and the increased deshielding of all hydrogen atoms in the IL cation can be established, as well as it can be noted that this deshielding is more pronounced on the hydrogens of the imidazolium ring than in the hydrocarbon tail. As deshielding is caused by the presence of electron-withdrawing groups, it can easily be seen that increased IL concentration will promote cation-cation and anion-cation interactions. As the concentration of IL increases and the

water content decreases the pure form of the IL is approached, and successive alterations occur to the solutions' molecular structure and properties.[95,96] In fact, depending of the IL concentration in an aqueous solution, different rates of dissociation and ion hydration are verified, as the water content determines if they are more or less dissociated or hydrated – this has a significant effect on the properties of the hydrotropic solution and thus very likely on the hydrotropic effect;[97] hence the fairly low 0,5 M and 1,5 M IL concentrations tested throughout this work, where hydrotrope-solute interactions are better evaluated. In terms of molecular structuring of an aqueous [C_4mim]Cl solution, the methylimidazolium ring is the favourite moiety for hydrogen bonding with water through C-H-O bonds,[96] contributing for the higher deshielding, when compared to the tail, upon reducing water-cation interactions by increasing IL concentration. Finally, the highest deshielding of hydrogen 5 (H5) can be backed by the fact that it seems to be the hydrogen more likely to interact with chloride through hydrogen bonding with a strong ionic character, due to its greater acidity relative to the other ring and tail hydrogens.[98–100]

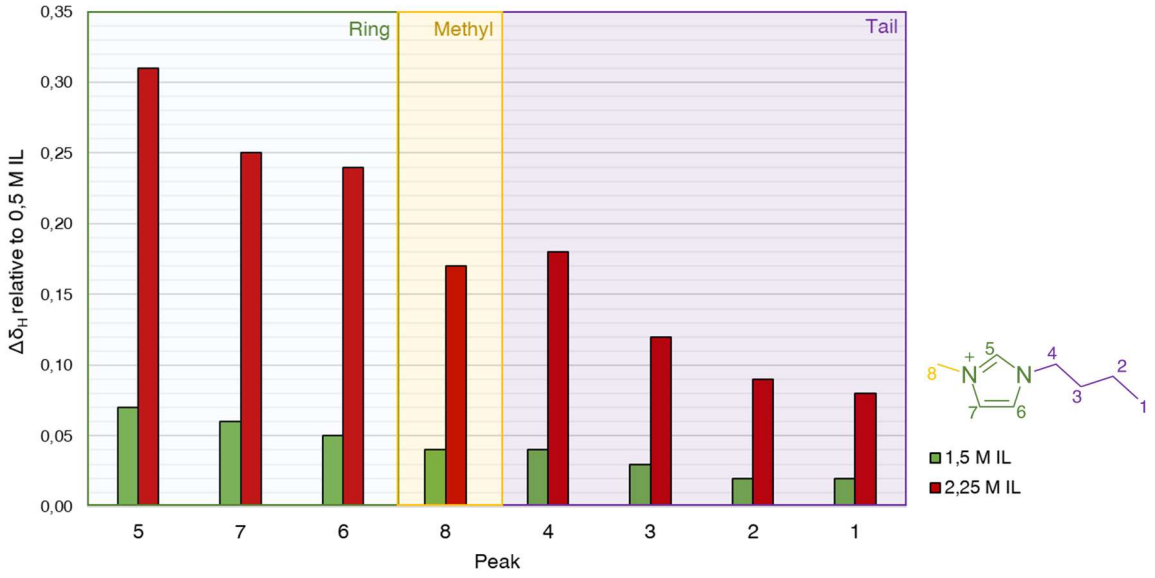

Figure 12. Chemical shifts of the hydrogens of the C_4mim cation in 1,5 and 2,25 M solutions of [C_4mim]Cl in water when compared to a 0,5 M solution.

b) In the absence of salt

Extremely important towards an understanding of the molecular interactions at play in hydrotropy is the analysis of IL solutions with a dissolved hydrophobic solute, vanillin in this case. Figure 13 provides the chemical shifts in the cation observed when vanillin is added to saturation. These shifts seem to be maximized when the solute is added to saturation,

as previous work on NMR of hydrotropic solutions showed a consistent increase in chemical shifts with the increasing concentration of added solute, and supporting the theory that the hydrotrope aggregates around the solute as the latter is added.[101] Thus, herein we test the chemical shifts on saturated solutions, where they should be at their maximum deviance in what concerns solute concentration. Ionic liquid concentration is also a parameter that influences the obtained chemical shifts, and as so both 0,5 M and 1,5 M IL concentrations will be probed in regards of hydrotrope-solute interactions. It is also important to notice that for [C_4mim]Cl the hydrotropic effect at 1,5 M is significantly stronger than at 0,5 M as can be noted from the hydrotropic curve of the ionic liquid presented in Figure 1, as well as in accordance with the typical hydrotropic solubility curve with its characteristic shape – as so, the 1,5 M IL concentration will be the main focus of attention. In general, for 1,5 M IL there is a clear distinction between the interactions of the IL ring versus the tail, as the ring sees little change in shielding whereas the addition of vanillin provided a significant shielding in all hydrogens of the hydrocarbon tail, which seems to indicate a preferred tail-solute interaction over a ring-solute one. These shifts point towards hydrocarbon chain interactions with non-polar regions of vanillin, which will be supported by MD data below, and are in accordance with previous findings,[3] while also pointing towards continued IL ring hydration, once again supported by MD data. At this point it should be important to notice how the hydrophilicity of the functional groups present is directly linked to the observed shifts. Regarding the 1-butyl-3-methylimidazolium cation, the matter is straightforward, as there is an evident dichotomy consisting of a hydrophobic hydrocarbon chain and a hydrophilic imidazolium ring, besides the hydrophobic methyl group. Regarding the vanillin molecule, a more comprehensive evaluation is needed as it possesses several functional groups with different rates of hydrophilicity that could be arranged in the following fashion: the most hydrophilic group is the hydroxyl, as such the most likely to remain hydrated, as will be later seen in the MD results; followed closely by the aldehyde group; then the less hydrophilic ether linkage; and finally the non-polar hydrocarbon ring. Bearing in mind this arrangement of functional groups, the following NMR results will be more evidently explained.

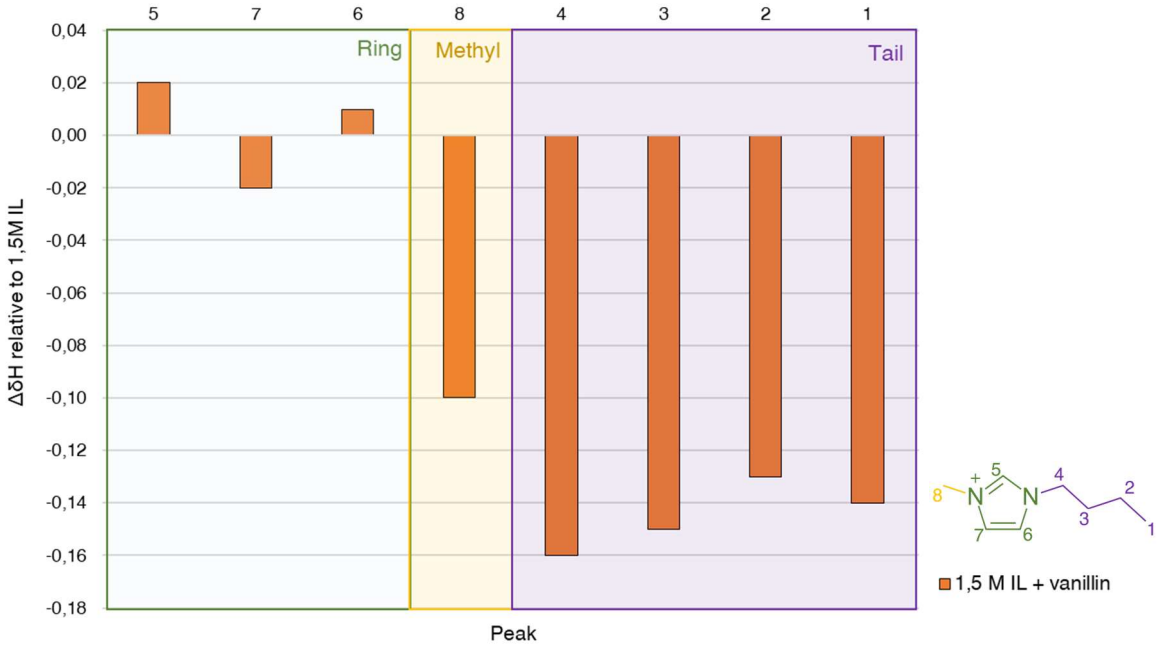

Figure 13. Chemical shifts of the hydrogens of the IL cation in a 1,5 M solution of [C_4mim]Cl in water, saturated with vanillin, when compared to an aqueous 1,5 M IL solution with no solute.

Further insight could be obtained by looking at the chemical shifts in the hydrogens of the vanillin molecule, as represented in Figure 14, when comparing vanillin dissolved to saturation in a hydrotropic IL aqueous solution to vanillin dissolved to saturation in water. All hydrogens within the molecule are more shielded when it is dissolved in the IL solution. This effect is especially pronounced in the hydrogens of the methoxy group and hydrogens 2 and 3 of the hydrocarbon group, most likely involved in solute-hydrotrope and solute-solute interactions; hydrogen 4 shows shielding to a lesser extent most probably because it is the closest to the highly electronegative hydroxy group of vanillin, an area most likely to remain hydrated and thus less available to interact with the hydrotrope. The significant shielding of H2 and H3 of the ring and H5 seems to point towards the fact that IL-vanillin interactions are mostly made with the participation of the hydrocarbon chain of the [C_4mim]$^+$ cation and the ring and methoxy group of vanillin, its most hydrophobic sites, thus revealing favoured hydrophobic hydrotrope-solute interactions. This once again supports the hydrotropy model proposed by Shimizu *et al.*[38] and is in accordance with previous works.[101]

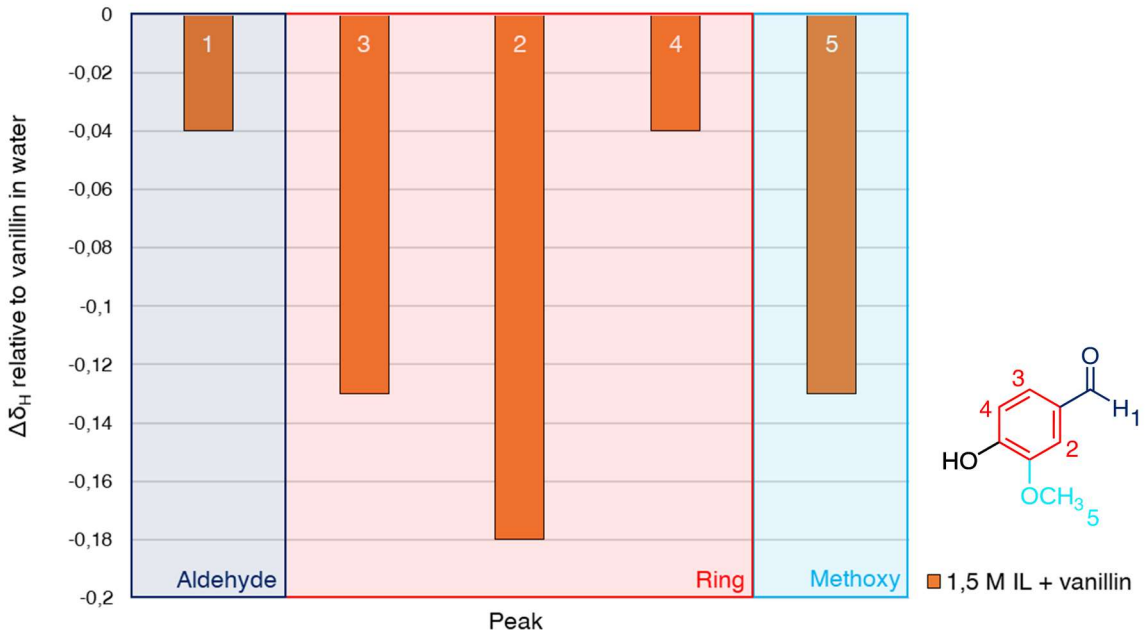

Figure 14. Chemical shifts of the hydrogens of vanillin in a 1,5 M solution of [C_4mim]Cl in water, saturated, when compared to vanillin dissolved in water, saturated.

As previously mentioned, the influence of the IL concentration was also assessed. Figures 15 and 16 provide the resulting chemical shifts of the IL cation and vanillin in ternary IL/vanillin/water systems with 0,5 M IL. The amount of shielding suffered by the IL cation tail is lesser in this condition, as more molecules should be freely solvated and not involved in vanillin solubilisation. The ring shows slight shielding as well. The methyl group is once again considerably shielded, hinting at possible hydrophobic interactions with vanillin. The vanillin chemical shifts profile is quite similar to the one obtained above for 1,5 M IL, with two main differences: H4, that is considerably more shielded in 0,5 M IL, and H5 that suffers the opposite effect. Considering that H4 of vanillin is the closest to the highly hydrophilic hydroxyl group, and H5 is part of a not so much hydrophilic one, it seems that the site-specific IL-vanillin interactions are the more pronounced the more IL is present, and as so may be linked directly to the hydrotropic solubilization typical curve for [C_4mim]Cl: 0,5 M finds itself before the exponential leap in effect, and sees less site-specificity, whereas 1,5 M finds itself in the leap area, seeing increased site-specificity in hydrophobic interactions.

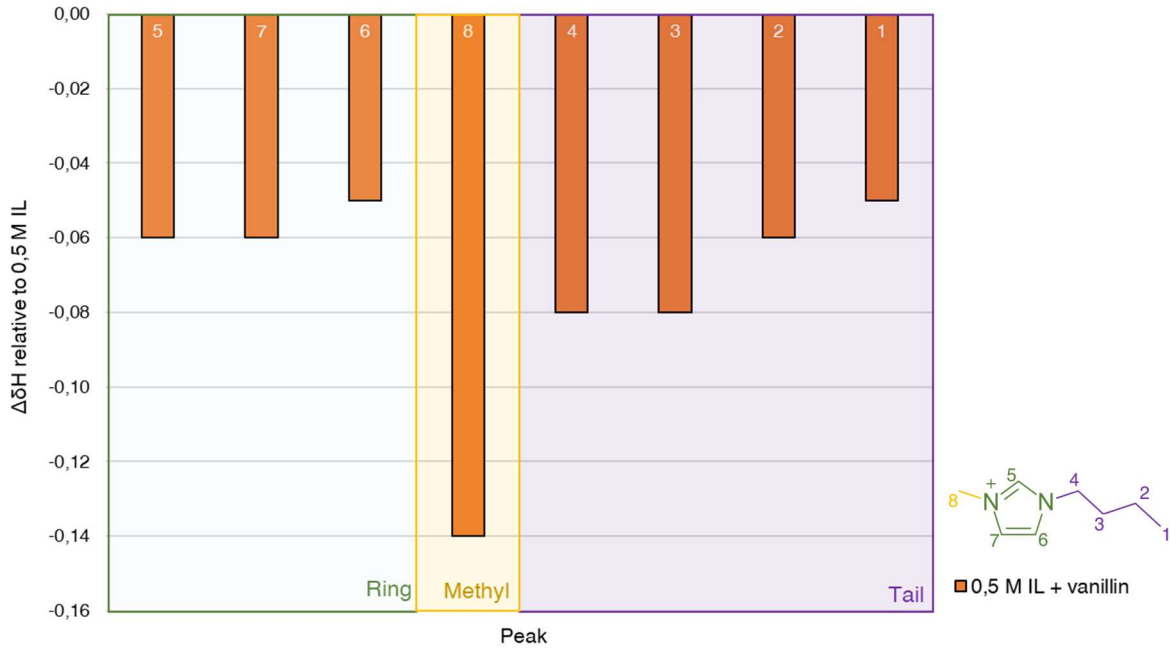

Figure 15. Chemical shifts of the hydrogens of the C_4mim cation in a 1,5 M solution of [C_4mim]Cl in water, saturated with vanillin, when compared to the same solution without vanillin.

Grouping the information from both cation and solute shifts together, the results point to the fact that the major hydrotrope-solute interaction is the one between the cation tail and the vanillin ring and methoxy group. This evidenced hydrophobic interaction is in support of a hydrotropic solubilisation mechanism where the hydrotrope accumulates around the solute, forming aggregates with it where the apolar moieties are associated while the polar moieties are kept mostly in contact with water. The hydrogen bonding between water molecules, being stronger than hydrophobic moieties-water interactions, are what drives the aggregation of hydrotrope and solute, and therefore lead to the increased solubilisation of hydrophobic molecules. It can then be said, based on the present NMR results on hydrotrope-solute interactions, that these same interactions are site-specific, as significant interaction site selectivity is evidenced for these molecules. This could be the reasoning behind the high selectivity of hydrotropes, as well as a point of distinction between hydrotropes and surfactants – while solubilization via surfactants forms aggregates *a priori*, solubilization via hydrotropes forms aggregates upon solute addition through site-specific interactions, a possible explanation for the higher selectivity of the latter.

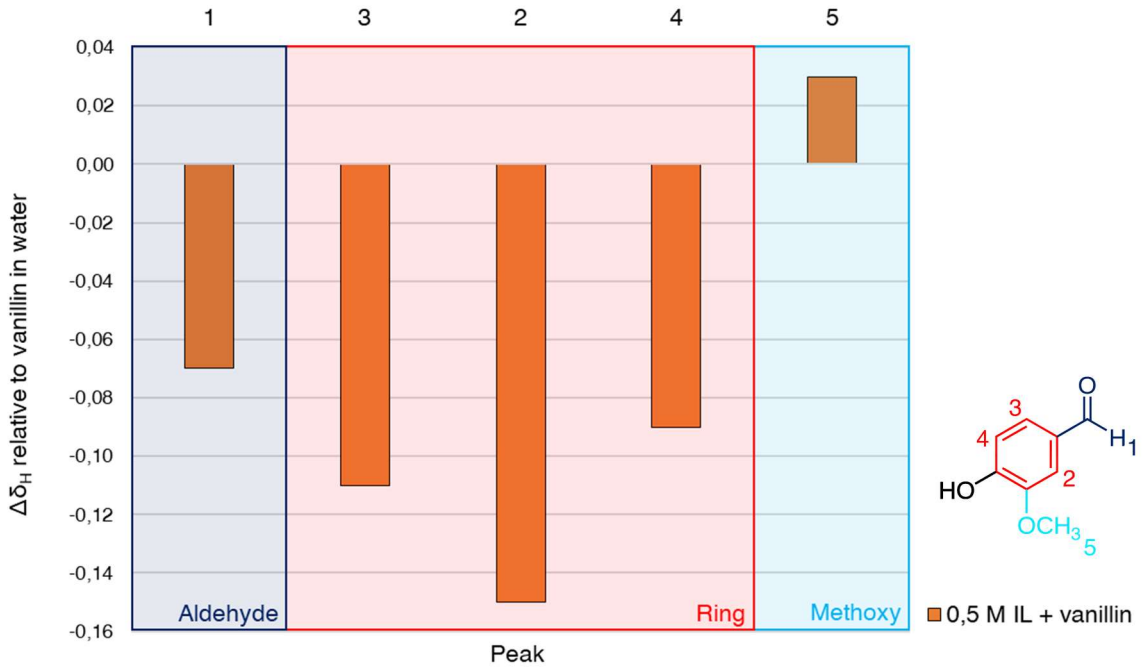

Figure 16. Chemical shifts of the hydrogens of vanillin in a 1,5 M solution of [C_4mim]Cl in water, saturated, when compared to vanillin dissolved in water, saturated.

c) Salted ionic liquid aqueous solutions

Beyond the simple hydrotrope and solute interactions in the hydrotropic solubilization of vanillin, the doping of IL aqueous solutions, with and without vanillin, with different salts, was also tested with the NMR technique. Previously noted the differences in chemical shifts concerning hydrotrope and solute concentrations, it should now be noted that the addition of salts provided consistent shifts independently of the hydrotrope concentration, and for the sake of brevity 1,5 M IL solutions will be the ones considered, as they provided clearer spectra with the most signal, and 1,5 M is a concentration where the hydrotropic effect is already significantly at play, more so than 0,5 M. 1,5 M [C_4mim]Cl solutions with added lithium, sodium, magnesium, and yttrium chloride at a concentration of 1 M revealed a strongly consistent pattern in their chemical shifts throughout all cation hydrogens, but a surprisingly inconsistent behaviour in terms of shielding/deshielding throughout cations of different valences, as can be seen in Figure 17. Both monovalent cation salts, NaCl and LiCl, provided deshielding of all hydrogens, more pronouncedly with sodium chloride, while $MgCl_2$ and YCl_3 provided shielding of all hydrogens, much more pronouncedly with yttrium chloride. Considering these chemical shift differences, one could organize the salt cations from the one that provides the most deshielding to the one providing the most shielding:

$Na^+ > Li^+ > Mg^{2+} > Y^{3+}$. This organization, while clearly resembling the Hofmeister series, is contradictory in regard of the monovalent cation salts, as they are portrayed in this analysis as salting-in salts, while salting-out in the hydrotropic solubility tests. Therefore, the own HS should be avoided as an all-around explanation for the behaviour of these salted systems. In fact, the HS is not always observed, as reversed and altered forms of it seem to have a place in ion-surface interactions. Surface charge, surface hydrophobicity, pH and even salt concentration seem to alter the order of ions in the series, and such a complexity of factors can deviate, in a work such as the present, the obtained ion sequence from the one of the original HS, which is in itself very robust mostly when considering the salting of proteins.[60] Also of note is the anti-parallelism between deshielding-inducing and shielding-inducing salts in the cation moieties they affect, as deshielding-inducing salts alter chemical shifts more significantly in the ring than in the tail, whereas shielding-inducing salts alter them in the opposite way. The salt cations in question, being salting-out cations, typically show stronger interactions with water molecules than water molecules among themselves. The mentioned salt cation sequence also runs from the salt that exhibits weakest interactions with water to the one that exhibits the strongest, and as so it is as well running from the salt inducing the least IL dehydration to the one inducing the most. Considering that dehydrating the IL promotes cation-cation interactions it is seen that the more the added salt is positioned towards the right in the $Na^+ > Li^+ > Mg^{2+} > Y^{3+}$ deshielding sequence, the more aggregation of the IL can be observed, hence the strong shielding, and the greater the hindrance towards vanillin solubility. This is a valid explanation once again for the stronger deshielding of the tail when in comparison to the ring, as hydrophobic interactions should be central in IL aggregation.

Regarding NaCl and LiCl, the fact that they provide increased deshielding to all hydrogens cannot pass as expected. As mentioned, this contradicts the results obtained in the hydrotropy curves in the previous section, as they still salt-out vanillin despite their opposite behaviour in this analysis. There is extensive literature on the LiCl doping in ionic liquids, aiming to utilise ILs in Li-ion batteries. However, these works dope the pure IL, which has very different bulk properties than the aqueous solutions at use in this work, as previously mentioned. Nevertheless, it should be noted that in pure ILs LiCl doping seems to potentiate longer charge separation, as it leads to the formation of charged clusters due to increased ion-ion interactions.[102] As Li^+ and Na^+ have the same valence as the $[C_4mim]^+$ cation, these salt cations may be more easily included in the IL network, more so than their more charged Mg^{2+} and Y^{3+} counterparts, possibly explaining the verified chemical shift differences.

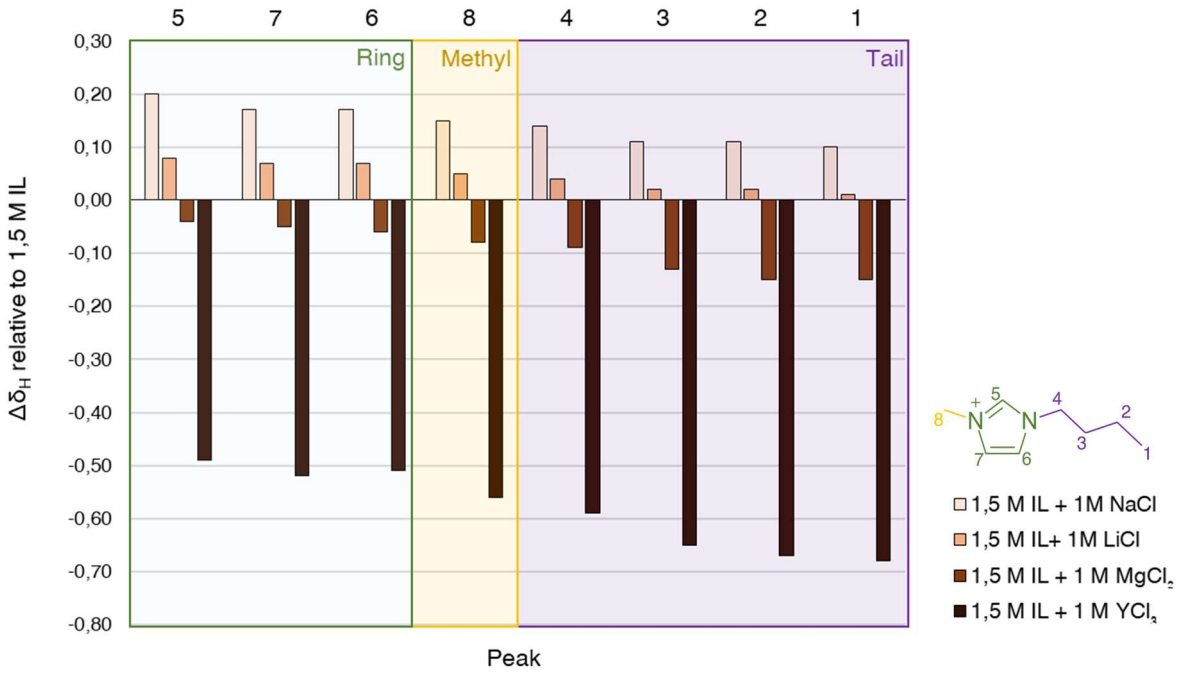

Figure 17. Chemical shifts of the hydrogens of the C_4mim cation in 1,5 M solutions of [C_4mim]Cl in water with 1,0 M of added salts, when compared to a similar solution without added salt.

Overall, the cation tail always tends to have a less electronegative environment than the ring, as any added salt either shields it more or deshields it less. As so, the addition of salt seems to be a promoter of tail-tail interactions, that is, of hydrophobic interactions, hinting at increased IL cation interactions, where the hydrophobic tails are in contact and away from water, and the hydrophilic rings are away from the tails and in closer contact with the water. To complement the obtained data, an additional DLS analysis was performed on salted 1,5 M IL solutions, with the intent to identify possible aggregate presence and aggregate size change according to the added salts. All salts were added in a concentration of 1 M, as to emulate the NMR analyses. The results obtained, represented in Figure 18, show a slight increase in aggregate size as salts with higher valence cations are added, consistent with the NMR shifts obtained. Although this data seems to be in accordance, the existence of IL aggregates at these concentration ranges, without the presence of any solute, is debatable, as the detected aggregates approach the lower detection limit of the equipment. Cláudio *et al.*[3] did not verify the presence of [C_4mim][Tos] aggregates at a concentration of 0,64 M through DLS measurements. However, Yin *et al.*[103] did verify aggregates at both 0,8 M and 1,6 M concentrations for the same IL, proposing that 0,64 M might be too low of a concentration to form detectable aggregates. In comparison with the results herein

presented, [C_4mim]Cl aggregates are significantly smaller in diameter, and some are very near or even below the equipment's lower range of sensitivity, placed at 0,3 nm. Regardless, the contribution of salting to the increase of aggregate size is evidenced, and complements well the data obtained by NMR, supporting dehydration of the IL upon salt addition, consequent increase in hydrotrope-hydrotrope interactions and aggregation, and subsequent decrease in vanillin solubility.

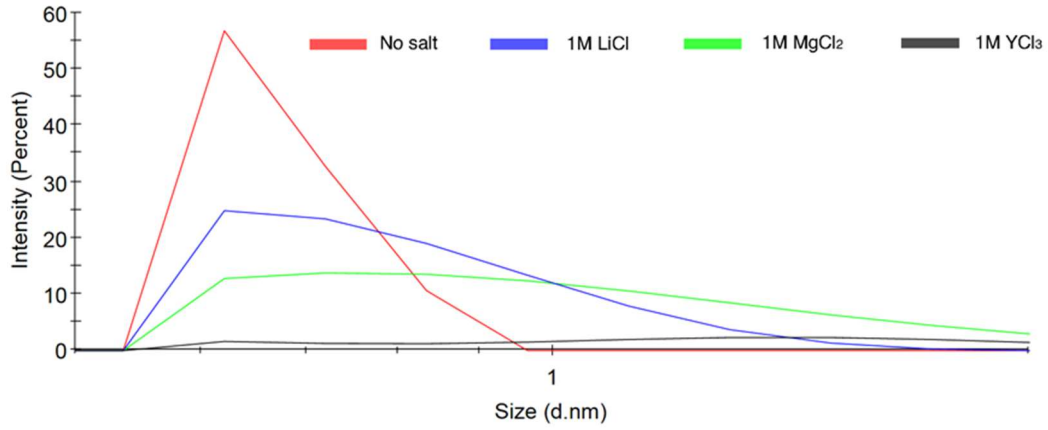

Figure 18. DLS measurement of aggregate presence in 1,5 M [C_4mim]Cl salted solutions without vanillin, logarithmic scale.

d) Salted ionic liquid aqueous solutions with vanillin

Following the same rationale as the previous tests, 1,5 M [C_4mim]Cl solutions with added sodium, magnesium, and yttrium chloride at 1,0 M with the addition of vanillin to saturation were tested. A similar trend as the aforementioned, depicted in Figure 19, can be observed, where $Na^+ > Mg^{2+} > Y^{3+}$ runs from the least shielding-inducing cation to the most shielding-inducing. However, the striking difference seen with the addition of vanillin is that now every salt induces shielding in every hydrogen of the IL cation. In terms of moieties, sodium chloride induces the most shielding in the ring, whereas yttrium chloride induces it on the tail. The present behaviour of NaCl is very peculiar: without vanillin, it induced more deshielding in the ring and less in the tail of the IL cation, whereas with the addition of vanillin the opposite is verified, as it induced more shielding in the ring and less in the tail. Magnesium chloride affects both equally. As mentioned before, regarding the previous analysis, the more strongly a cation binds water the more it dehydrates the IL cation, hence the shielding trend: stronger binding cations will favour aggregate formation, possibly leading to increased hydrotrope-hydrotrope interactions. With this promoted IL

aggregation there are less IL cations available to take part in the hydrotropic solubilization of vanillin, which justifies the decreased solubility verified in the hydrotropic solubility tests earlier presented. These two approaches are then seemingly in accordance, as yttrium chloride is more detrimental to vanillin solubility than magnesium and sodium chloride, while promoting the most shielding of the hydrogens of the IL cation.

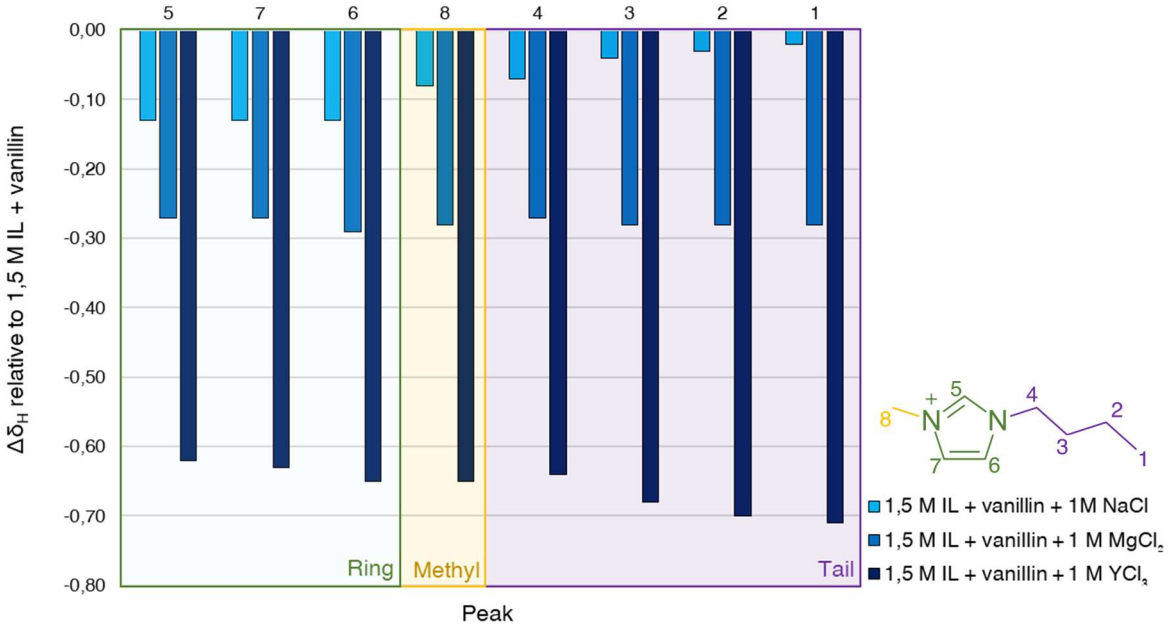

Figure 19. Chemical shifts of the hydrogens of the C_4mim cation in 1,5 M solutions of [C_4mim]Cl in water, with added vanillin to saturation and with 1,0 M of added salts, when compared to a similar solution without added salt.

Another look at the same condition, depicted in Figure 20, provides the chemical shifts observed for the hydrogens of vanillin. Shielding is observed, this time equally throughout all the molecules' hydrogens. Once again NaCl provides the least shielding, YCl_3 the most, and $MgCl_2$ is in-between. Thus, salting of IL/water/vanillin systems seems to affect the chemical environment of all vanillin hydrogens equally. It is evident that this shielding is caused by an increase in hydrophobic interactions, creating a greater local hydrophobic environment for vanillin.

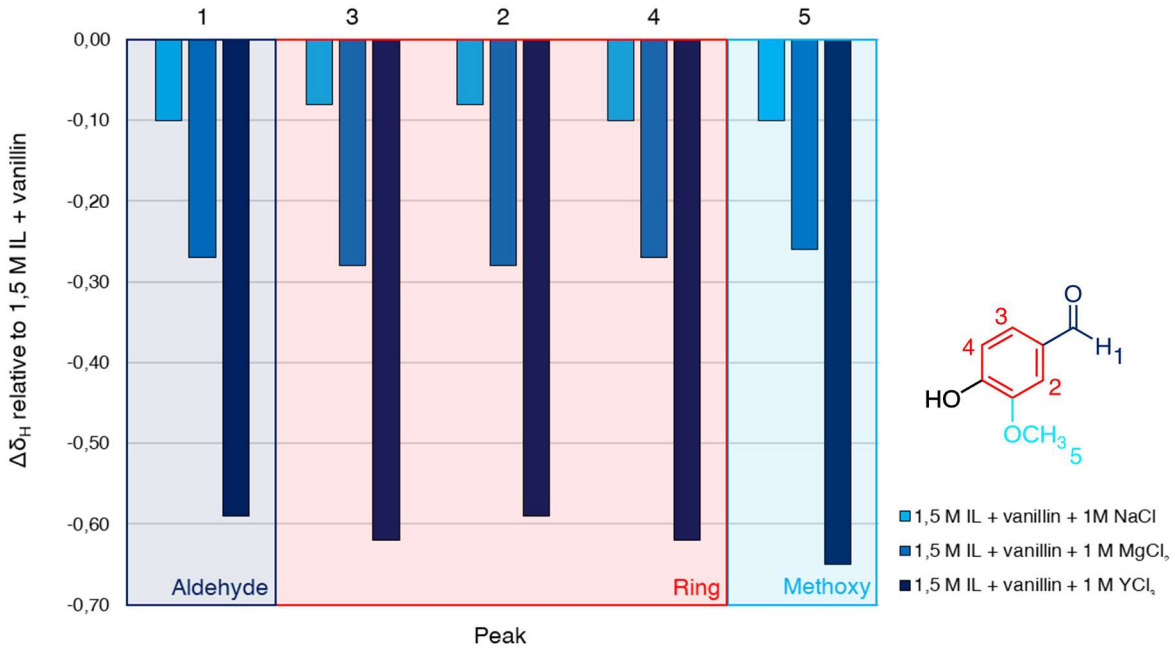

Figure 20. Chemical shifts of the hydrogens of vanillin in 1,5 M solutions of [C_4mim]Cl in water, with added vanillin to saturation and with 1,0 M of added salts, when compared to a similar solution without added salt.

In general, these results show a stark dissimilarity when compared to the salting effect on the IL, with no solute. After testing all binary interactions in separate, hydrotrope-hydrotrope and hydrotrope-water first, then hydrotrope-salt, then hydrotrope-solute, the final tested quaternary system of hydrotrope/solute/water/salt appears to have interactions strongly independent than those presented before. Despite the general salting-out effect of the added salts coming with no surprise, the analyses of binary interactions by themselves cannot explain with accuracy the behaviour exhibited by the last system. For instance, the nuanced behaviour of deshielding of the IL cation upon addition of 1 M Na/LiCl disappears with the addition of solute; also, the site-specific hydrotrope-solute interactions seen through the NMR shifts of both vanillin and the IL cation on the IL/water/vanillin system also cease to be in effect with the addition of 1 M of salt. In the quaternary system, hydrophobicity seems to be enhanced synergistically both by hydrotrope-solute interactions, in accordance with the previously mentioned hydrotropy model, as well as by the salting-out effect observed upon salt addition. The behaviour of [C_4mim]Cl has been well probed, as vanillin showed to provide a nucleation point where the IL aggregates, a behaviour only enhanced by the addition of salt, to an extent proportional to the charge of the salt cation. We can therefore cautiously conclude that the binary interactions studied were unable to predict accurately the behaviour of the quaternary system. Figure 21 presents the same chemical shifts normalized to the salt cation valence, and shows that the relationship between it and

the shift a given salt induces, in both IL cation and vanillin, is not necessarily linear, but rather increases beyond a linear fashion with valence. To further help visualize the behaviour of the quaternary system, the chemical shifts of the IL cation were also plotted with the salted IL in water as reference, such as seen in Figure SI:6, better probing the influence of the presence of solute. It is verified that the addition of vanillin did not increase hydrophobic interactions with added yttrium chloride as much as it did with the other salts, likely because there was less IL available to interact with vanillin, as the IL/salt/water system already had the most IL cation aggregation.

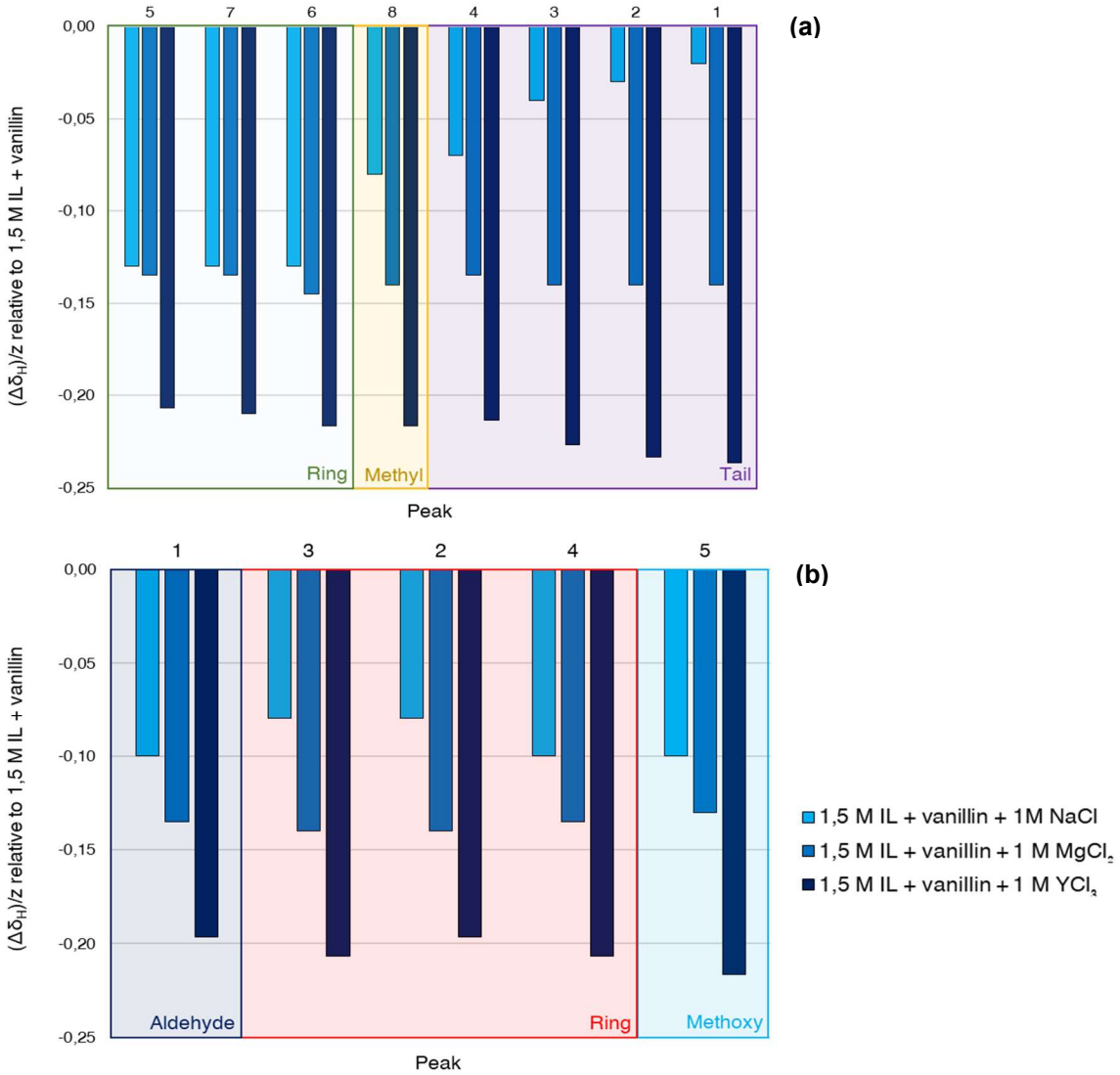

Figure 21. Chemical shifts, normalized to the valence of the salt cation added, *z*, of the hydrogens of the ionic liquid cation (a) and vanillin (b) in 1,5 M solutions of $[C_4mim]Cl$ in water, with added vanillin to saturation and with 1,0 M of added salts, when compared to a similar solution without added salt.

The same solutions of the quaternary IL/vanillin/water/salt systems were analysed by DLS to detect and size eventual aggregate formation. The analysed salts were once again sodium, lithium, magnesium, and yttrium chloride. Presented in Figure 22, the results provide a clear view over how the previously mentioned salt cation series is also applied in terms of aggregation: $Na^+ < Li^+ < Mg^{2+} < Y^{3+}$ is in this case a sequence running from the salt inducing the smallest aggregates to the one inducing the biggest. Rationalizing these results with the ones previously presented one can link the phenomenon of decreased solubility via salt addition with the formation of aggregates of increasing size. The formation of consistently bigger aggregates along the series, especially well depicted in the yttrium chloride curve in the normal scale, seem to point towards an increasingly proximity of phase separation. Such results find themselves in agreement with all former, as it was seen that salts with higher valence originated increased hydrophobic interactions and ionic liquid aggregation. They also present great similarity with the discussed DLS analysis for IL aggregates in aqueous solution, presented in the previous section, albeit with evidently much larger aggregates, which reinforces the theory that the presence of solute is essential to significant aggregation and to the hydrotropic effect.

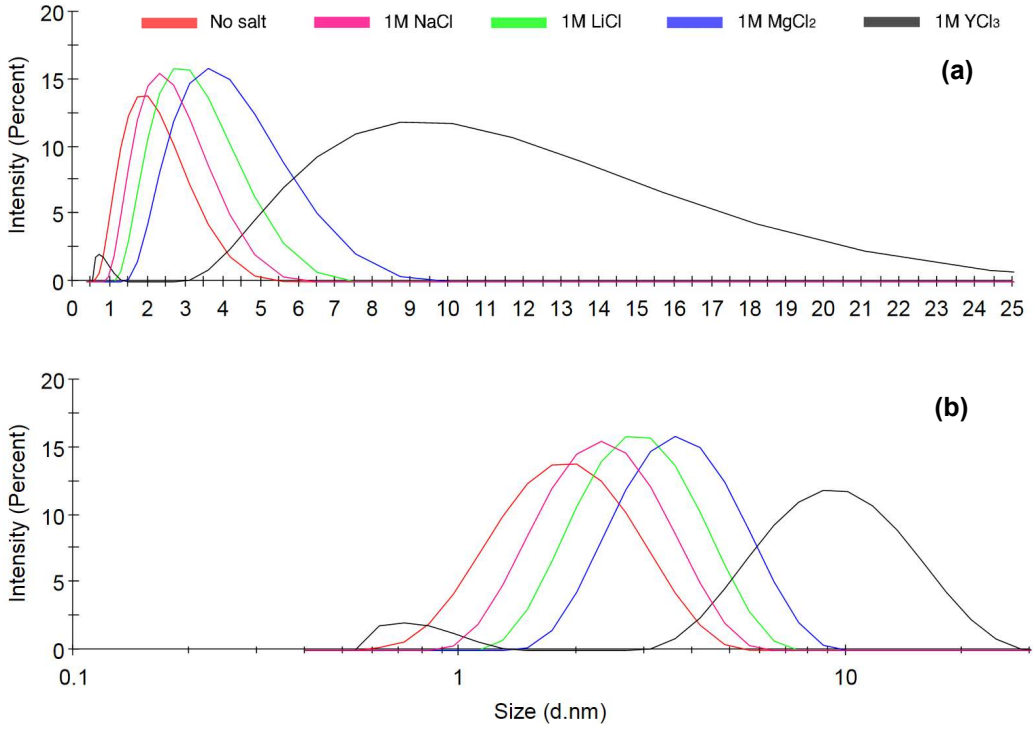

Figure 22. Aggregate presence in 1,5 M [C_4mim]Cl salted solutions saturated with vanillin in a (a) normal and (b) logarithmic scale.

3. Molecular Dynamics

The discussed work was further complemented with Molecular Dynamics simulations, aiming to obtain further insight on the relevant intermolecular interactions at play in the hydrotropic solubilisation of vanillin. Vanillin is a very weak base possessing a hydroxyl group that can be protonated or unprotonated (pKa of 7,4).[104] For the MD studies performed in this work, the protonated form of vanillin was used. The molecular dynamics all-atomistic systems herein described consisted of five different conditions, namely (a) 100 [C_4mim]Cl molecules in water, corresponding to a concentration of 0,51 M, (b) 10 vanillin molecules in water, below solubility limit, corresponding to a concentration of 0,055 M, (c) 10 vanillin molecules in aqueous [C_4mim]Cl, below solubility limit, corresponding to a concentration of 0,050 M (d) 20 vanillin molecules in aqueous [C_4mim]Cl, above solubility limit, corresponding to a concentration of 0,10 M and (e) 20 vanillin molecules in aqueous [C_4mim]Cl, above solubility limit, doped with 100 NaCl molecules. As the conditions containing IL always have 100 molecules of it, this number will be omitted from here on. It is important to consider that these systems are not only quite diluted in terms of IL concentration as well as they contain a low numerical amount of IL and vanillin molecules, not necessarily portraying with fidelity the experimental conditions; rather, these systems are aimed at probing the specific interactions existing between the IL and vanillin, and how these change with solute concentration and with the addition of charged particles (100 NaCl). Even the addition of salt is done at a very dilute concentration, not necessarily one that could macroscopically provoke a change in the systems properties, but one that could change specific intermolecular interactions. Thus, the objective of this section is not to reproduce computationally the work done experimentally, but to complement it with clues related to the relevant interactions that could shed more light on the reasoning behind the behaviour of each experimental condition.

a. Probing aggregate formation

The Solvent Accessible Surface Area (SASA) analysis provides information on the molecular environment of a given molecule or set of molecules by returning the area of that molecule that is accessible to a solvent, or in this case, the area that is accessible to water, and so can provide clues over which interactions are potentiated or hindered between conditions.

The profile for the SASA of the IL cation is shown in Figure 23. An expected decrease of the area is observed as vanillin is added, due to the increase of hydrotrope-solute

interactions, the decrease being more pronounced with 20 vanillin molecules added, as a bigger number of IL cation molecules take part in hydrotropic solubilization. This data supports the idea that the addition of solute potentiates aggregation and is consistent with vanillin being a point of nucleation to IL accumulation. The bigger reduction in area seen from the addition of 10 to 20 vanillin, when compared to the reduction from no vanillin to 10, suggests that only above the solubility the hydrotropic effect becomes considerable, as it is in that condition that significant aggregation is achieved. Regarding the addition of 100 NaCl, it is possible to verify a slight downshift in the SASA profile, in line with the rationale that the addition of salt will dehydrate the IL cation and promote its aggregation, if ever so slightly due to the low amount of salt added. This more system-wide initial approach allows the assessment of the general behaviour of the simulated systems, which shows to be consistent with the NMR experimental data patent on Figures 13 and 14, as solute concentration is directly linked to the rate of IL aggregation.

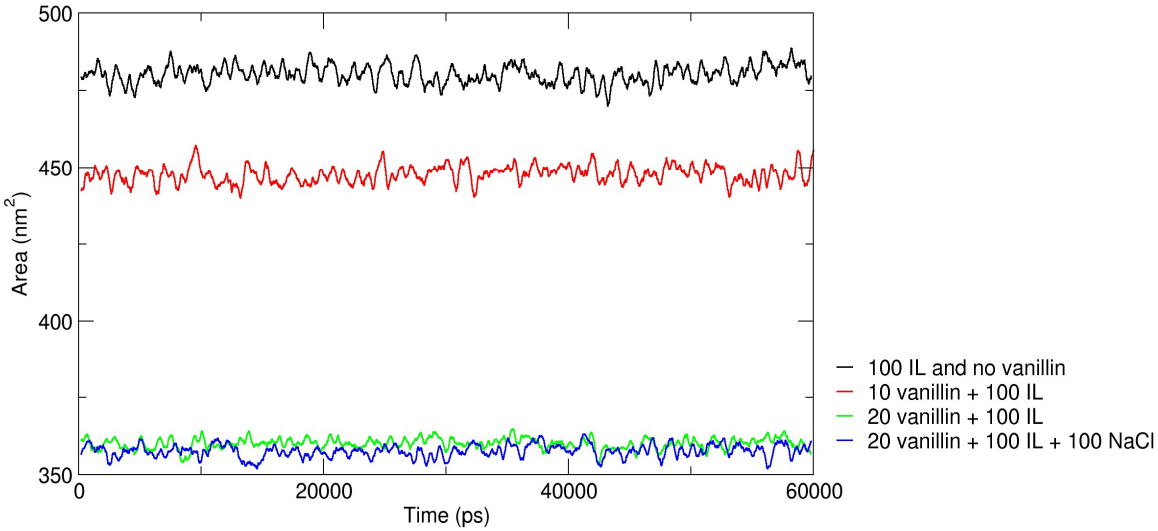

Figure 23. Solvent-accessible surface area for the $[C_4mim]^+$ cation in all conditions.

To further assess the presence and composition of aggregates in the simulated systems the *gmx density* tool was used to generate the density curves of all water, cation, and vanillin molecules across the box. This tool generates the partial density of a selected molecule type across the box. Aggregates would be expressed in these curves as peaks for vanillin and/or the IL cation, coinciding with depressions in the water curve, as water density would be lower in the aggregate location. Figure 24 compiles all the density curves obtained for the five systems. The IL/water system (a) showed good correspondence between the visible peaks and depression, pointing towards a location with higher cation

density than bulk; however, the density difference between the peak and bulk is of only approximately 2 $kg.m^{-3}$ and as so aggregate presence should be considered with caution. The vanillin/water system (b), as it simulates a condition under the vanillin solubility limit and presents no significant peaks nor depressions is in accordance with the expected since vanillin should be homogenously solvated. With the introduction of vanillin in IL on condition (c) aggregation was to be expected to an extent, given the aggregative effect of a hydrotrope around a solute. In fact, there is a visible region of slight IL aggregation, around 2 $kg.m^{-3}$ above bulk density, where hydrotropic solubilization of vanillin should be expressed. Despite this region not fully overlapping the visible slight vanillin peak, it overlaps well with a depression in water density; the vanillin peak was not necessarily expected to overlap the IL cation one, as this condition is under vanillin solubility even without the presence of the hydrotrope, and as so there should be a considerable amount of vanillin solvated non-hydrotropically. Condition (d) introduces vanillin beyond saturation and shows good overlapping of both vanillin and cation peaks with a water depression, although the variations in density are once again small. This suggests the hydrotropic effect is being potentiated as much as possible, as vanillin is very likely to be found near IL cations. Therefore, once again significant IL+vanillin aggregation is only seen with 20 added vanillin molecules, above the solubility limit, in a consistent fashion with the previous SASA profile results that showed a much higher decrease for conditions with 20 vanillin. Finally, condition (e) introduces a low amount of NaCl, a salt expected to bring about less vanillin solubility and increased IL aggregation. However, this small amount of 100 salt molecules was likely to produce no discernible differences in the simulated system. Overall, the analysis of densities sets the base for further analysis as it correctly points to the existence of strong hydrotrope-solute interactions and it is in good agreement with the discussed SASA profiles for a similar reason.

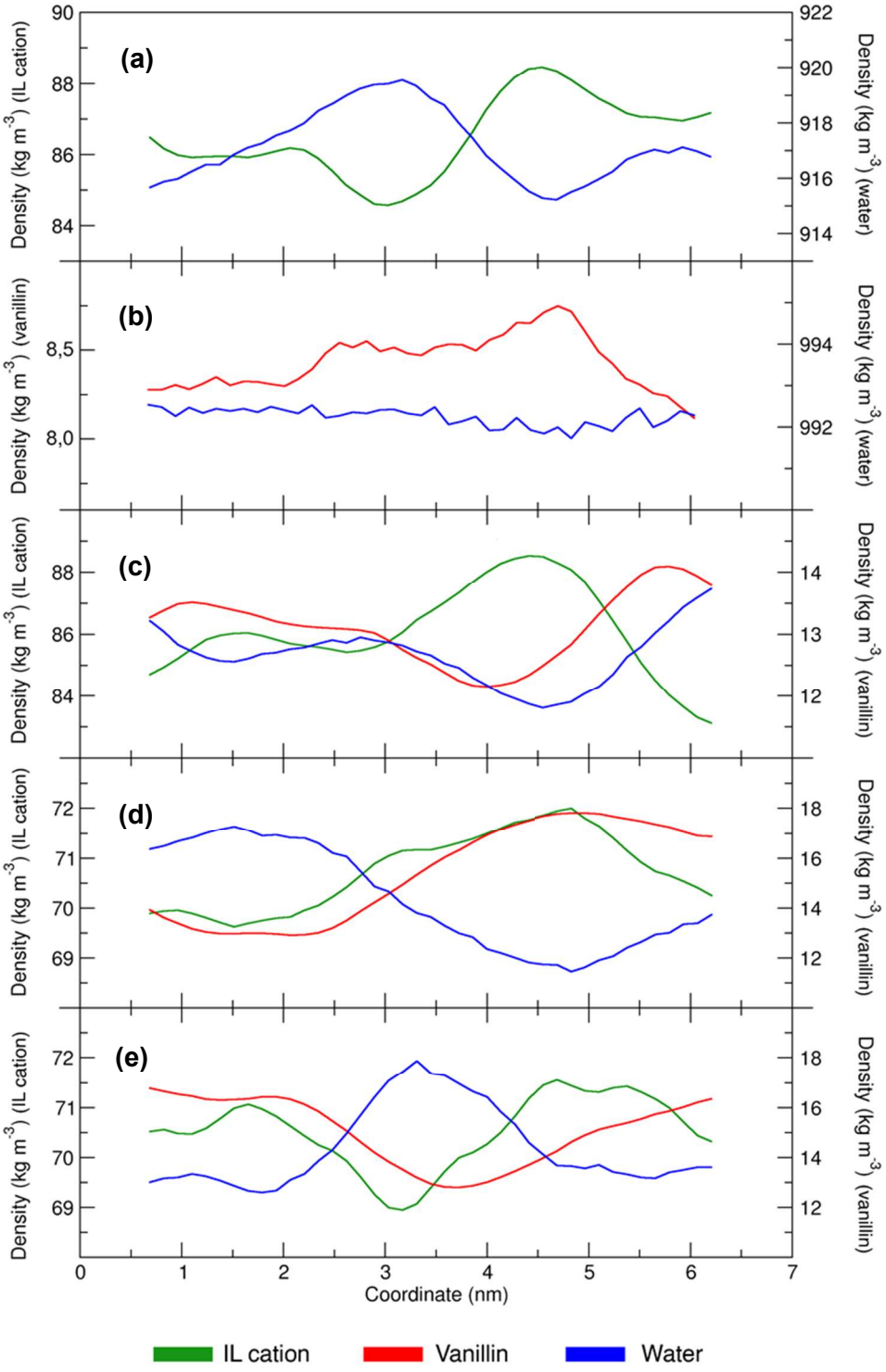

Figure 24. Density curves for the IL cation, vanillin, and water across the simulation boxes. The five conditions are (a) IL in water, (b) 10 vanillin in water, (c) 10 vanillin in IL and water, (d) 20 vanillin in IL and water, (e) 20 vanillin in IL and water with 100 NaCl molecules. Note that in (b) and (c) vanillin is present below its solubility limit, and in (d) and (e) above it. The depicted curves are smoothed running averages of the actual raw curves.

b. Probing site-specific solute-hydrotrope interactions

The probing of site-specific interactions was exclusively focused on selected hydrogen atoms of the IL cation and some hydrogen and oxygen atoms of the vanillin molecule, as these are the ones more likely involved in intermolecular interactions. For the IL cation, four hydrogen atoms were selected for RDF determination: H1, H2 and H3, making up all hydrogens of the imidazolium ring, and H10, a hydrogen located about halfway in the hydrocarbon chain. For the vanillin molecule hydrogen H0S of the hydrocarbon ring, and the O0A, O0H and O0N, oxygens of the hydroxyl, methoxy, and aldehyde functional groups, respectively, were selected. Models of the molecules with explicit labelling of the referred atoms can be found in Figure 25. Together with the RDF plots (full lines), coordination numbers (CN) were also plotted (dashed lines), showing the average number of particles within the defined distance *r*. Visual inspection of the systems was also performed, including the visualization of hydrogen bonds (H-bonds) whenever they occurred. These bonds were obtained by the VMD "hbonds" representation option, which allows the definition of two parameters: distance and angle cutoff. These parameters define the maximum distance to search for a hydrogen bond between an atom bonded to a hydrogen atom and an atom with no hydrogen bonded to it, and the maximum angle between those two atoms passing through the hydrogen, respectively. The default value for these parameters is 3,0 Å for the distance and 30º for the angle. Skarmoutsos *et al.*[105] have provided evidence that for imidazolium-based ILs a cutoff of 60º is the most appropriate, and as so herein a distance of 4,0 Å and an angle of 60º were utilized throughout for these parameters.

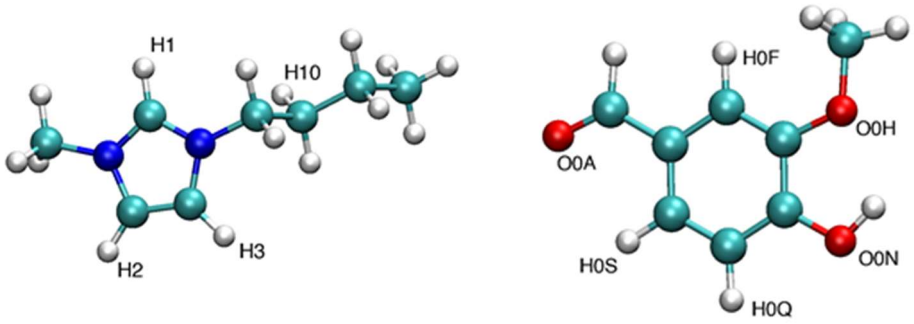

Figure 25. $[C_4mim]^+$ cation (left) and vanillin (right) all-atom models with labelling of the atoms for which RDF analyses were performed.

i. Ionic liquid-vanillin interactions

One of the most important interactions at study in this work is the hydrotrope-solute interaction or, in this case, the IL cation-vanillin interaction. The RDFs for the specific interactions between the H0S hydrogen of the vanillin ring with the various hydrogens of the IL cation are portrayed in Figure 26. In the first condition, 10 vanillin in aqueous IL, it is evident how most interactions are made between H0S and the H10 from the hydrophobic IL tail. This is evidence of how the addition of solute potentiates hydrophobic interactions via IL tail-vanillin ring interactions and is in accordance with the previously described experimental results, namely NMR analyses showcasing higher shielding in the IL cation tail than in its ring, in systems with vanillin, such as in Figure 16. A neat ordering of the remaining hydrogens ensues, with H1 the most involved in interactions, followed by H2 and H3, the latter showing a significant decrease in its CN throughout as well. Chloride ions can play a part here, as it seems to be the ring hydrogen less likely to interact with it, possibly staying more easily hydrated and being the least likely hydrogen to lose nearby water because of ring-ring interactions. This effect is lost upon addition of vanillin beyond the solubility limit, where it is seen that it is H2 that is now presenting the major divergence as it interacts less, as seen in both RDF and CN plots. With this addition the H10 profile becomes different than the other three, seeing that its first peak remains in place and all others move towards shorter distances. This is suggestive of an increase in ring-ring interactions, since there is also an increase in contact probability with H0S, especially for H3. Although the H10 peak remains at longer distances than the remaining, the region around and below 0,25 nm shows an increase, translating into close IL cation tail-vanillin ring contact, possibly due to dispersive interactions. Finally, it is clearly seen that the added quantity of 100 NaCl molecules did not cause significant differences in the RDF profiles, nor on the CN, as the middle and bottommost spectra are virtually identical, although a slight increase in probability and CN can be seen, hinting increased IL-vanillin interactions. It is also important to emphasize the difference between passing from 10 to 20 vanillin, that is, below and above the solubility limit, as the latter is likely to form vanillin aggregates akin to precipitate. This could dampen the probability of site-specific interactions that would be present were the solution saturated and no further. The probability of finding some IL cation molecules within these insoluble aggregates also exists. Thus, interactions between H0S and the IL cation evidence once more the importance of hydrophobic interactions towards hydrotropic solubilisation.

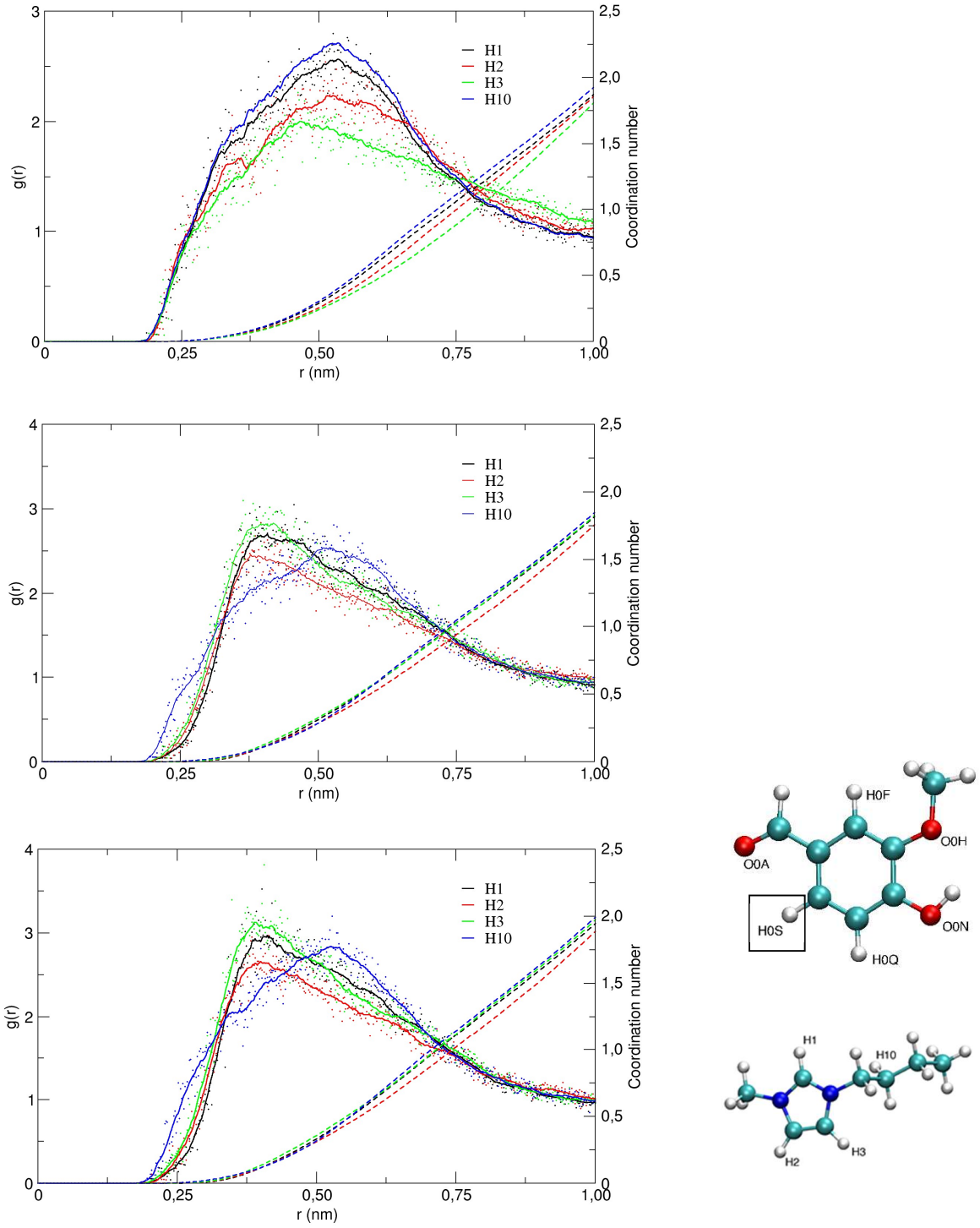

Figure 26. Radial distribution functions for the H0S hydrogen of the vanillin ring as reference, and the four hydrogens of the IL cation as selection, for the following conditions: 10 vanillin molecules in aqueous IL (top), 20 vanillin molecules in aqueous IL (middle), and 20 vanillin molecules in aqueous IL with 100 NaCl molecules added (bottom).

The second interactions considered will be the interactions between the oxygen atoms of the vanillin aldehyde, hydroxyl and methoxy groups with the various hydrogens of the IL cation. The profiles obtained for the aldehyde oxygen, O0A, are depicted in Figure 27, and the remaining in Figures SI:7 and SI:8, included in the additional information section as the general qualitative behaviour is similar between the three groups. The stark difference from the previous RDFs is undoubtedly the profile for H10 in the first condition, 10 vanillin in aqueous IL, for which the first peak is immensely more pronounced than the remaining and the CN likewise. Besides this one, the H10 profile also presents three other minor peaks, although much bigger than those of the other hydrogens. Thus, at this condition, the vanillin functional groups are very likely to be in close contact with the hydrophobic tail of the IL ring. Given the low *r* distance of the H10 peak, especially in the first condition, it is very likely that hydrophobic tail-vanillin functional group interactions are solvophobic interactions. As vanillin is added beyond solubility, the H10 peak decreases in comparison to the other RDF peaks. The remaining RDF peaks increase denoting increased ring-ring interactions in this condition, at enough proximity to hint at solvophobic interactions and hydrogen bonding. The difference in *r* between H10 and the remaining peaks for the hydroxyl and methoxy groups, which distance roughly coincides with the intramolecular distance between the ring and H10, suggests the IL to be oriented with the polar head closer to the vanillin ring, and the tail away from it, while the broadness of the peak suggests a wider range of potential interaction geometries. In the simulated systems beyond solubility limit conditions, H2 generally becomes once again the ring hydrogen that will less interact with the vanillin oxygens. H3, the hydrogen closest to the hydrophobic tail, remains in overall the more interactive of the three ring hydrogens. The loss of definition in peaks and their increased broadness above solubility when compared to below may be indicative that the larger the aggregates become, the less ordering there is within them. This is why the peak for H10 in condition (c) is so large and well defined, as aggregates are smaller and well-ordered; the increase in size means increased molecular density, and as so, given the various possible interaction geometries, a bigger variety of atoms at varying distances will fall within the RDF radius and provide a less well-defined plot. This agrees well with the NMR data that showed the loss in site specificity in vanillin-IL aggregates of bigger sizes. In all cases, the addition of salt had little effect beyond slightly improving all interactions, evidencing increased overall aggregation. Figure 28 provides an example of IL-vanillin clustering showcasing the discussed interactions. Overall, results point towards two markedly different behaviours: below the solubility limit of vanillin aggregation is moderate and hydrophobic interactions are very exclusive and as so very easily identifiable in the RDF plots. Above this limit,

hydrophobic interactions lose their exclusivity and ring-ring interactions become more prominent. It is also at this concentration of vanillin that significant aggregation is seen, as evidenced by the SASA profiles.

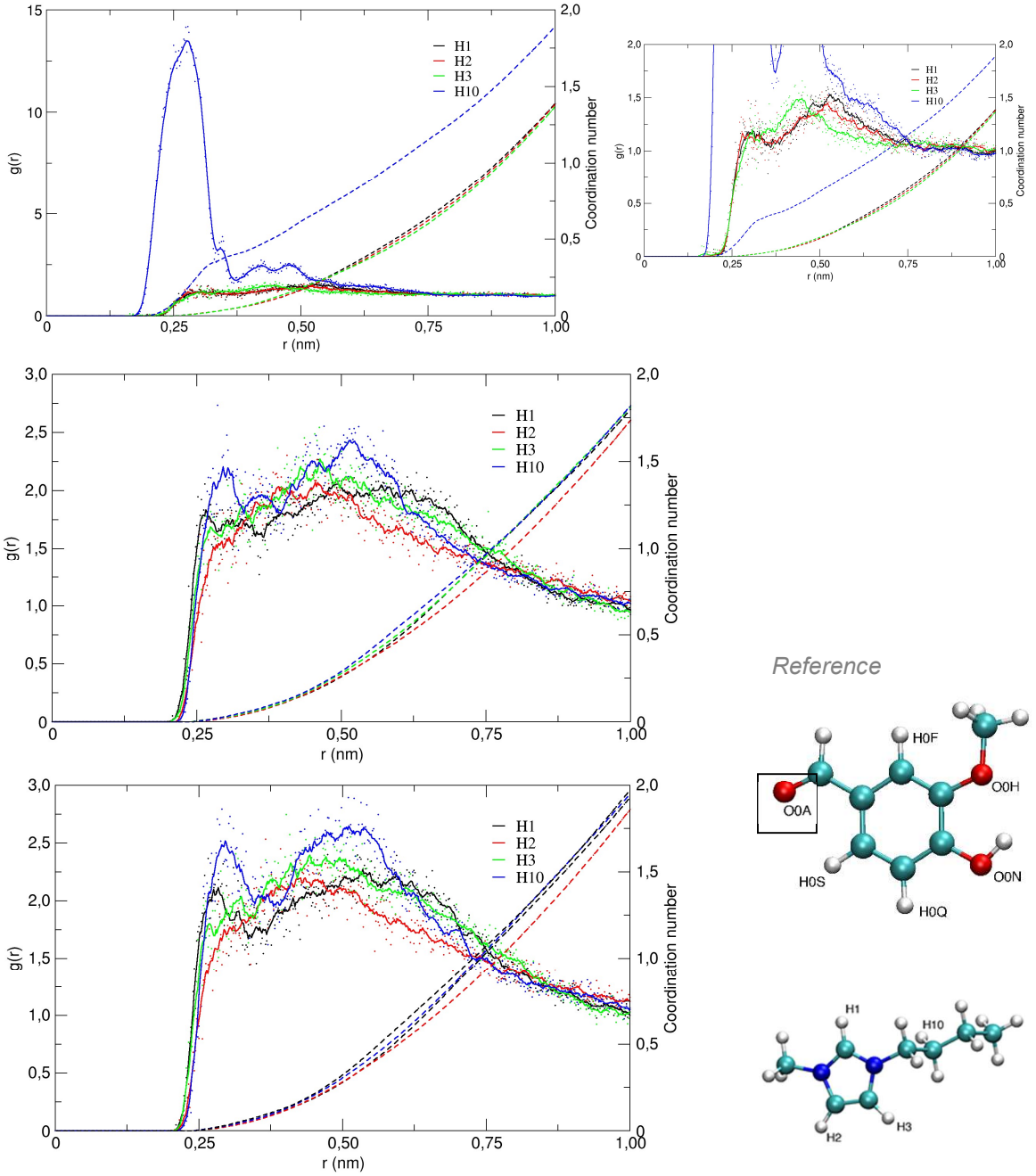

Figure 27. Radial distribution functions for the O0A oxygen of the vanillin aldehyde group as reference, and the four hydrogens of the IL cation as selection, for the following conditions: 10 vanillin molecules in aqueous IL (top, with respective ampliation on the right), 20 vanillin molecules in aqueous IL (middle), and 20 vanillin molecules in aqueous IL with 100 NaCl molecules added (bottom).

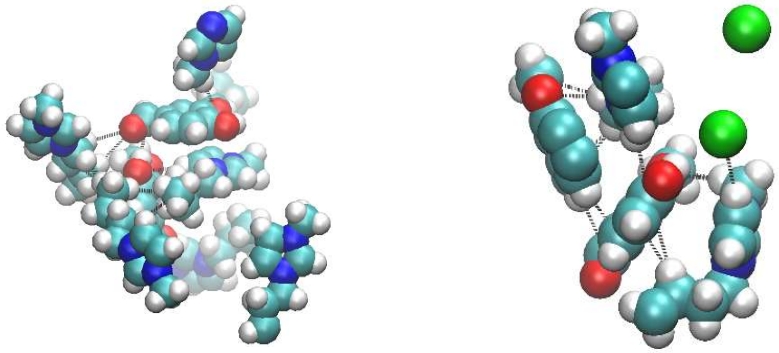

Figure 28. Different examples of IL-vanillin aggregates and possible hydrogen bonding. Depicted are vanillin (with red oxygen atoms), the IL cation (with blue nitrogen atoms) and chloride (green). Snapshots taken from system (e) 20 vanillin in 100 IL with added 100 NaCl.

Figure 29 depicts SDFs for IL-vanillin interactions as calculated from conditions (c) and (d), 10 and 20 vanillin in IL, respectively. The stronger hydration of the hydroxyl group is evident, while it is also an area where chloride seems to be more probable. Vanillin aggregation is potentiated, as expected through the formation of aggregates in a system containing both hydrotrope and solute. This aggregation is seen mainly via planar stacking of vanillin molecules, that is, with their rings parallelly arranged, and especially marked with 20 vanillin, suggesting ring stacking to be prominent at this vanillin concentration. It is also seen that the IL cation tail is more likely to interact than its polar head, although considerable ring-ring interactions are present. This once again evidences the importance of hydrophobic interactions in hydrotropic solubilisation, and is in accordance with previous data, such as the higher shielding evidenced for the IL tail when solute is present. This data also suggests that the great majority of IL-vanillin interactions are made in a planar fashion, with the IL placing itself above and below the vanillin hydrocarbon ring.

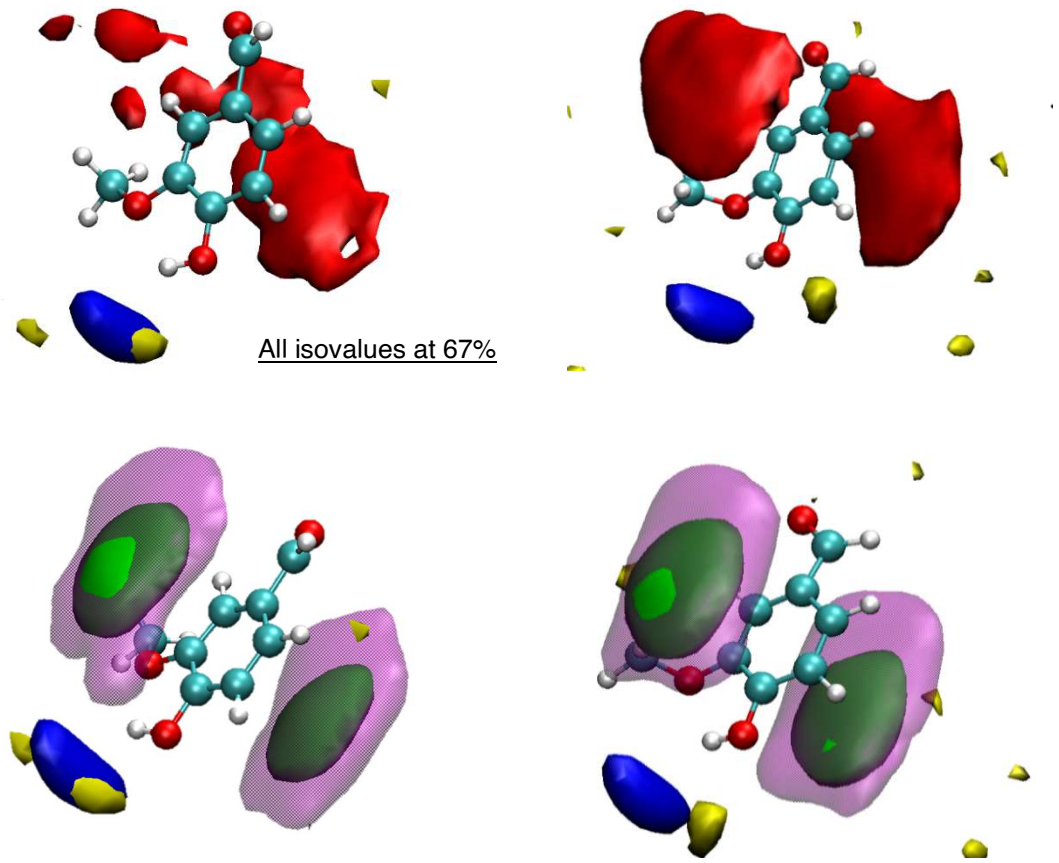

Figure 29. Spatial Distribution Functions of water (blue), chloride (yellow), vanillin (red), the IL cation head (green), and the IL cation tail (purple) with vanillin as the reference molecule, for condition (c) 10 vanillin in aqueous 100 IL (left) and (d) 20 vanillin in aqueous 100 IL (right).

The addition of 100 NaCl molecules, as in condition (e) 20 vanillin in aqueous IL with 100 NaCl, produced the SDF plots depicted in Figure SI:9, where the only alteration worth of noting in the IL-vanillin interactions, as the surface area of density of both IL head and tail around vanillin is increased in this condition when compared to the previous. Such increase points to the fact that the addition of salt promoted IL-vanillin interactions, probably due to the dehydrating effect this addition may have caused, forcing both hydrophobic interactions and ring stacking, as to accommodate aggregates with less area in contact with the solvent.

SDFs focusing on vanillin-IL interactions were also obtained with the $[C_4mim]^+$ cation as reference, depicted in Figure 30. The hydration sphere of the IL cation is well-defined, and the chloride presence near H1 and H2 is clear. With 20 vanillin the hydration sphere is

still maintained but the chloride density diminishes significatively. As to be expected considering the SDFs with vanillin as a reference, vanillin surrounding the IL cation is majorly found in parallel planes relative to the imidazolium ring. This ring stacking is possibly being stabilized by the chloride anions, given the good complementarity of the density surfaces of vanillin and Cl^- In fact, Matthews *et al.*[106] have verified that π-π interactions between imidazolium-chloride ionic liquid molecules in clusters are stabilised by the presence of anions between and at the periphery of the rings, and Gao *et al.*[107] noted the peculiarity in the stacking of imidazolium rings and how important C-H···X interactions are to this effect. Restricting the isovalues to 80% of its maximums makes it possible to better see the structuring of IL cation-vanillin aggregates. IL head aggregation is noted, albeit slightly uneven, at a distance superior to that of vanillin aggregation around the reference IL molecule, effectively creating a “sandwich-like” structure, where vanillin molecules are interspersed with IL cation molecules. Bumping isovalues to 90% makes this structuring even more neat. Finally, IL head hydration with very strict isovalues maintains the ring-like density profile, as it did even in IL in water only, showing the most hydration on H1 and H2.

The addition of salt produced the SDFs seen in Figure SI:10, where the hydration sphere around the IL head is maintained, but the density of Cl^- becomes completely uneven, no longer to be more likely found near H1 and H2. The stacking effect with inclusion of other IL heads besides the one of the reference can also be seen at lower isovalues, and is visualized very neatly at 80%. Worthy of the most attention however is the fact that at higher isovalues interactions between the reference and the IL tail in the plane of the imidazolium ring can be clearly seen, indicating thus increased IL aggregation and hydrophobic interactions upon addition of salt. The fact that this condition also presents, on the IL ring, poorer hydration than without salt is worth of mentioning as well.

One of the most interesting structuring details is the stacking of rings seen throughout all conditions with solute. These structures are depicted in Figure 31 and clearly correlate with the SDF plots showing the same stacking with the stacking effect through π-π interactions. Imidazolium rings are known to exhibit such behaviour between their molecules, effectively forming clusters via ring H-bonds with subsequent charge transfer and ring polarization, and π-π interactions stabilised by chloride anions.[106,108]

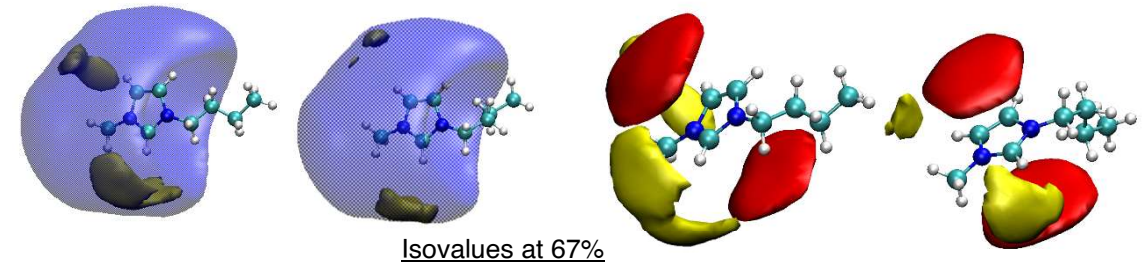

Isovalues at 67%

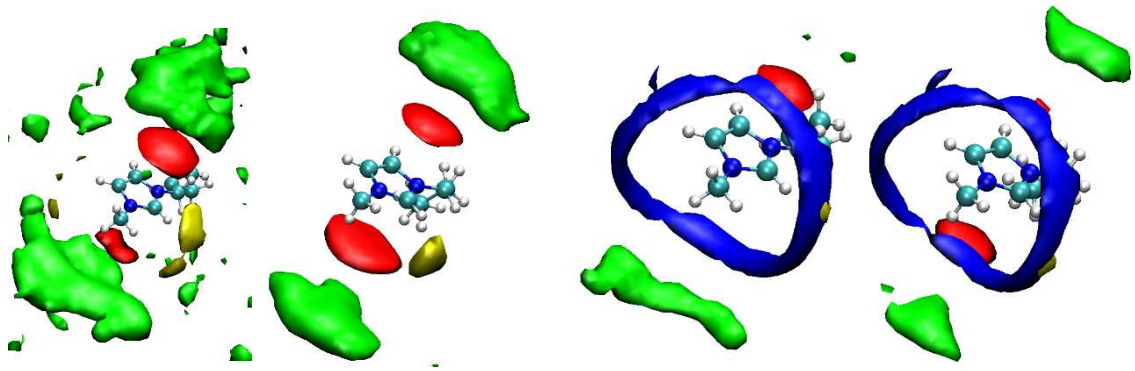

Isovalues at 80% Isovalues at 90% Isovalues at 80% Isovalues at 90%

Figure 30. Spatial Distribution Functions of water (blue), chloride (yellow), vanillin (red), and the IL cation head (green) with the IL cation as the reference molecule, for condition (c) 10 vanillin in aqueous 100 IL (left) and condition (d) 20 vanillin in aqueous IL (right).

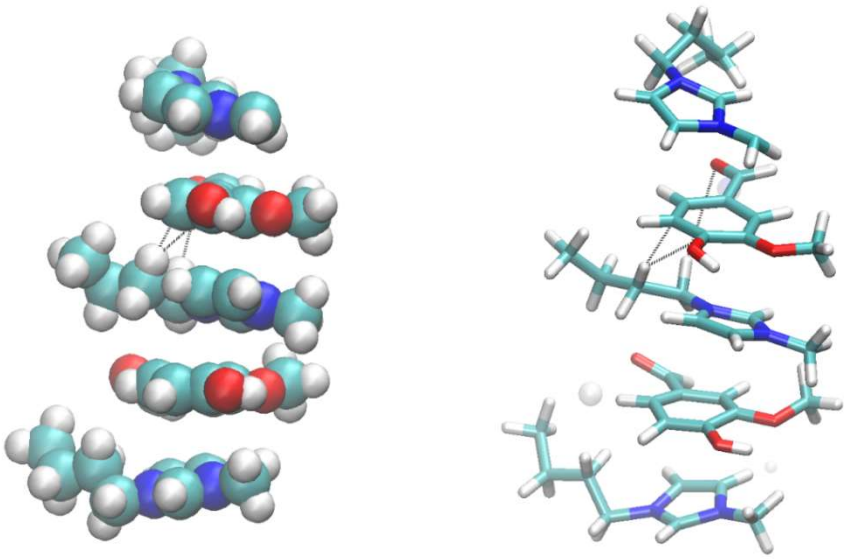

Figure 31. Vanillin (with red oxygen atoms) and IL cation (with blue nitrogen atoms) aggregates evidencing ring stacking. Van der Waals (left) and licorice (right) representations. Snapshot taken from system (d) 20 vanillin in 100 IL.

Table 4. Summary of radial distribution function values for the first peak obtained for the systems including both IL and vanillin.

System	Vanillin reference atom	H1		H2		H3		H10	
		Peak *r* (nm)	CN	Peak *r* (nm)	CN	Peak *r* (nm)	CN	Peak *r* (nm)	CN
(c)	H0S	0,53	0,37	0,51	0,28	0,46	0,18	0,53	0,40
	O0A	0,32	0,03	0,30	0,02	0,30	0,02	0,28	0,20
	O0H	0,50	0,18	0,65	0,45	0,50	0,14	0,26	0,13
	O0N	0,30	0,02	0,32	0,02	0,44	0,09	0,26	0,16
(d)	H0S	0,40	0,11	0,39	0,10	0,41	0,15	0,53	0,37
	O0A	0,30	0,03	0,44	0,16	0,46	0,21	0,29	0,02
	O0H	0,40	0,15	0,42	0,17	0,40	0,14	0,45	0,17
	O0N	0,35	0,10	0,35	0,08	0,38	0,13	0,33	0,05
(e)	H0S	0,40	0,12	0,39	0,10	0,40	0,15	0,53	0,41
	O0A	0,30	0,04	0,44	0,18	0,46	0,23	0,29	0,03
	O0H	0,40	0,15	0,42	0,18	0,38	0,15	0,45	0,19
	O0N	0,35	0,10	0,35	0,08	0,38	0,13	0,33	0,05

ii. Solute-water interactions

Binary vanillin-water interactions will now be considered. The subsequent RDF plots are depicted in Figure 32. In the condition in which vanillin was simply dissolved in water, the obtained RDF profiles show a much higher probability for all four atoms probed, as is evident. For all oxygens, the first sphere of hydration was well defined at 0,18/0,19 nm. The region of the second peak serves as a good measure of the hydrophilicity of the three functional groups the oxygens belong to, as the peak is higher in the hydroxyl group, the most hydrophilic, and lower in the methoxy group, the least hydrophilic of the three. Vanillin dissolved in aqueous IL shows significantly less hydration when compared to when dissolved in water, as all four profiles show less probability at all distances. Interestingly, there is a markedly different behaviour in regards to solute concentration between the ring hydrogen and the functional group hydrogens: the profile of H0S did not change from the conditions of 10 to 20 vanillin in aqueous IL, whereas the profile of the oxygens shows less hydration in the 20 vanillin condition than in the 10 vanillin one. Finally, there is a slight effect observed due to the addition of salt, as every profile, including the H0S profile, shows a small decrease in water probability, which agrees with the fact that this addition induces a slight salting-out effect, consistent with a slight increase in hydrotrope aggregation, forcing water contact with vanillin, a hydrophobic solute, and thus reducing its solubility.

Binary IL-water interactions, for which the obtained RDF plots are compiled in Figure 33, show how H10 barely registered any difference between tested conditions. Considering the hydrophobicity of the IL cation tail, it is understandable the inexistence of significant peaks, especially at shorter values of *r*, as water is less likely to be found around these moieties. H2 is the most well hydrated hydrogen of the imidazolium ring, followed by H1 and finally by H3. It is evident that the addition of vanillin alters IL cation-water interactions. As seen in the experimental section, the addition of a solute will promote IL cation nucleation around it, mostly through hydrophobic cation tail-vanillin ring interactions. Therefore, water must be successively pushed out of the nucleation zones as solute concentration increases and would be more likely to interact with the ring. The addition of 100 NaCl molecules provided again virtually no change in any profile.

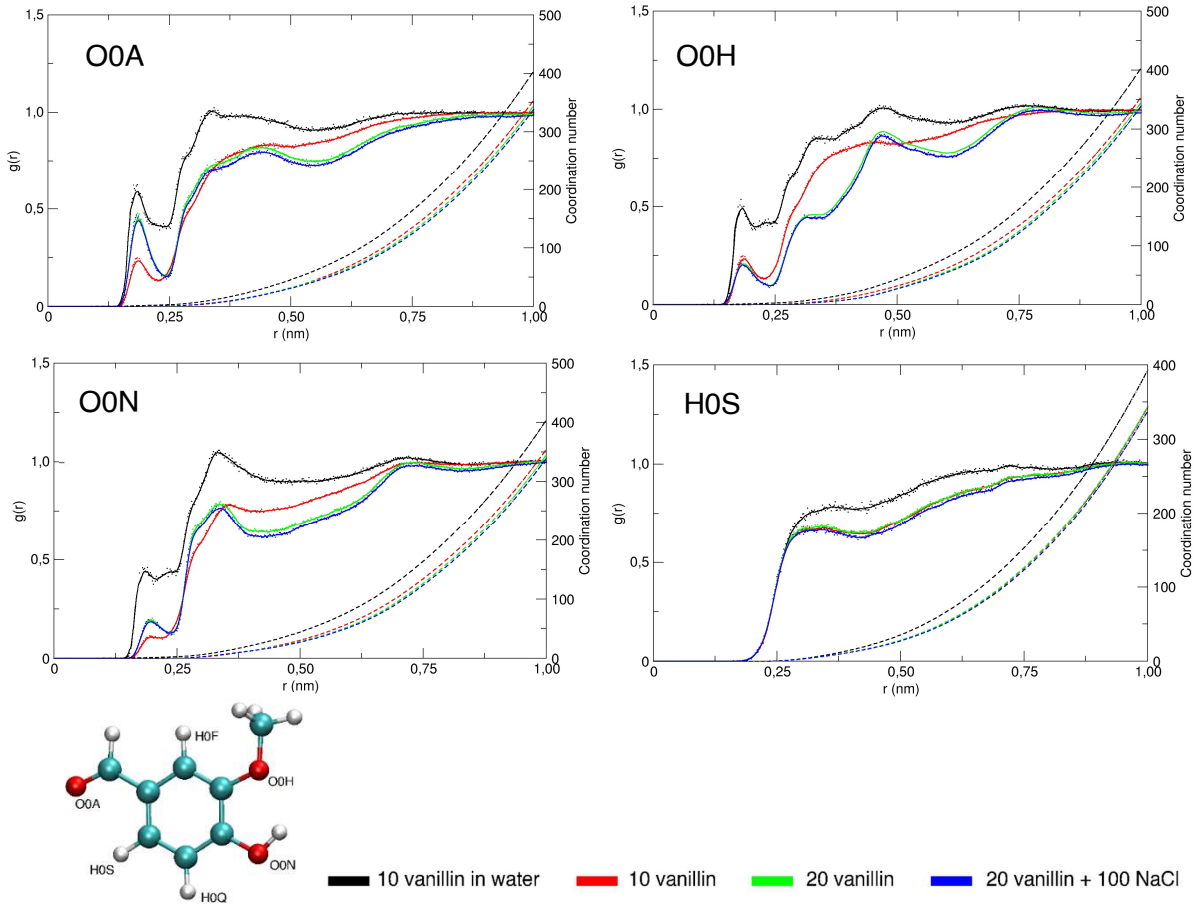

Figure 32. Radial distribution functions for the three selected functional group oxygens and hydrocarbon ring hydrogen of vanillin as reference, and water as selection.

The SDFs concerning the IL and vanillin interactions with water can be found in Figures SI:11 and SI:13. A more restrictive isovalue allows to see that the preferential hydration zones are around hydrogens 1 and 2 of the imidazolium ring, which denotes the more hydrophobic character of hydrogen 3 and shows the availability of the methyl group. It is very important to note how this data places the most probability of chloride interactions on H1, the hydrogen in between the nitrogen atoms of the ring, fact that supports the NMR data showing this hydrogen as suffering the most deshielding upon increase in IL concentration in aqueous solution, and the emulates the neat pure IL molecular organization.

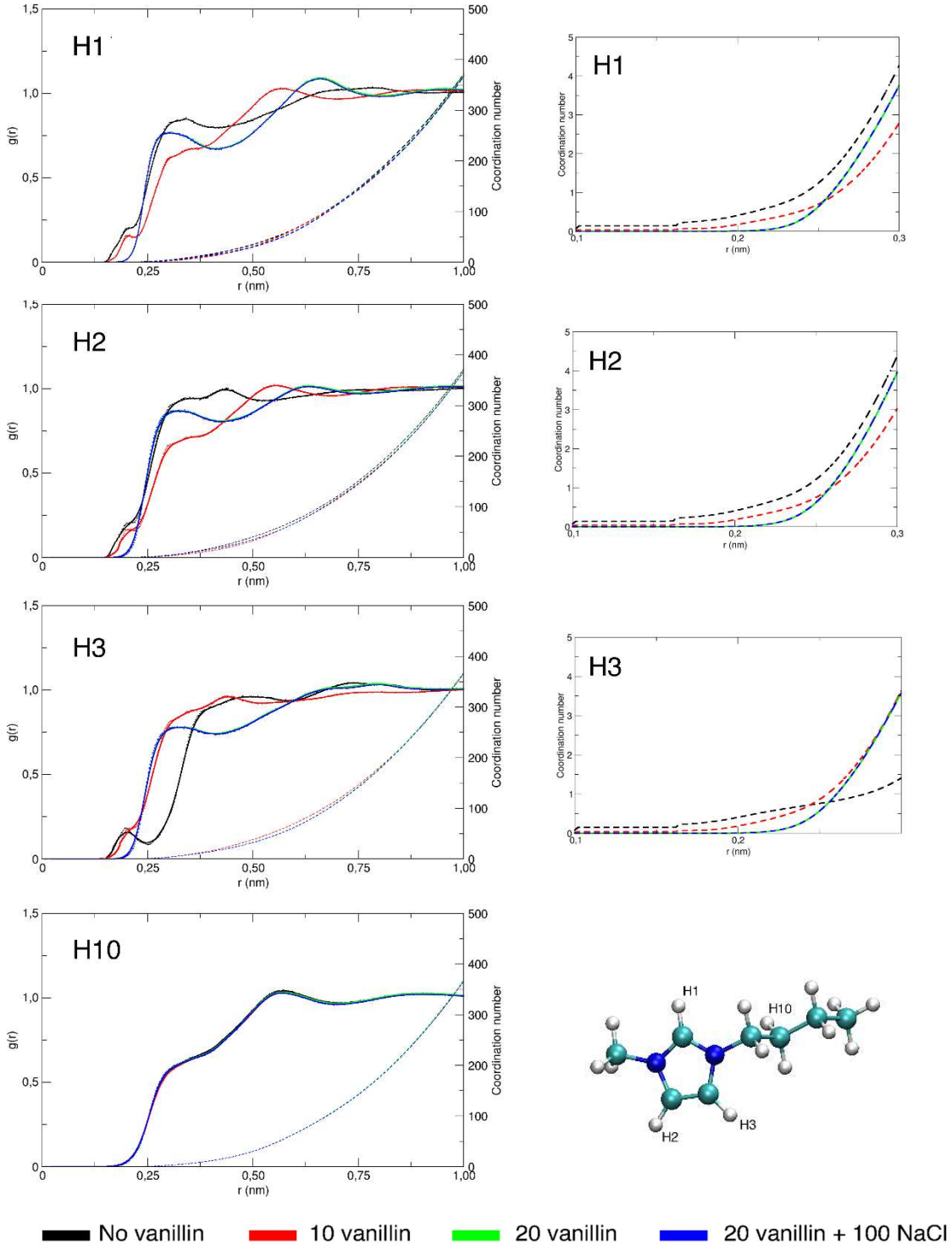

Figure 33. Radial distribution functions for the four selected hydrogens of the IL cations as reference, and water as selection.

Table 5. Summary of radial distribution function values for the first peak obtained for the systems including IL or vanillin in water.

System	H1		H2		H3		H10	
	Peak *r* (nm)	CN	Peak *r* (nm)	CN	Peak *r* (nm)	CN	Peak *r* (nm)	CN
(a)	0,34	8,3	0,35	10,3	0,48	28,6	0,57	54,7
(c)	0,34	5,8	0,35	7,2	0,35	8,8	0,57	52,9
(d)	0,30	3,8	0,31	4,9	0,31	4,4	0,57	53,3
(e)	0,30	3,8	0,31	4,9	0,31	4,4	0,57	53,1
System	H0S		O0A		O0H		O0N	
	Peak *r* (nm)	CN	Peak *r* (nm)	CN	Peak *r* (nm)	CN	Peak *r* (nm)	CN
(b)	0,37	11,1	0,18	1,4	0,18	1,3	0,19	1,4
(c)	0,33	5,3	0,18	0,1	0,18	0,1	0,20	0,1
(d)	0,34	6,3	0,18	0,2	0,19	0,2	0,20	0,2
(e)	0,34	6,2	0,18	0,1	0,18	0,1	0,19	0,1

4. Summary of findings

Herein it is evidenced that the addition of chloride salts promotes the salting-out, and thus a decrease in solubility, of vanillin, a hydrophobic solute, in aqueous solutions of [C_4mim]Cl. This decrease in solubility is subject to differences according to which salt is added, and tends to follow a trend majorly in accordance with the salt cation valence and the Gibbs free energy of hydration, that is, the higher the valence and the lesser the free energy, the stronger the detrimental effect to hydrotropic vanillin solubility. Nevertheless, oddnesses in the solubility behaviour for some salts recommend caution when applying a trend and state that these parameters are insufficient to act as a full description of how chloride salts influence vanillin solubility in IL solutions. A more nuanced behaviour is expressed, and for a correct prediction of solubility behaviour other parameters should be accounted for, particularly those that affect how a given cation interacts at its hydration shell level. The same general trend is verified through NMR analyses of salted IL solutions saturated with vanillin, in which solutions doped with salts of higher valence show a more shielded environment for the IL cation and vanillin, suggesting induction of aggregation both by the presence of salt and the solute. This technique also allowed to understand how site-specificity in ionic liquid interactions with vanillin is high, and how it diminishes when salt is added to the equation, even at moderate concentrations such as 1 M. This suggestion for aggregation is confirmed through DLS analyses, in which the general trend of aggregation can be observed to be consistent with the aforementioned one, as higher valence salt cations promote bigger aggregates and lead the system closer to phase separation. A causal effect can be suggested throughout, as higher valence salts bind water with greater strength, dehydrating the IL and promoting its self-aggregation, leaving less of it available to interact with vanillin and promote its hydrotropic solubility – hence decreased solubility, higher shielding of both vanillin and IL cation, and bigger aggregates in solution. Molecular dynamics simulations also present evidence towards the fact that solute presence is crucial for potentiation of the hydrotropic effect and show how clustering of hydrotrope-solute is prominent. π-π interactions and ring stacking are very important interactions at play in this clustering, and chloride seems to play a stabilising role. RDF analyses also showed how bigger aggregates tend to become less ordered than smaller ones, effectively possessing more varied interactions and geometries, fact that separates hydrotropic solubilization from the more ordered micellar solubilization. The used all-atomistic models showed results consistent with experimental ones and with the literature, therefore posing themselves as adequate to the study of imidazolium-based hydrotropic systems. Thus, evidence is

presented in this work that supports hydrophobic hydrotrope-solute interactions as the main interactions at play towards the hydrotropic solubilization effect, in accordance to the statistical thermodynamic descriptions of the hydrotropic mechanism.[38] It is also displayed how the addition of salts induces greater IL aggregation, once again mostly through hydrophobic interactions, and how this aggregation is prejudicial to the hydrotropic effect – despite hydrophobic interactions being increased upon salting, the hydrotrope aggregation will diminish the number of hydrotrope molecules available to contribute to solubilization, and so will hinder the hydrotropic effect. It is of extreme importance to note how this directly contradicts the theory that hydrotrope aggregates (pre-clustering) are beneficial or even required to hydrotropic solubilisation that some authors reported in the past.

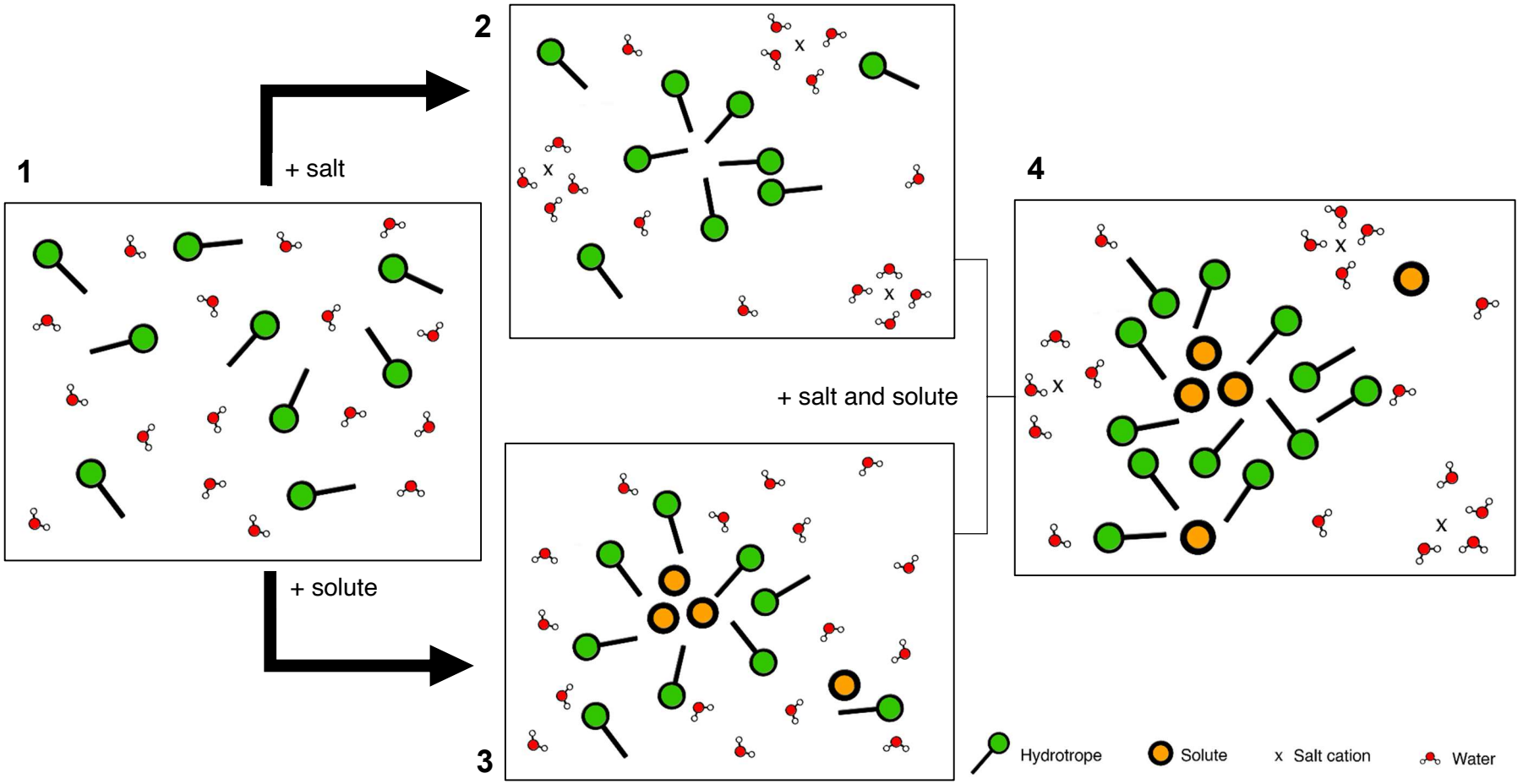

Figure 34. General interactions studied throughout this work. From the hydrotrope in solution (1), the addition of salt will promote hydrotrope aggregation, with preference for interactions involving the hydrophobic tail. This aggregation is due to dehydration induced by strong ion-water interactions (2). The addition of solute will promote aggregation of the hydrotrope but around the solute, central in hydrotropy. The main interactions are hydrophobic (3). The addition of both salt and solute will promote larger and less organized aggregates, but the salting will hinder solubility (4).

Chapter IV
Conclusions and future work

The main goal of this work was the gaining of insight over the effect of the presence of inorganic salts on hydrotropy, using aqueous solutions of $[C_4mim]Cl$, an imidazolium-based ionic liquid, and vanillin, a sparingly soluble hydrophobic organic compound. Along with this objective, furthering the knowledge over the generality of the hydrotropic effect was aimed at as well, both experimentally and using molecular dynamics simulations. The behaviour of the aqueous ionic liquid solutions when salted was found to be insufficiently explained by any singular parameter, exhibiting many nuances throughout the tested salts. The Gibbs free energy of hydration of the salt cation added may be one of the best ways to predict how the salting will affect hydrotropic solubility, but other thermodynamic and chemical specificities play a considerable part. It was found that salting these solutions promotes aggregation of the ionic liquid by dehydrating it, effectively originating larger aggregates the more this dehydrating effect was felt. These larger aggregates were also found to hinder vanillin solubility, clueing how pre-clustering of the hydrotrope is not beneficial towards hydrotropy. The model of hydrotropy proposed by Shimizu and colleagues was supported by the present work, as hydrotropy was found to be linked with hydrotrope and solute aggregation and driven mainly by hydrophobic interactions. Site specificity of hydrotrope-solute interactions was evidenced and seen to be dampened by the addition of salt. The molecular dynamics approach was found to complement well the experimental one, providing consistent results and showing the adequacy of the utilized models and force-fields towards imidazolium-based hydrotropy description. Hydrophobic interactions were found to be central in the presence of both hydrotrope and solute. Aggregation of the hydrotrope around the solute was probed and visualized, and several ionic liquid-vanillin sites of interaction seen. π-π interactions, translated into ring stacking, were particularly prominent throughout the simulations, and agree well with previous literature on molecular dynamics with imidazolium-based compounds. Larger aggregates, occurring with vanillin added above solubility limit, were found to be less ordered than smaller ones, possessing varied more varied interactions and geometries. Simulations then supported the importance of hydrophobic interactions and hydrotrope-solute aggregation in hydrotropy. Figure 34 schematizes the major interactions probed throughout this work, and so summarizes its main conclusions.

As so, hydrotropy reaffirms itself as a promising technique in the field of separations and drug solubilization. The particularities of solubilization behaviour in salted environments may have interesting and creative biological applications, since different *in vivo* locations possess different electrolyte environments.

Future essays to complete the partial picture portrayed in this work would be useful, namely NMR and DLS analyses, with a similar method to the herein used, salting IL solutions with and without vanillin with KCl and $CaCl_2$. Similarly, the same approach with additional salts such as CsCl might prove interesting. These analyses would allow a more comprehensive understanding of the behaviour of hydrotropy with IL liquid aqueous solutions doped with inorganic salts, permitting the more precise establishment of an eventual correlation with thermodynamic parameters such as the Gibbs free energy of hydration, with the different arrangements of the direct, indirect or reverse Hofmeister Series, or with more particular chemical properties of the cations. This is important towards the achievement of a sufficiently accurate predictive model for imidazolium-based hydrotropy in salted or otherwise electrolyte-heavy environments. As this work probed the effect of the salt cation, a logical next step would be the testing of the effect of the anion. In that sense, a preliminary effort was made in this work by testing 1 M of sodium acetate ($NaCH_3COO$), thiocyanate (NaSCN), and nitrate ($NaNO_3$) in both 0,5 M and 1,5 M [C_4mim]Cl aqueous solutions with posterior saturation with vanillin. It was assessed that all these systems phase separated, except sodium nitrate in 0,5 M IL that returned a vanillin concentration of around 45,4 ± 2,9 $g.L^{-1}$, effectively providing a slight salting-in effect.

Vanillin is a sparingly soluble compound in water, and despite its solubility being massively increased in [C_4mim]Cl, the simulation of a system analogous to the ones experimentally performed throughout this work requires the presence of several tens of thousands of molecules, only to have present within them few dozens of vanillin molecules. For a system with a considerable high amount of solvated vanillin molecules, the computational requirements are elevated. The development of accurate coarse-grained models for the necessary molecules would allow to efficiently simulate significantly sized systems, while lessening these requirements, and as so would be interesting for future work. An increase in scale of the systems described in this work would then be useful as well, as more significant conclusions could be extrapolated. In the course of this work, an attempt was made at the development of adequate CG models for this finality. Figures 35 and 36 depict the attempted AA to CG mapping that unfortunately presented unwanted and excessive aggregation and as so will need to be further improved. Similarly, the simulation of systems at higher salt concentrations is in demand, as well as the development and application of adequate models for divalent and trivalent salt cations.

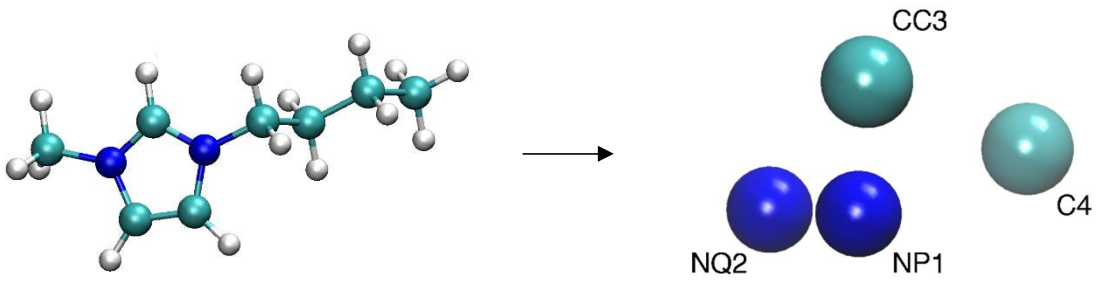

Figure 35. All-atom (left) to coarse-grain (right) modelling by the MARTINI model attempted in this work for the $[C_4mim]^+$ cation. The ring was represented by beads NP1, of bead type SP5, polar ring bead with very high polar affinity, NQ2, of bead type SQd, charged ring bead acting as hydrogen bond donor, and CC3, of bead type SP1, polar ring bead with low polar affinity, and the tail by bead C4, of bead type SC1, apolar bead with low polar affinity.

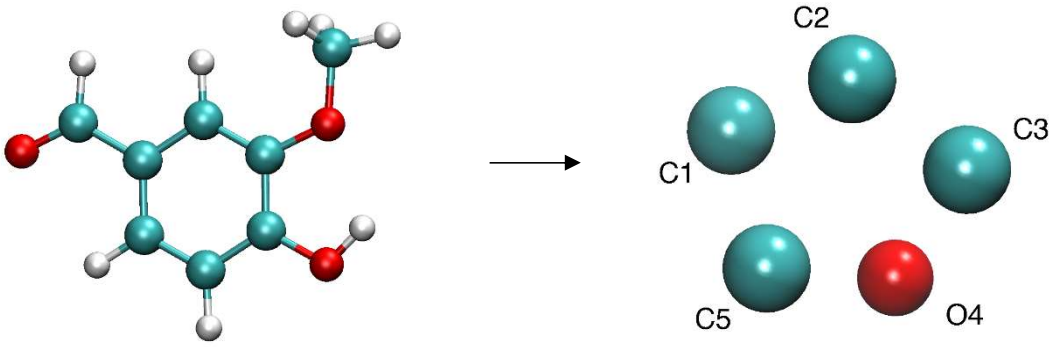

Figure 36. All-atom (left) to coarse-grain (right) modelling by the MARTINI model attempted in this work for the vanillin molecule, with beads C1, of bead type SNda, nonpolar bead acting as both donor and acceptor of hydrogen bonds, C2, of bead type SC4, apolar bead with high polar affinity, C3, of bead type SQa, charged bead acceptor of hydrogen bonds, O4, of bead type SC5, apolar bead with high polar affinity, and C5, of bead type SC4.

Chapter V
Bibliography

1. Poliakoff, M. & Licence, P. Sustainable technology: Green chemistry. *Nature* **450**, 810–812 (2007).
2. Earle, M. J. & Seddon, K. R. Ionic liquids: Green solvents for the future. *ACS Symp. Ser.* **819**, 10–25 (2002).
3. Cláudio, A. F. M. *et al.* The magic of aqueous solutions of ionic liquids: Ionic liquids as a powerful class of catanionic hydrotropes. *Green Chem.* **17**, 3948–3963 (2015).
4. Sintra, T. E. *et al.* Enhanced dissolution of ibuprofen using ionic liquids as catanionic hydrotropes. *Phys. Chem. Chem. Phys.* **20**, 2094–2103 (2018).
5. Barzegar-Jalali, M. & Jouyban-Gharamaleki, A. A general model from theoretical cosolvency models. *Int. J. Pharm.* **152**, 247–250 (1997).
6. Bockris, J. O., Bowler-Reed, J. & Kitchener, J. A. The salting-in effect. *Trans. Faraday Soc.* **47**, 184 (1951).
7. Edwards, D. A., Liu, Z. & Luthy, R. G. Surfactant Solubilization of Organic Compounds in Soil/Aqueous Systems. *J. Environ. Eng.* **120**, 5–22 (1994).
8. Kunieda, H. & Friberg, S. E. Critical Phenomena in a Surfactant/Water/Oil System. Basic Study on the Correlation Between Solubilization, Microemulsion, and Ultralow Interfacial Tensions. *Bulletin of the Chemical Society of Japan* vol. 54 1010–1014 (1981).
9. Rasenack, N. & Müller, B. W. Micron-Size Drug Particles: Common and Novel Micronization Techniques. *Pharm. Dev. Technol.* **9**, 1–13 (2004).
10. Agrawal, Y. & Patel, V. Nanosuspension: An approach to enhance solubility of drugs. *J. Adv. Pharm. Technol. Res.* **2**, 81 (2011).
11. Xua, S. & Dai, W. G. Drug precipitation inhibitors in supersaturable formulations. *Int. J. Pharm.* **453**, 36–43 (2013).
12. Kim, H., Kim, H. W. & Jung, S. Aqueous solubility enhancement of some flavones by complexation with cyclodextrins. *Bull. Korean Chem. Soc.* **29**, 590–594 (2008).
13. Modi, A. & Tayade, P. Enhancement of dissolution profile by solid dispersion (kneading) technique. *AAPS PharmSciTech* **7**, 1–6 (2006).
14. Jain, P., Goel, A., Sharma, S. & Parmar, M. Solubility Enhancement Techniques with Special Emphasis on Hydrotropy. *Int. J. Pharma Prof. Res.* **1**, 34–45 (2010).
15. Kunz, W., Holmberg, K. & Zemb, T. Hydrotropes. *Curr. Opin. Colloid Interface Sci.* **22**, 99–107 (2016).
16. Neuberg, C. Hidrotropy. *Biochem. Z* **76**, 107–108 (1916).
17. Hough, W. L. *et al.* The third evolution of ionic liquids: Active pharmaceutical ingredients. *New J. Chem.* **31**, 1429–1436 (2007).

18. Kim, J. Y., Kim, S., Papp, M., Park, K. & Pinal, R. Hydrotropic solubilization of poorly water-soluble drugs. *J. Pharm. Sci.* **99**, 3953–3965 (2010).
19. Tavare, N. S. & Colonia, E. J. Separation of eutectics of chloronitrobenzenes through hydrotropy. *J. Chem. Eng. Data* **42**, 631–635 (1997).
20. Ferraz, R., Branco, L. C., Prudêncio, C., Noronha, J. P. & Petrovski, Ž. Ionic liquids as active pharmaceutical ingredients. *ChemMedChem* **6**, 975–985 (2011).
21. Gaikar, V. G. & Sharma, M. M. Separations with hydrotropes. *Sep. Technol.* **3**, 2–11 (1993).
22. Hodgdon, T. K. & Kaler, E. W. Hydrotropic solutions. *Curr. Opin. Colloid Interface Sci.* **12**, 121–128 (2007).
23. Srinivas, V. *et al.* Molecular organization in hydrotrope assemblies. *Langmuir* **13**, 3235–3239 (1997).
24. Subramanian, D., Boughter, C. T., Klauda, J. B., Hammouda, B. & Anisimov, M. A. Mesoscale inhomogeneities in aqueous solutions of small amphiphilic molecules. *Faraday Discuss.* **167**, 217–238 (2013).
25. Balasubramanian, D., Srinivas, V., Gaikar, V. G. & Sharma, M. M. Aggregation behavior of hydrotropic compounds in aqueous solution. *J. Phys. Chem.* **93**, 3865–3870 (1989).
26. Barton, A. F. M. Solubility Parameters. *Chem. Rev.* **75**, 731–753 (1975).
27. Shimizu, S. & Matubayasi, N. The origin of cooperative solubilisation by hydrotropes. *Phys. Chem. Chem. Phys.* **18**, 25621–25628 (2016).
28. Setschenow, J. Über die Konstitution der Salzlösungen auf Grund ihres Verhaltens zu Kohlensäure. *Zeitschrift für Phys. Chemie* **4U**, (1889).
29. Sanghvi, R., Evans, D. & Yalkowsky, S. H. Stacking complexation by nicotinamide: A useful way of enhancing drug solubility. *Int. J. Pharm.* **336**, 35–41 (2007).
30. Frank, H. S. & Franks, F. Structural Approach to the Solvent Power of Water for Hydrocarbons; Urea as a Structure Breaker. *J. Chem. Phys.* **48**, 4746–4757 (1968).
31. Buchanan, P., Aldiwan, N., Soper, A. K., Creek, J. L. & Koh, C. A. Decreased structure on dissolving methane in water. *Chem. Phys. Lett.* **415**, 89–93 (2005).
32. Rezus, Y. L. A. & Bakker, H. J. Observation of immobilized water molecules around hydrophobic groups. *Phys. Rev. Lett.* **99**, 1–4 (2007).
33. Booth, J. J., Abbott, S. & Shimizu, S. Mechanism of hydrophobic drug solubilization by small molecule hydrotropes. *J. Phys. Chem. B* **116**, 14915–14921 (2012).
34. Shimizu, S. & Matubayasi, N. Hydrotropy: Monomer-micelle equilibrium and minimum hydrotrope concentration. *J. Phys. Chem. B* **118**, 10515–10524 (2014).

35. Russo, J. W. & Hoffmann, M. M. Measurements of surface tension and chemical shift on several binary mixtures of water and ionic liquids and their comparison for assessing aggregation. *J. Chem. Eng. Data* **56**, 3703–3710 (2011).
36. Subramanian, D. & Anisimov, M. A. Phase behavior and mesoscale solubilization in aqueous solutions of hydrotropes. *Fluid Phase Equilib.* **362**, 170–176 (2014).
37. Hopkins Hatzopoulos, M. *et al.* Are hydrotropes distinct from surfactants? *Langmuir* **27**, 12346–12353 (2011).
38. Booth, J. J., Omar, M., Abbott, S. & Shimizu, S. Hydrotrope accumulation around the drug: The driving force for solubilization and minimum hydrotrope concentration for nicotinamide and urea. *Phys. Chem. Chem. Phys.* **17**, 8028–8037 (2015).
39. Jain, P., Goel, A., Sharma, S. & Parmar, M. Solubility Enhancement Techniques with Special Emphasis on Hydrotropy. *Online* **1**, 34–45 (2010).
40. Maheshwari, R. K. & Jagwani, Y. Mixed hydrotropy: Novel science of solubility enhancement. *Indian J. Pharm. Sci.* **73**, 179–183 (2011).
41. Madan, J. R., Kamate, V. J., Dua, K. & Awasthi, R. Improving the solubility of nevirapine using A hydrotropy and mixed hydrotropy based solid dispersion approach. (2017).
42. Madan, J. R., Pawar, K. T. & Dua, K. Solubility enhancement studies on lurasidone hydrochloride using mixed hydrotropy. **5**, (2015).
43. McKee, R. H. Use of Hydrotropic Solutions in Industry. *Ind. Eng. Chem.* **38**, 382–384 (1946).
44. Kayali, I., Qamhieh, K. & Olsson, U. Formulating middle phase microemulsions using extended anionic surfactant combined with cationic hydrotrope. *J. Dispers. Sci. Technol.* **32**, 41–46 (2011).
45. Kayali, I., Qamhieh, K. & Olsson, U. Microemulsion phase behavior of aerosol-ot combined with a cationic hydrotrope in the dilute region. *J. Dispers. Sci. Technol.* **31**, 183–187 (2010).
46. Khan, Z. A. *et al.* Mixing behavior of cationic hydrotropes with anionic surfactant sodium dodecyl sulfate. *J. Dispers. Sci. Technol.* **32**, 1452–1458 (2011).
47. Rogers, R. D. & Seddon, K. R. Ionic Liquids - Solvents of the Future? *Science* **302**, 792–793 (2003).
48. Sowmiah, S., Srinivasadesikan, V., Tseng, M.-C. & Chu, Y.-H. On the Chemical Stabilities of Ionic Liquids. *Molecules* **14**, 3780–3813 (2009).
49. Cláudio, A. F. M., Freire, M. G., Freire, C. S. R., Silvestre, A. J. D. & Coutinho, J. A. P. Extraction of vanillin using ionic-liquid-based aqueous two-phase systems. *Sep.*

Purif. Technol. **75**, 39–47 (2010).

50. Cláudio, A. F. M. *et al.* Optimization of the gallic acid extraction using ionic-liquid-based aqueous two-phase systems. *Sep. Purif. Technol.* **97**, 142–149 (2012).
51. Walton, N. J., Mayer, M. J. & Narbad, A. Vanillin. *Phytochemistry* **63**, 505–515 (2003).
52. Dhinakaran, M., Morais, A. B. & Gandhi, N. N. Extraction of vanillin through hydrotropy. *Asian J. Chem.* **25**, 231–236 (2013).
53. Batista, M. L. S., Neves, C. M. S. S., Carvalho, P. J., Gani, R. & Coutinho, J. A. P. Chameleonic behavior of ionic liquids and its impact on the estimation of solubility parameters. *J. Phys. Chem. B* **115**, 12879–12888 (2011).
54. Rengstl, D., Kraus, B., Van Vorst, M., Elliott, G. D. & Kunz, W. Effect of choline carboxylate ionic liquids on biological membranes. *Colloids Surfaces B Biointerfaces* **123**, 575–581 (2014).
55. Hofmeister, F. Zur Lehre von der Wirkung der Salze - Dritte Mittheilung. *Arch. für Exp. Pathol. und Pharmakologie* **25**, 1–30 (1888).
56. Freire, M. G. *et al.* Aqueous biphasic systems: A boost brought about by using ionic liquids. *Chem. Soc. Rev.* **41**, 4966–4995 (2012).
57. Shahriari, S., Neves, C. M. S. S., Freire, M. G. & Coutinho, J. A. P. Role of the Hofmeister series in the formation of ionic-liquid-based aqueous biphasic systems. *J. Phys. Chem. B* **116**, 7252–7258 (2012).
58. Li, C. *et al.* Phase behavior for the aqueous two-phase systems containing the ionic liquid 1-butyl-3-methylimidazolium tetrafluoroborate and kosmotropic salts. *J. Chem. Eng. Data* **55**, 1087–1092 (2010).
59. Yang, Z. Hofmeister effects: an explanation for the impact of ionic liquids on biocatalysis. *J. Biotechnol.* **144**, 12–22 (2009).
60. Schwierz, N., Horinek, D., Sivan, U. & Netz, R. R. Reversed Hofmeister series—The rule rather than the exception. *Curr. Opin. Colloid Interface Sci.* **23**, 10–18 (2016).
61. Noubigh, A., Cherif, M., Provost, E. & Abderrabba, M. Solubility of gallic acid, vanillin, syringic acid, and protocatechuic acid in aqueous sulfate solutions from (293.15 to 318.15) K. *J. Chem. Eng. Data* **53**, 1675–1678 (2008).
62. Sadeghi, R., Mostafa, B., Parsi, E. & Shahebrahimi, Y. Toward an understanding of the salting-out effects in aqueous ionic liquid solutions: Vapor-liquid equilibria, liquid-liquid equilibria, volumetric, compressibility, and conductivity behavior. *J. Phys. Chem. B* **114**, 16528–16541 (2010).
63. Xu, A., Wang, J. & Wang, H. Effects of anionic structure and lithium salts addition on

the dissolution of cellulose in 1-butyl-3-methylimidazolium-based ionic liquid solvent systems. *Green Chem.* **12**, 268–275 (2010).

64. Singh, T. & Kumar, A. Aggregation behavior of ionic liquids in aqueous solutions: Effect of alkyl chain length, cations, and anions. *J. Phys. Chem. B* **111**, 7843–7851 (2007).
65. Dorbritz, S., Ruth, W. & Kragl, U. Investigation on aggregate formation of ionic liquids. *Adv. Synth. Catal.* **347**, 1273–1279 (2005).
66. Allen, M. P., Attig, N., Binder, K., Grubm, H. & Eds, K. K. Introduction to Molecular Dynamics Simulation. **23**, (2004).
67. Cui, Y. Hydrotropic Solubilization by Urea Derivatives: A Molecular Dynamics Simulation Study. *J. Pharm.* **2013**, 1–15 (2013).
68. Das, S. & Paul, S. Mechanism of Hydrotropic Action of Hydrotrope Sodium Cumene Sulfonate on the Solubility of Di-t-Butyl-Methane: A Molecular Dynamics Simulation Study. *J. Phys. Chem. B* **120**, 173–183 (2016).
69. Bastos, H., Bento, R., Schaeffer, N., Coutinho, J. A. P. & Pérez-Sánchez, G. Using coarse-grained molecular dynamics to rationalize biomolecule solubilization mechanisms in ionic liquid-based colloidal systems. *Phys. Chem. Chem. Phys.* **22**, 24771–24783 (2020).
70. Cui, Y., Xing, C. & Ran, Y. Molecular Dynamics Simulations of Hydrotropic Solubilization and Self-Aggregation of Nicotinamide. *J. Pharm. Sci.* **99**, 3048–3059 (2010).
71. Marrink, S. J. & Tieleman, D. P. Perspective on the martini model. *Chem. Soc. Rev.* **42**, 6801–6822 (2013).
72. Nielsen, S. O., Lopez, C. F., Srinivas, G. & Klein, M. L. Coarse grain models and the computer simulation of soft materials. *J. Phys. Condens. Matter* **16**, (2004).
73. Van Der Spoel, D. *et al.* GROMACS: Fast, flexible, and free. *J. Comput. Chem.* **26**, 1701–1718 (2005).
74. Lindahl, E., Abraham, M. J., Berk, H. & Van Der Spoel, D. GROMACS 2019.4 Manual. *GROMACS Doc.* (2019).
75. Humphrey, W., Dalke, A. and Schulten, K. VMD - Visual Molecular Dynamics. *J. Molec. Graph.* **14**, 33–38 (1996).
76. Berendsen, H. J. C., Postma, J. P. M., Van Gunsteren, W. F., Dinola, A. & Haak, J. R. Molecular dynamics with coupling to an external bath. *J. Chem. Phys.* **81**, 3684–3690 (1984).
77. Parrinello, M. & Rahman, A. Polymorphic transitions in single crystals: A new

molecular dynamics method. *J. Appl. Phys.* **52**, 7182–7190 (1981).

78. Ponder, J. W. & Case, D. A. Force Fields for Protein Simulations. in *The Journal of Physical Chemistry B* vol. 108 27–85 (2003).
79. Jorgensen, W. L., Maxwell, D. S. & Tirado-Rives, J. Development and testing of the OPLS all-atom force field on conformational energetics and properties of organic liquids. *J. Am. Chem. Soc.* **118**, 11225–11236 (1996).
80. Berendsen, H. J. C., Grigera, J. R. & Straatsma, T. P. The missing term in effective pair potentials. *J. Phys. Chem.* **91**, 6269–6271 (1987).
81. Hockney, R. W., Goel, S. P. & Eastwood, J. W. Quiet high-resolution computer models of a plasma. *J. Comput. Phys.* **14**, 148–158 (1974).
82. Brehm, M., Thomas, M., Gehrke, S. & Kirchner, B. TRAVIS—A free analyzer for trajectories from molecular simulation. *J. Chem. Phys.* **152**, (2020).
83. Eisenhaber, F., Lijnzaad, P., Argos, P., Sander, C. & Scharf, M. The double cubic lattice method: Efficient approaches to numerical integration of surface area and volume and to dot surface contouring of molecular assemblies. *J. Comput. Chem.* **16**, 273–284 (1995).
84. Shimizu, S. & Matubayasi, N. Unifying hydrotropy under Gibbs phase rule. *Phys. Chem. Chem. Phys.* **19**, 23597–23605 (2017).
85. Marcus, Y. The hydration entropies of ions and their effects on the structure of water. *J. Chem. Soc. Faraday Trans. 1 Phys. Chem. Condens. Phases* **82**, 233–242 (1986).
86. Marcus, Y. Thermodynamics of Solvation of Ions. *J. Chem. Soc., Faraday Trans.* **89**, 713–718 (1993).
87. Lommelen, R., Onghena, B. & Binnemans, K. Cation Effect of Chloride Salting Agents on Transition Metal Ion Hydration and Solvent Extraction by the Basic Extractant Methyltrioctylammonium Chloride. *Inorg. Chem.* **59**, 13442–13452 (2020).
88. De Robertis, A., Rigano, C., Sammartano, S. & Zerbinati, O. Ion association of Cl- with Na^+, K^+, Mg^{2+} and Ca^{2+} in aqueous solution at 10 ≤ T ≤ 45 ° C and 0 ≤ I ≤ 1 mol l-1. A literature data analysis. *Thermochim. Acta* **115**, 241–248 (1987).
89. Friesen, S., Hefter, G. & Buchner, R. Cation Hydration and Ion Pairing in Aqueous Solutions of MgCl 2 and CaCl 2. *J. Phys. Chem. B* **123**, 891–900 (2019).
90. Sun, Z., Zhang, W., Ji, M., Hartsock, R. & Gaffney, K. J. Aqueous Mg2+ and Ca2+ ligand exchange mechanisms identified with 2DIR spectroscopy. *J. Phys. Chem. B* **117**, 12268–12275 (2013).
91. Ikeda, T., Boero, M. & Terakura, K. Hydration properties of magnesium and calcium ions from constrained first principles molecular dynamics. *J. Chem. Phys.* **127**,

(2007).

92. Azam, S. S., Hofer, T. S., Randolf, B. R. & Rode, B. M. Hydration of sodium(I) and potassium(I) revisited: A comparative QM/MM and QMCF MD simulation study of weakly hydrated ions. *J. Phys. Chem. A* **113**, 1827–1834 (2009).
93. Mähler, J. & Persson, I. A study of the hydration of the alkali metal ions in aqueous solution. *Inorg. Chem.* **51**, 425–438 (2012).
94. Ragnarsdottir, K. V., Odkers, E. H., Sherman, D. M. & Collins, C. R. Aqueous speciation of yttrium at temperatures from 25 to 340°C at Psat: An in situ EXAFS study. *Chem. Geol.* **151**, 29–39 (1998).
95. Bernardes, C. E. S., Minas Da Piedade, M. E. & Canongia Lopes, J. N. The structure of aqueous solutions of a hydrophilic ionic liquid: The full concentration range of 1-ethyl-3-methylimidazolium ethylsulfate and water. *J. Phys. Chem. B* **115**, 2067–2074 (2011).
96. Chang, H. C. *et al.* Structural organization in aqueous solutions of 1-butyl-3-methylimidazolium halides: A high-pressure infrared spectroscopic study on ionic liquids. *J. Phys. Chem. B* **112**, 4351–4356 (2008).
97. Ma, C., Laaksonen, A., Liu, C., Lu, X. & Ji, X. The peculiar effect of water on ionic liquids and deep eutectic solvents. *Chem. Soc. Rev.* **47**, 8685–8720 (2018).
98. Hunt, P. A., Kirchner, B. & Welton, T. Characterising the electronic structure of ionic liquids: An examination of the 1-butyl-3-methylimidazolium chloride ion pair. *Chem. - A Eur. J.* **12**, 6762–6775 (2006).
99. Saha, S., Hayashi, S., Kobayashi, A. & Hamaguchi, H. O. Crystal Structure of 1-Butyl-3-methylimidazolium Chloride. A Clue to the Elucidation of the Ionic Liquid Structure. *Chem. Lett.* **32**, 740–741 (2003).
100. Hunt, P. A., Ashworth, C. R. & Matthews, R. P. Hydrogen bonding in ionic liquids. *Chem. Soc. Rev.* **44**, 1257–1288 (2015).
101. Abranches, D. O. *et al.* Unveiling the mechanism of hydrotropy: Evidence for water-mediated aggregation of hydrotropes around the solute. *Chem. Commun.* **56**, 7143–7146 (2020).
102. Aguilera, L., Völkner, J., Labrador, A. & Matic, A. The effect of lithium salt doping on the nanostructure of ionic liquids. *Phys. Chem. Chem. Phys.* **17**, 27082–27087 (2015).
103. Yin, T., Chen, Y. & Shen, W. Aggregation of an ionic-liquid type hydrotrope 1-Butyl-3-methylimidazolium p-toluenesulfonate in aqueous solution. *Colloids Surfaces A Physicochem. Eng. Asp.* **564**, 95–100 (2019).

104. Serjeant, E.P., D. B. *Ionisation Constants of Organic Acids in Aqueous Solution. International Union of Pure and Applied Chemistry (IUPAC)*. (Pergamon Press, Inc., 1979).
105. Skarmoutsos, I., Dellis, D., Matthews, R. P., Welton, T. & Hunt, P. A. Hydrogen bonding in 1-butyl- and 1-ethyl-3-methylimidazolium chloride ionic liquids. *J. Phys. Chem. B* **116**, 4921–4933 (2012).
106. Matthews, R. P., Welton, T. & Hunt, P. A. Hydrogen bonding and π–π interactions in imidazolium-chloride ionic liquid clusters. *Phys. Chem. Chem. Phys.* **17**, 14437–14453 (2015).
107. Gao, W., Tian, Y. & Xuan, X. How the cation-cation π-π Stacking occurs: A theoretical investigation into ionic clusters of imidazolium. *J. Mol. Graph. Model.* **60**, 118–123 (2015).
108. Wang, Y. L., Laaksonen, A. & Fayer, M. D. Hydrogen Bonding versus π-π Stacking Interactions in Imidazolium-Oxalatoborate Ionic Liquid. *J. Phys. Chem. B* **121**, 7173–7179 (2017).

Supporting Information

Table SI:1. Experimental results for the hydrotropy tests referent to the 0,5 M IL condition. The vanillin concentration expressed is the mean value deriving from three independent tests. Note that the value in the absence of salt was obtained from a previous study, and as such is not subject to any deviation.

NaCl		
[NaCl] mol.kg^{-1}	[Van] g.L^{-1}	± σ
0,000	43,23	0,00
0,482	35,47	0,44
1,017	30,19	1,11
1,490	28,93	0,61
1,985	26,15	0,89
2,451	24,42	0,51
2,978	23,44	0,48
3,320	21,01	0,21

KCl		
[KCl] mol.kg^{-1}	[Van] g.L^{-1}	± σ
0,000	43,23	0,00
0,496	40,76	2,26
1,000	39,03	0,32
1,521	33,11	0,25
2,006	32,18	0,08
2,623	28,35	0,54

LiCl		
[LiCl] mol.kg^{-1}	[Van] g.L^{-1}	± σ
0,000	43,23	0,00
1,060	33,17	2,49
1,960	25,21	0,67
4,050	17,76	0,35
6,030	15,20	0,37
6,950	13,78	0,19
7,930	15,08	0,12
8,940	12,85	0,16

$MgCl_2$		
[$MgCl_2$] mol.kg^{-1}	[Van] g.L^{-1}	± σ
0,000	43,23	0,00
0,498	40,76	2,26
1,011	39,03	0,32
1,490	34,55	2,30
1,991	32,18	0,08

$CaCl_2$		
[$CaCl_2$] mol.kg^{-1}	[Van] g.L^{-1}	± σ
0,000	43,23	0,00
0,537	35,33	0,44
1,075	27,62	0,84
1,613	19,92	0,46
2,135	19,67	0,15
2,700	19,27	0,76

YCl_3		
[YCl_3] mol.kg^{-1}	[Van] g.L^{-1}	± σ
0,000	43,23	0,00
0,506	30,04	1,11
1,015	21,33	0,45
1,504	18,17	0,42

Table SI:2. Experimental results for the hydrotropy tests referent to the 1,5 M IL condition. The vanillin concentration expressed is the mean value deriving from three independent tests. Note that the value in the absence of salt was obtained from a previous study, and as such is not subject to any deviation.

NaCl		
[NaCl] mol.kg^{-1}	[Van] g.L^{-1}	± σ
0,000	279,77	0,00
0,493	229,07	0,92
1,019	207,59	8,13
1,503	202,97	2,81
1,994	192,38	2,41
2,501	211,32	1,50

KCl		
[KCl] mol.kg^{-1}	[Van] g.L^{-1}	± σ
0,000	279,77	0,00
0,502	200,68	17,48
1,012	214,90	1,48
1,406	209,08	5,91
1,577	209,78	2,96

LiCl		
[LiCl] mol.kg^{-1}	[Van] g.L^{-1}	± σ
0,000	279,77	0,00
1,120	157,53	7,93
2,000	137,35	5,78
3,020	105,54	10,29
4,010	93,28	9,60
4,980	94,40	6,96
5,990	85,50	2,69
6,420	81,12	1,54

$MgCl_2$		
[$MgCl_2$] mol.kg^{-1}	[Van] g.L^{-1}	± σ
0,000	279,77	0,00
0,487	256,36	4,23
1,014	211,17	1,48
1,482	182,09	4,25
1,961	160,66	0,62

$CaCl_2$		
[$CaCl_2$] mol.kg^{-1}	[Van] g.L^{-1}	± σ
0,000	279,77	0,00
0,489	145,55	10,91
0,996	126,31	2,70
1,424	107,57	3,45
1,697	100,81	4,88

YCl_3		
[YCl_3] mol.kg^{-1}	[Van] g.L^{-1}	± σ
0,000	279,77	0,00
0,484	147,57	0,74

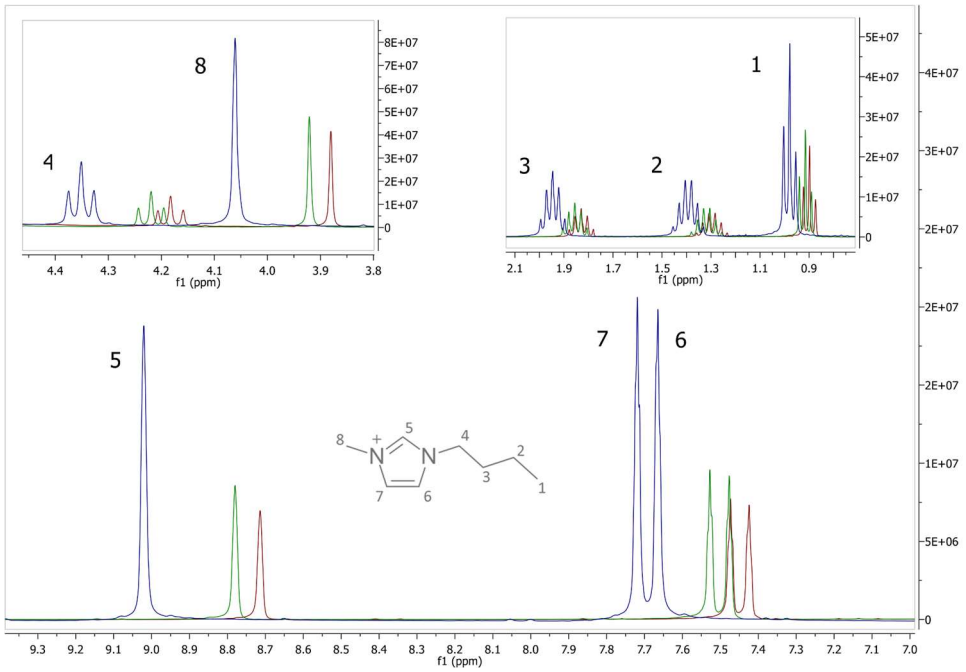

Figure SI:1. NMR spectra of [C_4mim]Cl in water, at different concentrations: 0,5 M (red), 1,5 M (green), and 2,25 M (blue).

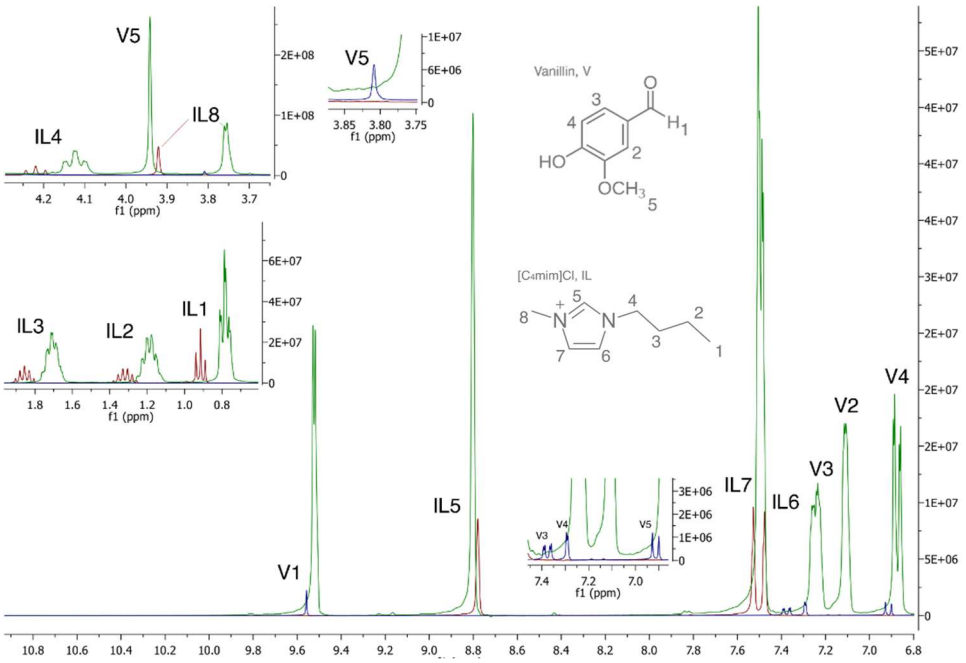

Figure SI:2. NMR spectra of [C_4mim]Cl and vanillin in water. 1,5 M IL in water (red), 1,5 M IL with vanillin to saturation (green), and vanillin in water to saturation (blue).

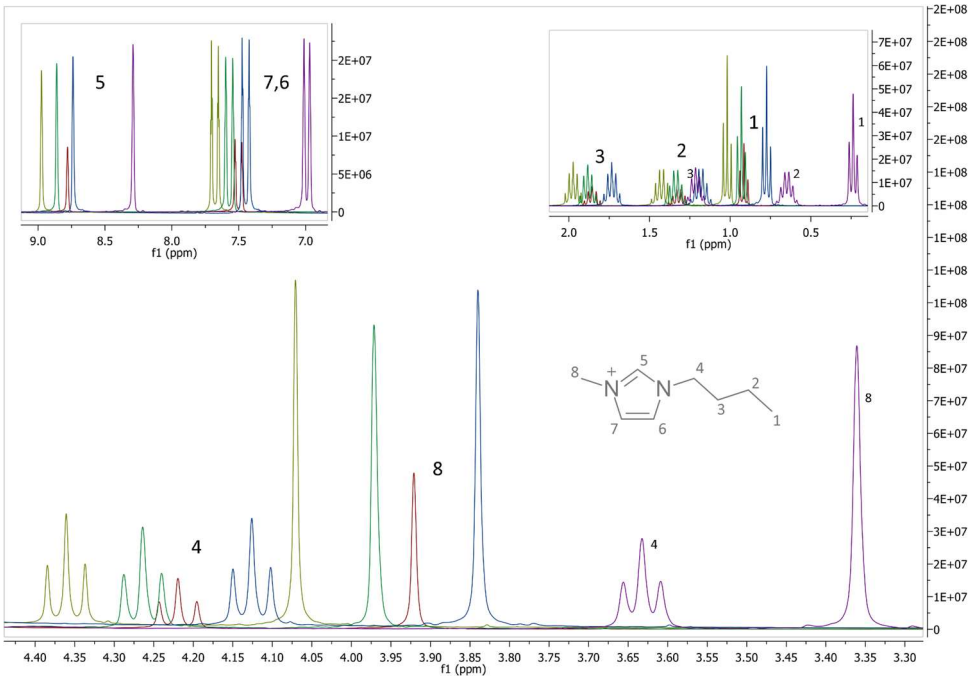

Figure SI:3. NMR spectra of 1,5 M [C_4mim]Cl in water with added salts: 1,5 M IL in water without added salt (red), 1 M NaCl (olive), 1 M LiCl (green), 1 M $MgCl_2$ (blue), 1 M YCl_3 (purple).

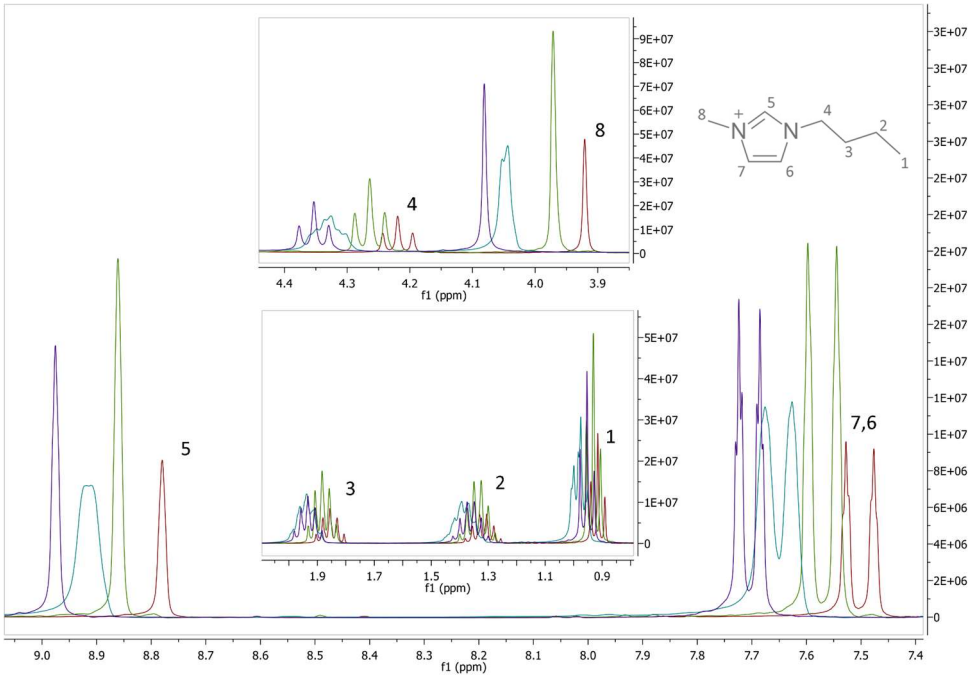

Figure SI:4. NMR spectra of 1,5 M [C_4mim]Cl in water with added LiCl: 1,5 M IL in water without added salt (red), 1 M LiCl (olive), 2 M LiCl (turquoise), 6 M LiCl (purple).

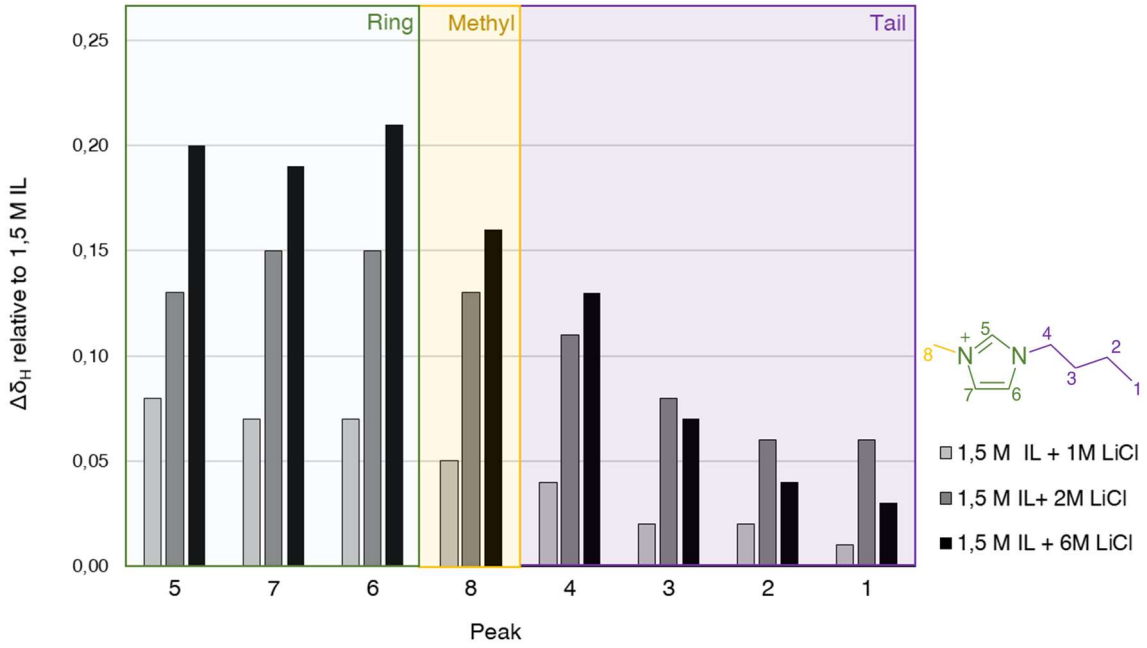

Figure SI:5. Chemical shifts of the hydrogens of the C_4mim cation in 1,5 M solutions of [C_4mim]Cl in water, with added LiCl, when compared to a similar solution without salt.

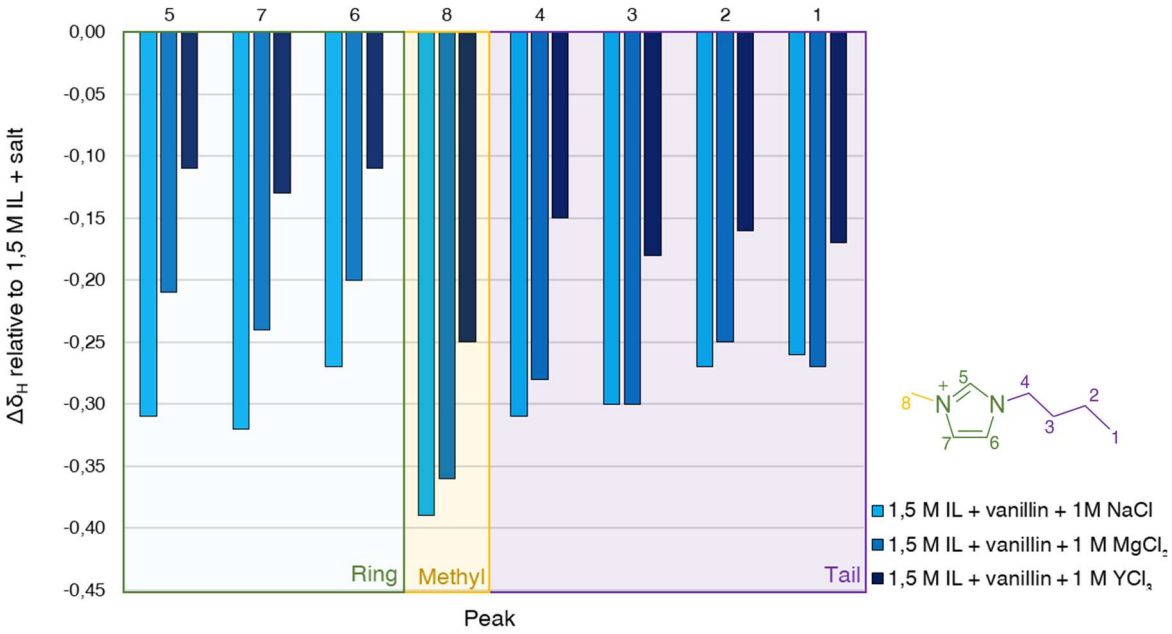

Figure SI:6. Chemical shifts of the hydrogens of the C_4mim cation in 1,5 M solutions of [C_4mim]Cl in water, with added vanillin to saturation and with 1,0 M of added salts, when compared to a similar solution without vanillin.

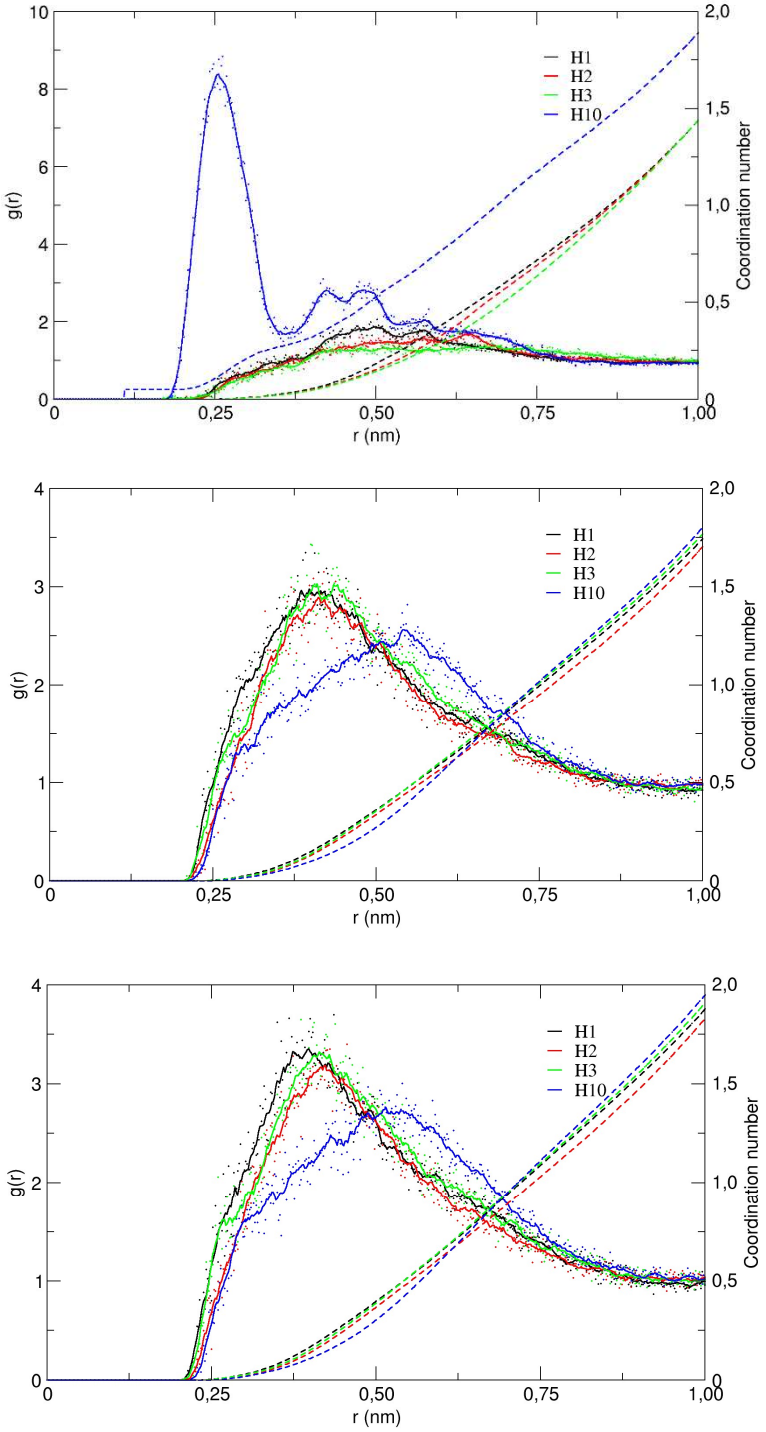

Figure SI:7. Radial distribution functions for the O0H oxygen of the vanillin methoxy group as reference, and the four hydrogens of the IL cation as selection, for the following conditions: 10 vanillin molecules in aqueous IL (top), 20 vanillin molecules in aqueous IL (middle), and 20 vanillin molecules in aqueous IL with 100 NaCl molecules added (bottom).

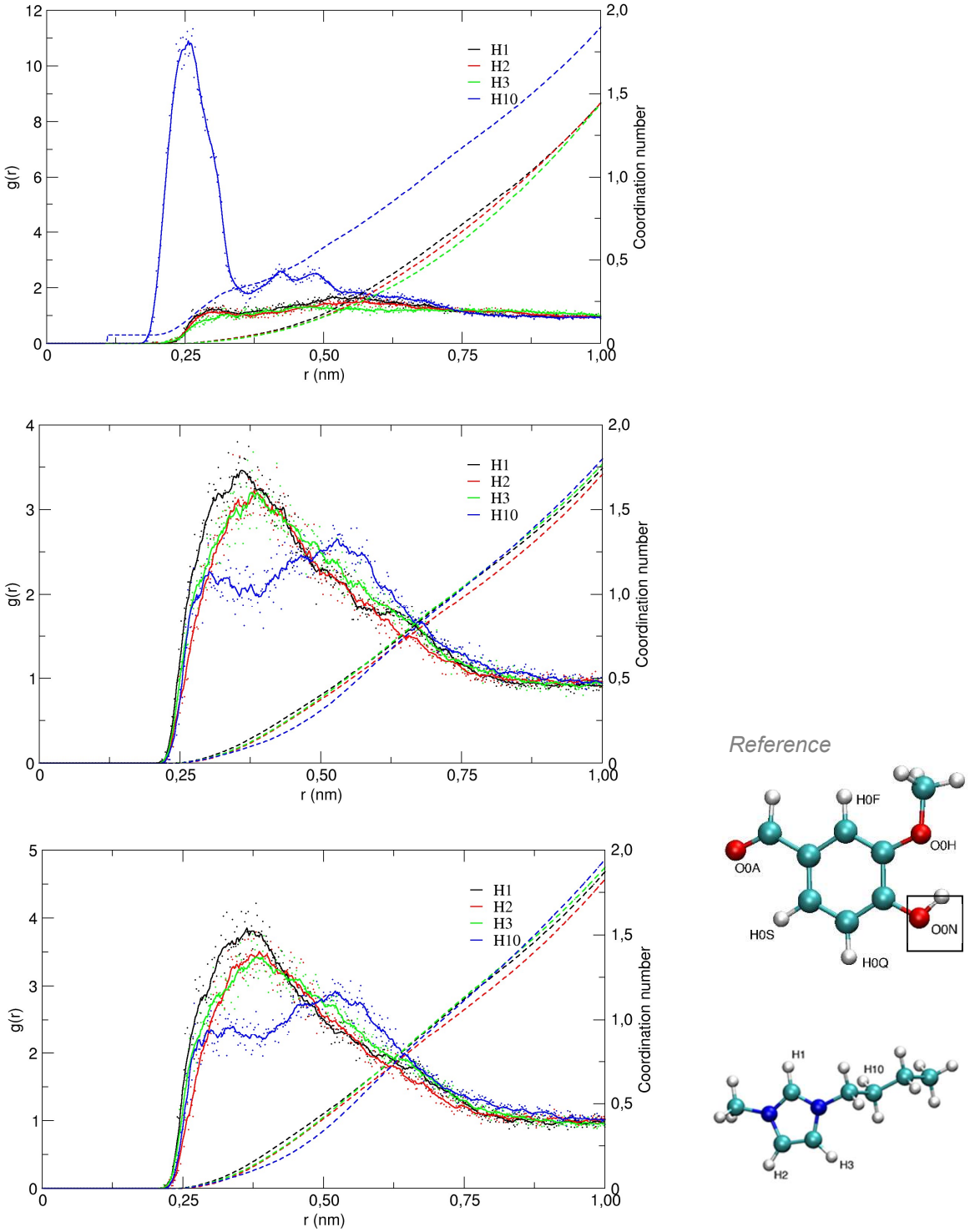

Figure SI:8. Radial distribution functions for the O0N oxygen of the vanillin hydroxyl group as reference, and the four hydrogens of the IL cation as selection, for the following conditions: 10 vanillin molecules in aqueous IL (top), 20 vanillin molecules in aqueous IL (middle), and 20 vanillin molecules in aqueous IL with 100 NaCl molecules added (bottom).

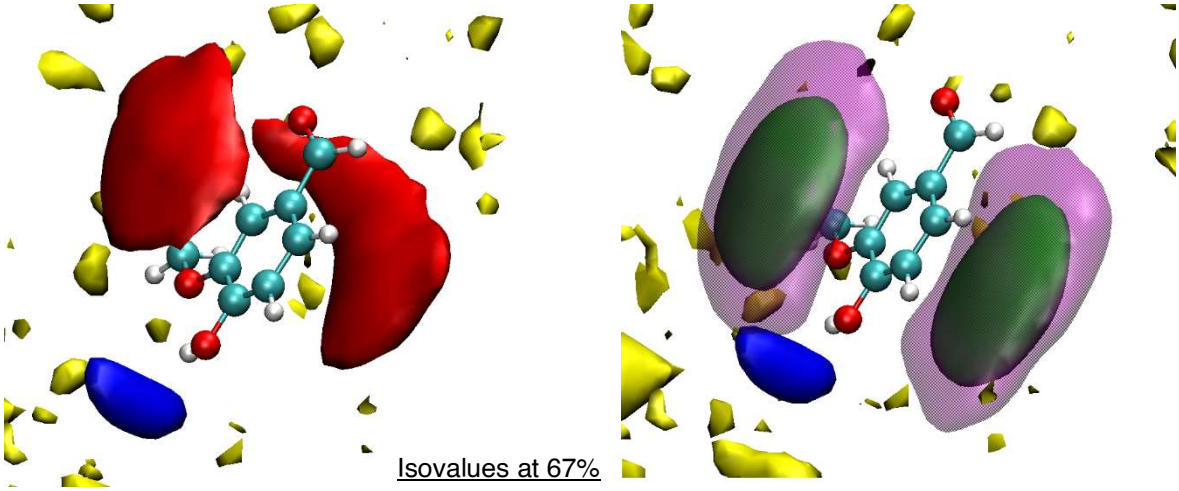

Figure SI:9. Spatial Distribution Functions of water (blue), chloride (yellow), vanillin (red), the IL cation head (green), and the IL cation tail (purple) with vanillin as the reference molecule, for condition (e) 20 vanillin in aqueous 100 IL with 100 NaCl.

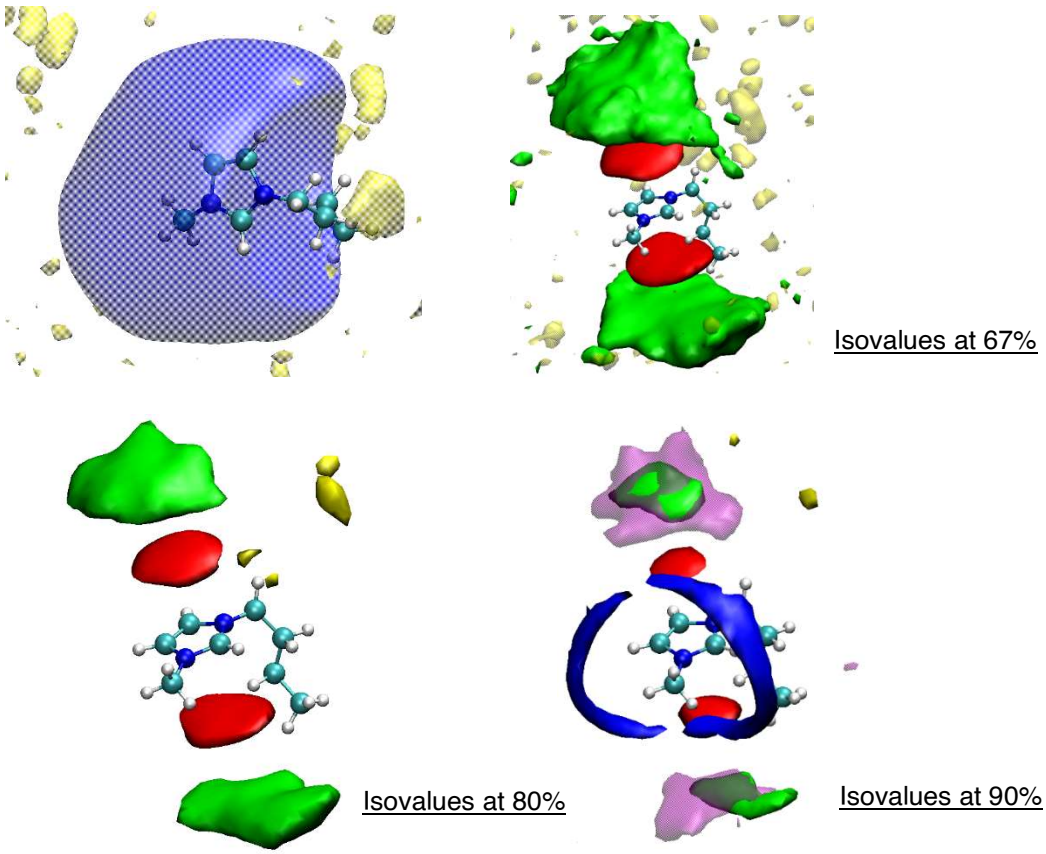

Figure SI:10. Spatial Distribution Functions of water (blue), chloride (yellow), vanillin (red), the IL cation head (green), and the IL tail (purple) with the IL cation as the reference molecule, for condition (e) 20 vanillin in aqueous 100 IL.

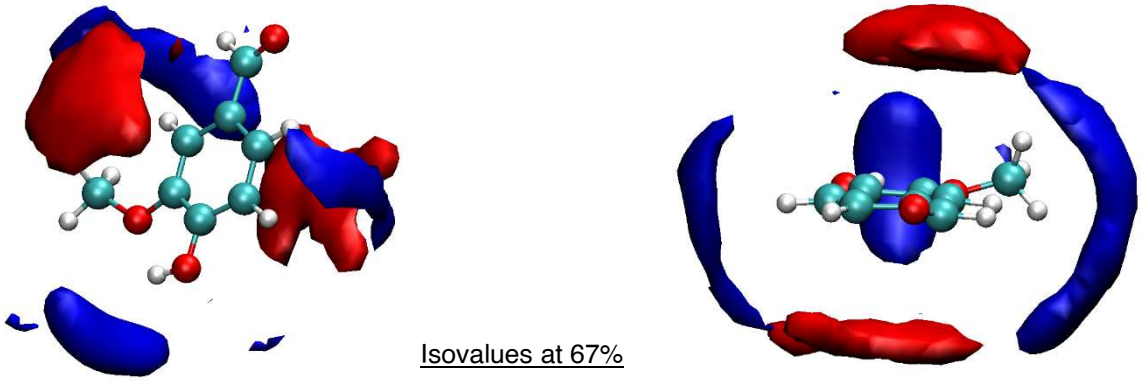

Figure SI:11. Spatial Distribution Functions of water (blue) and vanillin (red) with vanillin as the reference molecule, for condition (b) 10 vanillin in water.

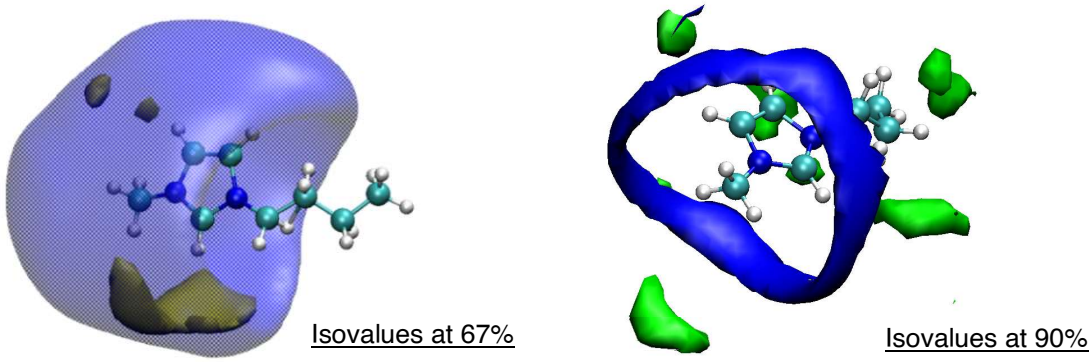

Figure SI:12. Spatial Distribution Functions of water (blue), chloride (yellow) and the IL cation imidazolium ring (green) with the $[C_4mim]^+$ cation as the reference molecule, for condition (a) 100 IL in water.

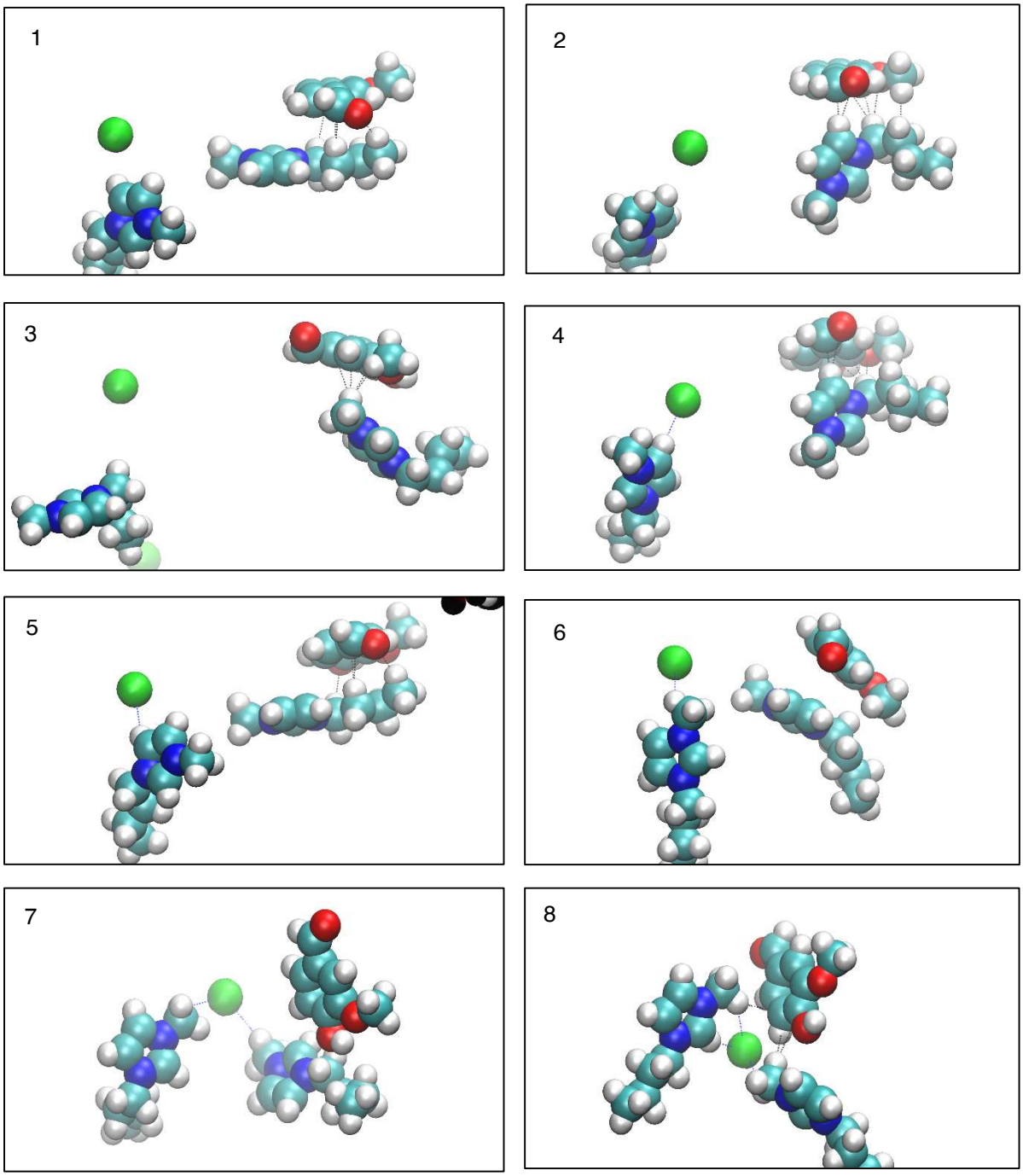

Figure SI:13. Sequence of eight frames depicting typical observed interactions between vanillin (with red oxygen atoms), the IL cation (with blue nitrogen atoms), and chloride (green). Deserving special emphasis, the planar interactions, the methyl chloride interactions, IL tail-vanillin interactions, and the possible structuring effect of chloride in frames 7 and 8. Water hidden for clarity. Snapshots taken from condition (d) 20 vanillin in aqueous IL.